2018

# INVESTIGATING SMOKE EXPOSURE AND CHRONIC OBSTRUCTIVE PULMONARY DISEASE (COPD) WITH A CALIBRATED AGENT BASED MODEL (ABM) OF IN VITRO FIBROBLAST WOUND HEALING.

James A. Ratti
*Virginia Commonwealth University*

INVESTIGATING SMOKE EXPOSURE AND CHRONIC OBSTRUCTIVE

PULMONARY DISEASE (COPD) WITH A CALIBRATED AGENT BASED MODEL

(ABM) OF *IN VITRO* FIBROBLAST WOUND HEALING.

A thesis submitted in partial fulfillment of the requirements for the degree of Master of Science of Biomedical Engineering at Virginia Commonwealth University.

by

JAMES ALEXANDER RATTI
B.S. Biomedical Engineering, VCU, 2013

Director: REBECCA L. HEISE
ASSOCIATE PROFESSOR, BIOMEDICAL ENGINEERING

Virginia Commonwealth University
Richmond, Virginia
May 2018

# Acknowledgements

I would first like to thank Dr. Rebecca Heise and Dr. Angela Reynolds for all of their insight, guidance, and encouragement throughout this project. I will forever be grateful to you for accepting me onto your team and teaching me these *in vitro* techniques and computational methods to study disease from an engineering perspective. This experience has inspired me to further explore the roles of mechanobiology within diseases and medicines for them in my future endeavors. I would also like to thank Dr. Christopher Lemmon for the advice regarding fibroblast biology and taking the time to serve on my committee; as well as all of the students and alumni of the Heise and Lemmon labs for all of the conversations, assistance and computers for simulations.

I would like to extend a special thanks to my partner Kat Beyer for all of her support, listening to me blather about science, and helping me stay grounded in the chaos.

Lastly, I would like to thank my family and friends for all of the support, invaluable life lessons and patience with my limited availability during these studies.

You all helped make this possible and I can't thank you enough.

Sincerely,

Alex Ratti

Table of Contents

# List of Tables

## List of Figures

# Abstract

INVESTIGATING SMOKE EXPOSURE AND CHRONIC OBSTRUCTIVE

PULMONARY DISEASE (COPD) WITH A CALIBRATED AGENT BASED MODEL

(ABM) OF *IN VITRO* FIBROBLAST WOUND HEALING.

By James Alexander Ratti, B.S.

A thesis submitted in partial fulfillment of the requirements for the degree of Master of Science in Biomedical Engineering at Virginia Commonwealth University.

Virginia Commonwealth University, 2018

Major Director:  Rebecca L. Heise
Associate Professor, Biomedical Engineering

COPD is characterized by tissue inflammation and impaired remodeling that suggests fibroblast maintenance of structural homeostasis is dysregulated. Thus, we performed *in vitro* wound healing experiments on normal and diseased human lung fibroblasts and developed an ABM of fibroblasts closing a scratched monolayer using NetLogo to evaluate differences due to COPD or cigarette smoke condensate exposure. This ABM consists of a rule-set governing the healing response, accounting for cell

x

migration, proliferation, death, activation and senescence rates; along with the effects of heterogeneous activation, phenotypic changes, serum deprivation and exposure to cigarette smoke condensate or bFGF. Simulations were performed to calibrate parameter-sets for each cell type using *in vitro* data of scratch-induced migration, viability, senescence-associated beta-galactosidase and alpha-smooth muscle actin expression. Parameter sensitivities around each calibrated parameter-set were analyzed. This model represents the prototype of a tool designed to explore fibroblast functions in the pathogenesis of COPD and evaluate potential therapies.

# Background

**Chronic Obstructive Pulmonary Disease (COPD) & Oxidative Stress**

With no cure available and treatments that are only able to manage symptoms –
COPD is currently the third leading cause of death among adults in the United States [1]. The
Global Initiative for Chronic Obstructive Lung Disease (GOLD), which provides yearly
updates of recommended methods for the treatment and prevention of COPD, defines it as
"a common, preventable, and treatable disease characterized by persistent respiratory
symptoms and airflow limitation that is due to airway and/or alveolar abnormalities,
usually caused by significant exposure to noxious particles or gases," such as cigarette
smoke or other pollutants [2,3]. This reduction in airflow is due to imbalanced tissue
remodeling that progressively produces both: (A) decreased elastic recoil, small airway
collapse, and loss of alveolar integrity within the parenchyma, along with (B) increased
airway resistance due to narrowed lumen diameters from inflammation, fibrosis and
smooth muscle proliferation within the bronchioles (Figure 1.1) [3–11].

While rare, sometimes heritable, forms of COPD also exist – such as alpha1-
antitrypsin deficiency disorder which causes tissue degradation through a lack of this
crucial antiprotease [12] – the most common risk factor for COPD is smoking tobacco
followed by exposure to other environmental pollutants and ageing. However, only 25%
of smokers will develop the accelerated decline of respiratory function that is associated

with clinically significant COPD [13], indicating some genetic risk factors may play a role as well [2–5,14–16]. For this reason, COPD has been classified as a hereditary autoinflammatory disease, as these are characterized by genetic mutations which produce an overactive or hyperresponsive innate immune system that typically present with periodic episodes or flares mediated by interleukin (IL)-1 [16].
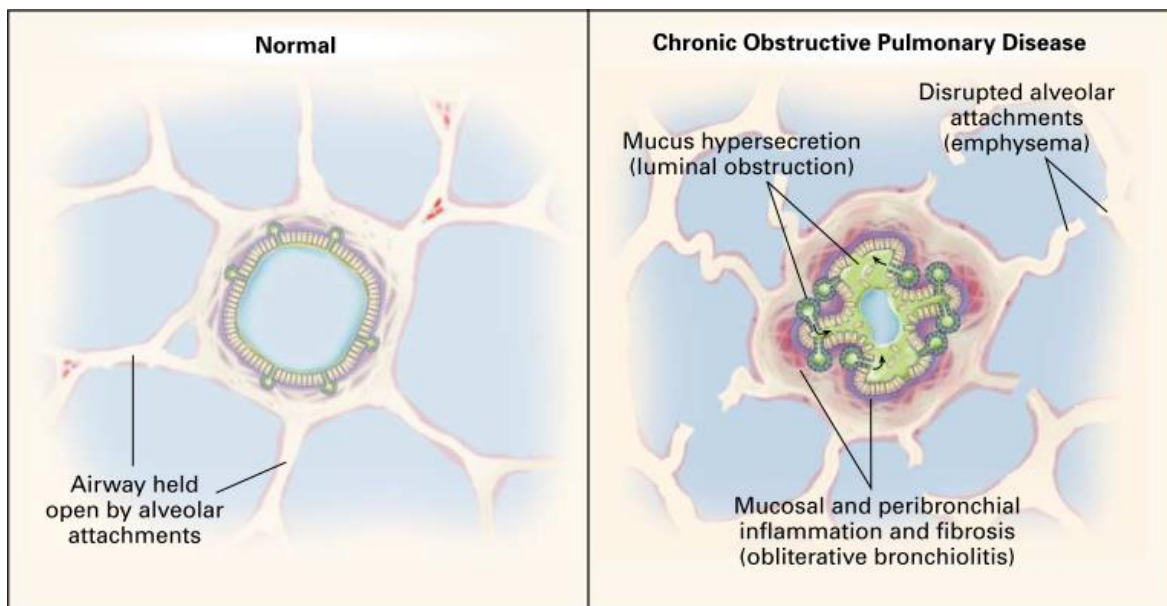


**Figure 1.1** – Mechanisms of airflow limitation in COPD. Reproduced with permission from [10], copyright Massachusetts Medical Society.

Due to this likelihood that genetic differences exist between smokers who do or do not develop COPD, specific cell lines have been isolated from human lungs with COPD (e.g. COPD-Diseased Human Lung Fibroblasts; DHLF) for comparison to genotypically-normal cell lines from healthy human lungs (e.g. Normal Human Lung Fibroblast; NHLF) for *in vitro* research involving COPD [9,17–19]. In particular, pulmonary fibroblasts isolated from people with COPD express increased levels of redox signaling (e.g. isoprostanes,

elevated NADH/NAD ratio), inflammatory signaling (e.g. PGE2, COX-2, TNFα, TGFβ, NLRP3-mediated IL-1β, IL-6), myofibroblast markers (e.g. αSMA), senescence markers (e.g. p16, p21, β-Gal, IL-1α, minimal telomeres), and fail to maintain extracellular matrix (ECM) homeostasis [3,6,9,16,18–23]. Additionally, lung fibroblasts have been shown to differentially inhibit global protein translation, proliferation, migration, and contraction of collagen gels within hours [9,21,24,25] – as well as increase senescence over several passages [18,20,26–28] – in response to prostaglandin-E2 (PGE2) *in vitro*, a common inflammatory pathway that has been shown to be dysregulated in COPD fibroblasts and directly correlates with the disease's severity [9,18,20,24,26].

The proposed inflammatory mechanisms behind COPD's pathogenesis are a modified response to respiratory irritants characterized by increased oxidative stress from activated immune cells, cigarette smoke, and other environmental factors that creates an amplified inflammatory response, an imbalance of proteases and antiproteases, and an increase in cellular proliferation, apoptosis and senescence. This is supported by a loss of alveolar epithelial cells and increased proliferation – evidenced by shortened telomeres among progenitor and non-senescent cells relative to uninflamed somatic cells – among samples from patients with COPD. Additionally, increased levels of markers for oxidative stress (e.g. $H_2O_2$, 8-isoprostane), inflammatory cells (e.g. Neutrophils, Macrophages, NK-cells), inflammatory mediators, proteases (e.g. MMPs, elastases, cathepsins), and markers of senescence have been found in samples from patients with COPD [2–6,14,19,29,30] – in fact,

this secretory profile is collectively termed the COPD-associated secretory phenotype (CASP). While it partially overlaps with some other lung diseases like

idiopathic pulmonary fibrosis [31], CASP most notably has the same upregulated secretory profile as the cellular senescence-associated secretory phenotype (SASP) [19]. Both secretory profiles are known to result from oxidative stressors like cigarette smoke and inflammation, indicating that cell senescence has an active role in COPD pathogenesis [6,18,37–40,19,20,29,32–36]. It is theorized that COPD pathogenesis occurs via chronic oxidative stress by inducing both apoptosis and senescence – and that senescent cells express a SASP that is self-promoting, induces senescence in surrounding cells, and progressively increases the amount of proteases in the extracellular space. Ongoing stimulation by oxidative stressors can amplify this pathway until the levels of senescent cells becomes self-sustaining, surpasses the ability of the immune system meant to remove them, and reduces the tissue's proliferative capacity to replace lost cells. The resulting imbalances in cellular apoptosis:proliferation and protease:antiprotease levels are thought to be independently responsible for driving the degradation of parenchymal tissue at the cellular and molecular levels, and may explain the observed persistence of inflammation in COPD patients who quit smoking [6,14,19,29,32].

Likewise, cigarette smoke and oxidative stress have been found to induce myofibroblast differentiation among lung fibroblasts – both directly and through miR210 containing extracellular vesicles from bronchial epithelial cells [23] – and epithelial-mesenchymal transition [41,42], which has been found to be increased in COPD as well [42]. The resulting loss of proliferative epithelial cells paired with an excess of fibroblasts, myofibroblasts and senescent cells is thought to drive the differential fibrotic and degradative changes seen in chronic bronchitis and emphysema, respectively.

Altogether, this review indicates that oxidative stress, PGE2 and NLRP3-mediated signaling play a major role in the pathogenesis of COPD by promoting inflammation, mesenchymal differentiation and cellular senescence that subsequently promotes differential ECM hypertrophy and degradation by tissue type; it's hoped that mechanisms which target and suppress these pathways will provide new and effective treatments. Potentially, multi-scale computational modeling of these pathways – from the molecular level up to the entire respiratory system – can be used to determine which combination of these pathways is sufficient to produce the observed clinical symptoms, or if additional factors (e.g. substrate stiffness, substrate composition, traction forces, cyclical stretch, metabolic regulation) need to be taken into account within a more complex model.

**Pulmonary Wound Healing**

Wound healing among embryonic and fetal tissues exhibits full functional regeneration of injured tissues without scarring, while wound healing of adult tissues often leads to the formation of scar tissue or fibrosis that can result in a repaired tissue with less functionality than before the injury [43–46]. In non-pathological tissues, adult wound healing progresses through three overlapping phases: (1) homeostasis and inflammation, (2) proliferation, construction and remodeling, then (3) resolution [36,44–46]. This process occurs in the lung just as it does throughout the body in general (Figure 1.2).
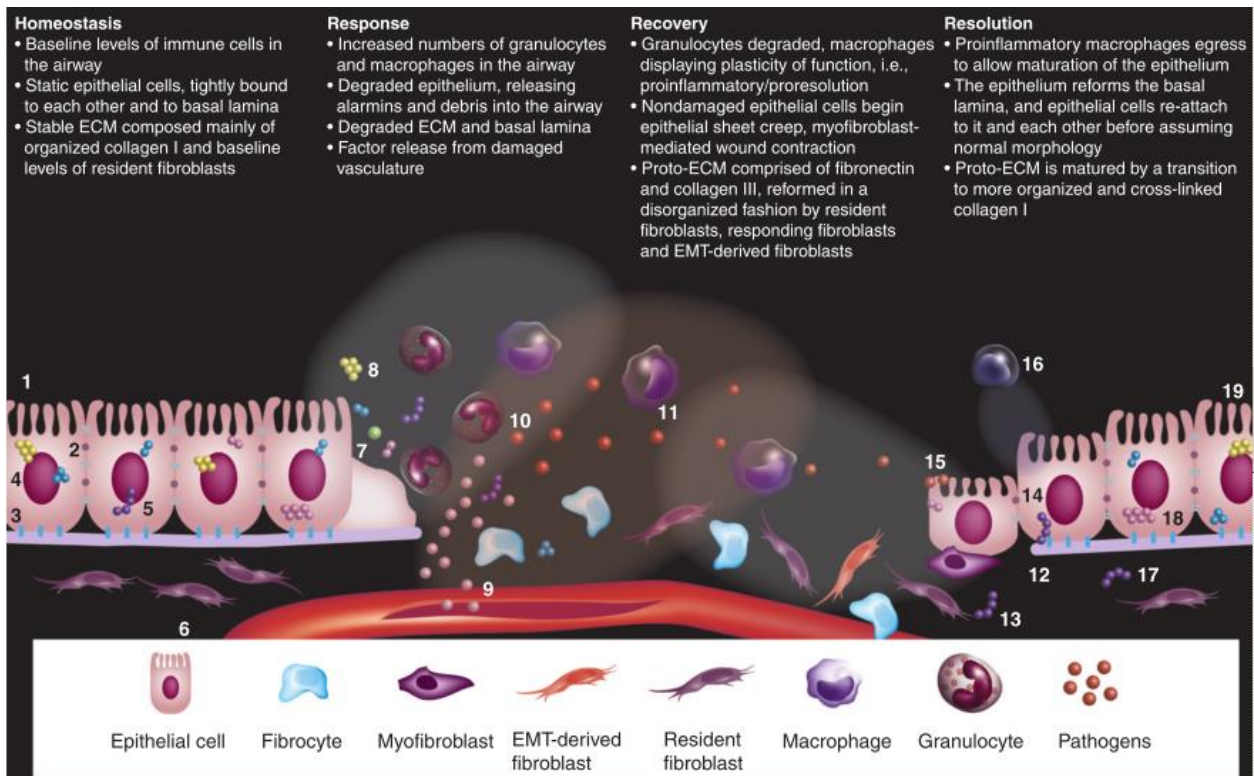
**Figure 1.2** – Phases of acute wound healing in the lungs. A damaged section of tissue experiences an inflammatory response, recovery of lost cell types and ECM components, and resolution of the healing process as the tissue returns to homeostasis. Reproduced with permission from [47], copyright the authors.

The initial phase of pulmonary haemostasis and inflammation occurs immediately following injury – physical trauma activates platelets to induce clotting and stop blood loss – while trauma, infections, toxins and oxidative stress can all stimulate the release of inflammatory growth factors and cytokines (e.g. TGFβ, IL-6, PGE2) from platelets, leukocytes (e.g. neutrophils and macrophages), and damaged resident cells (e.g. fibroblasts, epithelial cells, endothelial cells) which recruit other cells to the wound site to amplify this inflammatory signaling and initiate tissue repair. These recruited cells include additional activated leukocytes to remove dead cells, debris, and invading pathogens from

the wound; fibroblasts to replace and remodel the damaged ECM; endothelial cells for angiogenesis within the healing tissue; and other tissue-specific cells necessary for tissue function – such as bronchial and alveolar epithelial cells in the lungs, keratinocytes in the skin, or hepatocytes in the liver [36,44–51].

The next phase of pulmonary healing is characterized by the growth of granulation tissue – named for its granular appearance – through proliferation of these recruited cells to replace those lost to the injury, construction of new ECM through deposition and contraction of structural proteins (i.e. collagens and fibronectin), and active angiogenesis to provide the new tissue with sufficient circulation. Remodeling of the granulation tissue is effected through continued contraction and cross-linking of newly synthesized ECM by myofibroblasts, secreted matrix metalloproteases (MMPs), and tissue inhibitors of metalloproteases (TIMPs); the regulation of these effectors determines the resultant amount of scarring and fibrosis [11,43–46,48–50].

Resolution of wound healing in the lung is reached when the tissue structure is restored and excess myofibroblasts and epithelial cells are removed by apoptosis. This occurs primarily as the newly synthesized ECM is able to take external stress off myofibroblasts, although increased $NO_2$-signaling or activation of the Fas-apoptotic pathway by IL-6 sensitized by TNFα can also induce myofibroblast apoptosis. If chronic inflammation is present, tissue remodeling may persist and cause some cells to become senescent – from excessive stress, proliferation, or paracrine signaling from other senescent cells – and thereby target themselves for removal by leukocytes, cease synthesis of ECM proteins and TGFβ, and gradually upregulate their secretion of MMPs and pro-

senescence factors (e.g. IL-1α, PGE2, NF-κB, C/EBPβ). Dead or senescent cells cleared from tissues by the immune system are subsequently replaced through proliferation of surrounding cells if needed to resolve the chronic healing response. However, prolonged remodeling by myofibroblasts and senescent cells can cause permanent tissue dysfunction and preclude a full resolution of wound healing – if either myofibroblasts resist undergoing apoptosis and senescence, or if the number of senescent cells surpasses the immune system's ability to clear them, then tissue remodeling may become progressively and irreversibly hypertrophic (i.e. stiffer, fibrotic ECM) or degradative (i.e. softer, more gelatinous ECM), respectively [11,18,39,40,43–46,48–50,52,19,29,32–37].

**Fibroblast Heterogeneity & Activation**

As the primary mediators of ECM synthesis and remodeling, the main contributors to tissue repair are resident fibroblasts and myofibroblasts: mechanically-sensitive cells of mesenchymal origin with a dedifferentiated phenotype. These cells represent a heterogeneous population, where subpopulations from different locations within the lungs (i.e. stroma versus parenchymal regions) exist with differing signaling properties [45,48]. They regulate ECM properties through controlled secretion of structural proteins (e.g. collagen-I, fibronectin, elastin, laminin), proteases, antiproteases, and inflammatory signals (e.g. TGF-β, IL-6, TNF-α, PGE2, IL-1α) in response to inflammatory stimuli such as physical trauma, toxins, oxidative stress, or autocrine and paracrine inflammatory signaling from other fibroblasts, activated leukocytes, epithelial cells and endothelial cells. This regulation of ECM production and quality of remodeling is achieved via a controlled

progression of inactivated resident fibroblasts into activated "proto-myofibroblasts" that

may differentiate into myofibroblasts and eventually either apoptose or become senescent

to be targeted for clearance by the immune system [36,38,53–57,43–46,48–51]. However, within

COPD these cells express increased levels of inflammatory signals, myofibroblast and

senescence markers, reactive oxidative species (ROS; e.g. $OH^-$, $HO_2$, $O_2^-$, $H_2O_2$, $ONOO^-$,

etc.), and fail to maintain their native ECM [3,6,24,9,14,18–23].
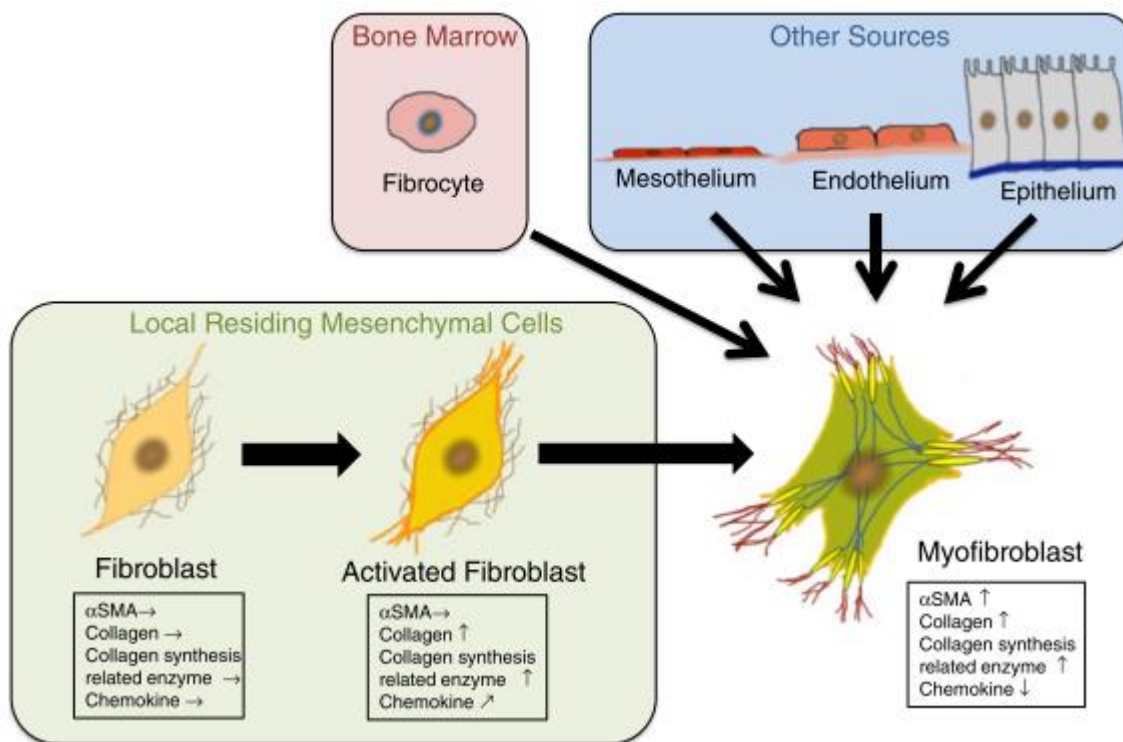


**Figure 1.3** – Fibroblast functions, activation into myofibroblasts and other sources. Reproduced with permission from [48], copyright the authors.

Inactivated resident lung fibroblasts are found in uninjured tissue and all phases of

wound healing within the intact, cross-linked ECM that stress-shields them and inhibits

their formation of stress fibers or focal adhesions with the ECM. However, once stimulated

by a change in the mechanical properties of the local ECM that indicates repairs are needed

– for example, provisional ECM (e.g. fibrin clot) stiffness ranges from 10-1000 Pa [49,50,52] –

these cells migrate to the wounded area. These inactive fibroblasts are naturally resistant to

Fas-mediated apoptosis, and will readily proliferate if isolated *in vitro*; they exhibit

nominal synthesis of ECM proteins (e.g. collagen-I, fibronectin); and form few or no stress

fibers, cell-cell, or cell-ECM interactions – those interactions that do form are often weakly

connected to nascent adhesions (a.k.a. focal complexes) – allowing them to quickly

migrate in response to an injury-induced chemokine or stiffness gradient [11,43,57,45,48–51,53–55].

In the combined presence of transforming growth factor-β (TGFβ) and NADPH

oxidase-4 (NOX4) [39,53–55], the ED-A slice variant of fibronectin, and a sufficient increase

in mechanical stresses – either of substrate stiffness ($\geq$ ~3 kPa [50]), shear stresses from the

edematous increase in extracellular fluid, extracellular stresses from the ECM or adjacent

cells, or intracellular stresses from contraction of the actin cytoskeleton – focal complexes

can form into focal adhesions (FAs; 2-6 μm long [49]) capable of supporting stress fibers and

higher traction forces (3-4 nN/μm$^2$ [49]). These mechanobiological signals spur fibroblasts to

progressively activate into a proto-myofibroblast  morphology followed by full

myofibroblast differentiation [45,48,58,59,49–51,53–57]. These proto-myofibroblasts are found in all

phases of wound healing from inflammation through remodeling, and will readily

proliferate if cultured *in vitro* similar to fibroblasts. One activated through force-controlled

release of TGFβ from reservoir proteins bound to the ECM ($\geq$ 5-9 kPa [50]), the actin

cytoskeleton is rapidly reorganized to form lamellipodia, numerous focal adhesions, N-

cadherin-type cell-cell interactions, and actin stress fibers devoid of alpha-smooth muscle

actin (αSMA). Additionally, these proto-myofibroblasts exhibit IL-6 mediated positive

reinforcement of upregulated proliferation, ECM synthesis and contractility, pro-survival

genes, and αSMA expression that's not yet incorporated into stress fibers [9,43,49–51,53,56,59].
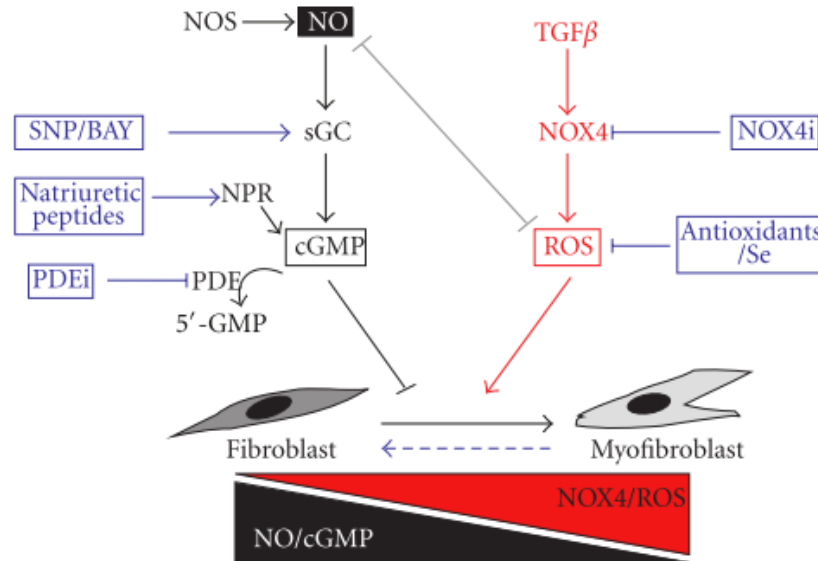


**Figure 1.4** – Myofibroblast differentiation mediated by oxidative stress and potential
inhibitors to recover the fibroblast phenotype. Reproduced with permission from [60],
copyright the authors.

With progressive activation of TGFβ and NOX4 signaling along with sufficient

increase in mechanical stimulation – either via substrate stiffness ($\geq$ ~20 kPa; thus, most *in*

*vitro* cultures of fibroblasts exhibit proto-myofibroblast phenotypes due to tissue culture

plastic's stiffness in the GPa range [49]), shear, extracellular adhesions, or internal

contractility – proto-myofibroblasts may fully differentiate into myofibroblasts as their

focal adhesions coalesce into super-mature focal adhesions (SMFAs; 8-30 μm long, 4-5

fold longer than FAs [49,50]) capable of supporting αSMA-containing stress fibers, 3-4 fold

increased traction stresses (~12 nN/μm$^2$ [49]), and OB-cadherin (type-11) junctions. While generally not found in the inflammatory phase of healing, myofibroblasts are primarily found within the proliferating and remodeling granulation tissue, can originate from multiple cell types besides resident fibroblasts (e.g. circulating fibrocytes, endothelial cells, epithelial cells, and smooth muscle cells), and don't proliferate if isolated *in vitro*, unlike inactive fibroblasts and proto-myofibroblasts. The main hallmark of myofibroblasts, their expression of αSMA-containing stress fibers, is mediated through production via multiple signaling pathways – including: SMAD2/3, Notch1-Jagged1 (required *in vitro*), Wnt, hedgehog, or oxidative stress mediated by NOX4 – and organization into stress fibers without disrupting the core actin fibril [49,50,61]. While myofibroblasts maintain upregulation of collagen-I and fibronectin, they cease secretion of cytokines. This causes them to continue synthesizing and contracting new ECM as long as the upregulated TGFβ remains to provide myofibroblasts resistance to Fas-mediated apoptosis; without protection from TGFβ, myofibroblasts may apoptose in response to IL-6-and-TNFα or NO$_2$ signaling, although their strongest stimulus for apoptosis is a loss of external stress indicative of sufficiently remodeled, structurally sound ECM signaling the end of healing [9,11,50,51,53–57,36,38,43–46,48,49].

**Cellular Senescence: Replicative & Stress-Induced**

As part of the tissue's chronic wound healing response, cellular senescence is essentially a cellular quarantining mechanism to suspend proliferation and prevent the spread of any damage to new cells – either until it is able to recover from the stimulus that

induced it, or until it's progressively amplified secretory profile attracts a leukocyte to clear it. Senescence can be induced by shortened telomeres from age or upregulated proliferation ("replicative senescence"); growth factors (e.g. IL-1β, PGE2), oncogenes, or stress-induced damage to intracellular components by toxins or oxidative stressors ("premature senescence" or "stress-induced senescence"); and terminal differentiation within inappropriate microenvironments ("developmental senescence"). While developmental senescence earned its name from the controlled senescence and clearance of excess cell types during development, it is also implicated as a mechanism of senescence for cells in wound resolution in response to TGFβ. In chronically inflamed wounds, replicative senescence may be triggered if continual turnover of proliferative cells causes them to prematurely reach their replicative limit. Likewise, premature stress-induced senescence may be induced by persistent exposure to oxidative stressors or pro-senescence growth factors [18,19,62–64,32–37,39,40].

One of the primary mechanisms of chronic lung injury and premature senescence is from sources such as cigarette and kitchen smoke, or activated leukocytes (i.e. respiratory burst activity). Excessive reactive oxygen species (ROS; $OH^-$, $HO_2$, $O_2^-$, $H_2O_2$, $ONOO^-$, etc.) are known to deactivate antiproteases, damage cells through oxidation of their DNA, proteins and lipids, and activate inflammatory transcription regulators NF-κB and ERK1/2 [3,6,60,65–67,14,18,19,32,33,36,38,39]. If levels of ROS surpass the ability of local antioxidants to buffer them, then this oxidative stress may either kill cells outright (i.e. cellular necrosis) – in which case they undergo uncontrolled autolysis, spill their contents into the extracellular space, and increase the amount of stressors exposed to neighboring cells – or trigger a

DNA damage response (DDR) that induces growth arrest to begin the cellular repair

process. If a DDR can't be repaired promptly however, the cell becomes senescent.
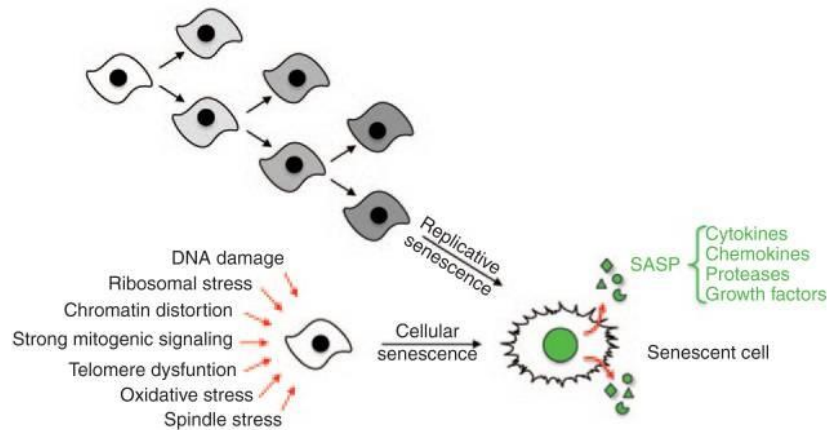


**Figure 1.5** – Induction of cellular senescence and the SASP. Reproduced with permission from [63], copyright American Society for Clinical Pharmacology and Therapeutics.

If a cell becomes senescent at any stage, it will increase its resistance to apoptosis,

slow its migration rate, spread out, flatten, and grow up to twice in size [19,33,35,64] –

suggesting an increase in applied traction forces [68,69] – and reorganize its chromatin into

heterochromatin, termed senescence-associated heterochromatic foci (SAHF), thus making

these changed irreversible [33–35,40,62,64]. Also, once growth arrest is initiated, senescent cells

begin developing the SASP by expressing IL-1α on their surface to bind adjacent surface-

bound receptors. This signaling occurs in autocrine and paracrine fashions to activate the

NF-κB and C/EBPβ transcription factors that mediate full expression of the SASP; this

includes IL-1α, proteases (i.e. MMPs), other cytokines (e.g. IL-6, IL-8) and growth factors

that targets the senescent cells for clearance by the innate immune system (e.g. neutrophils,

macrophages, NK-cells). Through this process senescent cells will upregulate their expression of β-Galactosidase (β-Gal), which serves as a useful, although not definitive, marker for senescent cells [15,18,38–40,62–64,19,20,32–37].

## Fibroblast Migration: Individual & Collective

Cellular migration is often represented as a biased random walk such as the Vischek or Ornstein-Uhlenbeck models [70–72]. Individual cells stochastically migrate up gradients of binding efficiency with the substrate – influenced by gradients of adhesion, topography, stiffness, chemokines and electrochemistry – which guide the intracellular polarization of actin polymerization and depolymerization [72–74]. In order to do so within two-dimensional environments, they search for new adhesions through the formation of transient, spatially-stochastic protrusions of filipodia and lamellipodia driven by actin polymerization against the opposing membrane tension through Cdc42-GTP and Rac1-GTP signaling, respectively; however, in three dimensions, cells will often form pseudopods or blebs for more efficient migration in that milieu [75–77]. Cells may bind to their substrate through transmembrane integrin receptors, or with other cells through cadherins, which form adhesive complexes with the actin cytoskeleton driven by ROCK/MLC mediated RhoA-GTP signaling. Myosin-II throughout the actin network, but concentrated near the rear of the nucleus, then generates tension upon these adhesions in the lamellipodium and ventral membrane which creates traction and causes the cell body to move forward; in a direction determined by the balance of adhered protrusions, weighted by their adhesion strength and stabilized by microtubules. These actomyosin forces also pull the membrane in from the

back and sides of the cell simultaneously through connections with the cortical actin

network – which induces actin depolymerization and adhesion complex disassembly at the

rear of the cell while generating hydrodynamic flow of the cytosol up to the front of the

cell – to recycle the actin monomers, bundles of myosin-II and associated adhesion

complex proteins needed for continued migration [78–82].
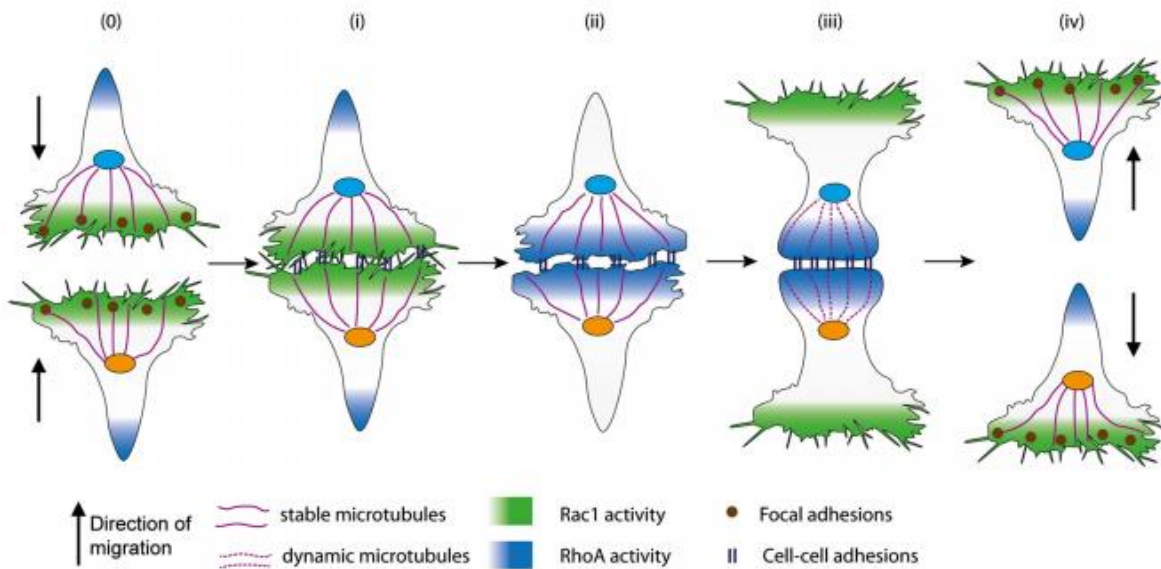


**Figure 1.6 –** Contact inhibition of locomotion among fibroblasts. Reproduced with permission from [83], copyright the authors.

The ratio of these cytoskeletal and force-generating protein within each cell determine

the rate of migration, directional persistence, and shape of each cell; those which migrate

faster and with more directional persistence take on a large wide canoe shape with smooth

edges (e.g. keratocytes), while slower wandering cells take on a narrow 'D' shape with

unstable edges (e.g. amoebae). Interestingly, cells which take on a canoe shape and migrate

faster with more directional persistence have a higher actin network density – indicating

we may be able to increase cell migration by upregulating cytoskeletal actin or increasing actin polymerization with an increase in temperature [84–86].

As a group, fibroblasts fall on the slower, less coordinated side of the spectrum of migration types described. They're commonly represented as spindle-shaped, however this shape is unstable as they lack persistent polarization and exhibit actin fibres oriented at unexpected angles with respect to the direction of motion [87–90]. In barrier removal assays they show little directional persistence, with an average 2 cell diameters between independent movements [91]. They're nematic cells which exhibit limited cadherin mediated cell-cell adhesion with contact-inhibited migration and proliferation; upon division, daughter fibroblasts disperse [83,87–90,92–95]. However, this contact inhibition is not complete – at confluence in vitro, cryptic lamellipodia extend below neighboring fibroblasts to migrate through monolayers at approximately a third the rate during pre-confluence [91,96,97] and will keep proliferating albeit at a lower rate [93,94]. Yet, if fibroblasts are not yet confluent and come into contact, they will form transient cell-cell connections which inhibit further migration and redirect their polarization and resultant migration away from each other (Figure 1.2), such that the mean velocity of a single cell is inversely proportional to the amount of cell-cell contacts [83,87–90,92,98,99]. This contact inhibition is reversible (i.e. confluent monolayers can recover prior migration and proliferation rates when passaged) and mediated by p27(Kip1) induction which also suppresses cellular senescence by deactivating mTOR; which also explains how cells maintain reversible quiescence within tissues or confluent monolayers [100,101].

As a result of this contact inhibition, jamming of fibroblast monolayers as cell densities increase have been modeled as liquid crystals [102], and barrier removal experiments have been performed *in vitro* to evaluate the release of contact inhibition on their migration [70,71,103]. Barrier removal experiments are preferred over scratch assays for the study of collective migration since the former method limits damage to cells, is more reproducible, and allows various monolayer geometries to be formed that allow for the evaluation of changes due to the orientation of individuals or level of orientation-order among the population. However, the cell damage produced by scratch assays is preferable to mimic wound healing despite the decreased reproducibility of these experiments. Thus, to model wound healing within the lung in vitro, we opted for a scratch closure assay.

**Agent Based Models**

To model our scratch closure assays *in silico*, we opted for an ABM to study how the dynamics of fibroblast activation and senescence affect their collective migration to evaluate changes due to treatments or exposures with computational efficiency. While comprehensive models taking a systems-biology approach to model fibroblast wound healing have also been formulated [104–106], these are computationally intensive. Many other types of stochastic active particle models are also well-suited for studying wound healing and collective cell migration, however these are all physics-based models that study how the dynamics of cell-substrate and cell-cell connections between particles generate phenomena such as actin polarity emergence [107], monolayer jamming [70,95,102], flocking [70,108], digitation features among epithelial sheets [71,109], angiogenesis [110], or collagen

deposition and contraction [111]. Fortunately, efforts to model inflammatory responses utilizing multiple cell states (e.g. damaged and healthy) and cell types (e.g. epithelial and immune) have exemplified the value of ABM techniques [112–116]. An ABM produced by Brown et al [113] even produced a model smoke particulate exposure on fibroblast maintenance of the ECM and macrophage-mediated inflammation that managed to approximate fibrotic features observed within mouse models of smoke exposure. However, this model was limited in its ability to account for the direct effects of smoke exposure on their myofibroblast activation or senescence.

In contrast with ordinary and partial differential equations that model pooled population dynamics in a top-down manner, ABMs represent a bottom-up approach that excel at modeling emergent collective behaviors due to interactions between individuals and their environment. Agents are mobile individuals interacting with an immobile lattice of patches according to a set of rules. Agents often represent cells while patches represent the substrate or sheet of epithelial cells. Models may incorporate multiple types of agent or patch with their own subset of rules, multiple layers in two dimensions, or three dimensions. To facilitate these models, several modeling platforms have been developed [114,115,117,118]. While slower than other platforms, NetLogo [119] is open-source, easy to use and has several built-in tools such as BehaviorSpace to assist with model analysis [114,115,118]. Some ABMs also include continuum mechanic modules to create a hybrid model [120].

Here, we model the collective migration dynamics of fibroblasts closing a scratched monolayer influenced by the differential stimulation of myofibroblast activation and senescence produced from a distribution of sensitivities to a constant environmental stimulus. This model is designed to evaluate differences between fibroblast populations to which the model is calibrated with *in vitro* data by representing their response as a set of parameters governing basal rates of migration, proliferation, senescence and myofibroblast differentiation.

**Project Objectives**

1. *In Vitro*: Quantify the *in vitro* scratch wound closure along with the percentage of cell death, cell senescence and myofibroblasts among human lung fibroblasts.
2. *In Silico*: Using NetLogo, develop an ABM of fibroblast wound healing to evaluate differences among parameter-sets calibrated to *in vitro* data from Objective 1.

# *In Vitro* Methods

**Cell Culture & Treatment Medias**

Normal Human Lung Fibroblasts (NHLF; CC-2512), and Diseased Human Lung Fibroblasts (DHLF; 195277) derived from COPD patients, were obtained from Lonza for all *in vitro* studies. NHLF and DHLF were only used for passages 5-9 and 2-3, respectively. Cells were expanded and cultured in Fibroblast Growth Media-2 (FGM; CC-3132, Lonza) that was refreshed every 2-3 days. When 80-90% confluent, cells were dissociated with 0.025% Trypsin/EDTA and passaged with a 1:7 split.

Cigarette Smoke Condensate (CSC) was obtained from Murty Pharmaceuticals (Lexington, KY) and diluted to a 0.125% (50 mg/ml) solution with Fibroblast Basal Medium (FBM; CC-3131, Lonza). According to the manufacturer, the CSC stock was prepared from smoking University of Kentucky's 3R4F Standard Research Cigarettes on an FTC Smoke Machine; total particulate matter on the filter was calculated from its weight gain, then DMSO was used to extract the condensate via soaking and sonication to produce an approximate 40 mg/ml solution. This stock was subsequently diluted in FBM and sterile-filtered (0.22 um pore size) to make the CSC treatments. DMSO diluted in FBM was used as a vehicle control.

**Metabolic Assays**

To assess the toxicity of CSC dilutions, evaluate the effect contribution of the dimethylsulfoxide (DMSO) vehicle and compare the metabolic effects of the treatment medias, cells were seeded into flat-bottomed 96-well plates (Corning) at a density of 62500 cells/cm$^2$ with 200 µl FGM. After 14 hours of growth, the seeding media was aspirated and replaced with 100 µl of the treatment medias. Following 0, 0.5, 2, 12, or 24 hours of treatment, media was replaced with 100 µl FBM plus 10 µl of either MTT (#11465007001, Sigma) or CCK-8 (Dojindo) reagent.

For MTT assays, cells were incubated with the MTT reagent for 4 hours, then 100 µl of the MTT Solubilization Solution was added and further incubated overnight to solubilize the MTT formazan reduction product. The optical density (OD) of formazan was then measured at 570 nm using a BioTek Epoch Spectrophotometer; background absorbance was also measured at 650 nm, and the difference between these optical densities (i.e. $OD_{570} - OD_{650}$) was calculated to represent the amount of MTT formazan resulting from reductive metabolic processes.

For CCK-8 assays, cells were incubated with the WST-8 reagent for 4 hours, then the media was aspirated and replaced with 100 µl DMSO to solubilize the WST-8 formazan reduction product over 10-15 minutes at room temperature. The optical density of WST-8 formazan was then measured at 450 nm; background absorbance was also measured at 600 nm, and the difference between these (i.e. $OD_{450} - OD_{600}$) was calculated to represent the concentration of WST-8 formazan resulting from reductive metabolic processes.

**Scratch Wound Healing Assays**

Wound healing was evaluated by proxy through the *in vitro* assessment of collective fibroblast migration within scratched monolayers. Cells were seeded with 2 ml of FGM at a density of 42100 cells/cm$^2$ (~400,000 cells/well) into clear tissue culture treated 6-well plates (Corning), after horizontal marks were drawn through the center of each well along the underside of the plate. After incubation for 14 hours, each cell monolayer was scratched vertically with a 20 μm pipette tip, rinsed with 30 mM HEPES Buffered Saline, and then covered with 2 ml of the treatment media. Each monolayer was imaged immediately after the scratch and at each time-point (i.e. a series of {0, 4, 8, 12, 24} or {0, 12, 16, 20, 24} hours) in two locations, one above the horizontal mark and the other below, on an Olympus IX71 Microscope under phase contrast with QCapture Pro 6.0 software. The same locations were imaged across successive time-points through the use of a reference point (i.e. a trivial portion of the horizontal mark visible through the bottom of the plate); however if this default reference was not usable (e.g. the scratch retracted near the mark in the center of the well, but not elsewhere), then filenames were notated and alternate features (e.g. whorl patterns distant from the scratch, scratches in the plastic, etc.) were utilized as substitute references. The denuded area was measured in triplicate using the freehand selections tool within ImageJ [121,122], and subsequently expressed as the percentage of scratch closure ($\%Healing = (Area_{initial} - Area_{current}) / Area_{initial})$). Measurements from technical repeats (i.e. triplicate measurements of duplicate images of triplicate wells) within each experimental group were averaged together to form a single biological repeat for statistical comparisons.

**Cytometric Stain Assays**

For all staining experiments, cells were seeded with 2 ml of FGM at a density of

42100 cells/cm$^2$ (~80,000 cells/well) into clear tissue culture treated 24-well plates

(Corning), then fixed and/or stained after 6, 14, 26, or 38 hours of incubation after seeding.

To evaluate population changes within the context of our scratch assay model, each cell

monolayer was scratched with a 20 µl pipette tip, rinsed with 30 mM HEPES Buffered

Saline, and then covered with 400 µl of the treatment media after 14 hours of growth. To

capture population changes caused by the scratch and wash step, separate experiments

were collected at 14 hours either with or without scratched monolayers. After staining, all

plates were viewed and imaged on an Olympus IX71 Microscope equipped with QCapture

Pro 6.0 software. Each well was imaged in three locations – with two centered on the

scratch, if present, and one distant from it – and each location was imaged using two

channels in order to determine the relative size of the targeted subpopulation of cells (i.e.

dead, senescent or myofibroblast) among the whole population in each image. The total

cell populations determined from each type of staining assay were pooled for each

experimental group to determine total population changes with time.

**Viability Stain**

Cell death was evaluated using a fluorescent viability staining kit (L3224, Invitrogen). Briefly, media was aspirated, 200 µl of the staining solution containing 2 µM calcein AM (live; FITC, ~450-500 nm) and 4 µM EthD-1 (dead; TRITC, ~500-550 nm) was applied and incubated at room temperature for 30 minutes. Cells were then imaged using a QImaging EXi Blue fluorescence microscopy camera with FITC and TRITC channels. The total cell population was calculated as the sum of all live and dead cells, thus the percentage of dead cells was calculated as $= 100 * (N_{dead} / (N_{live} + N_{dead}))$.

**Senescence Associated Beta-Galactosidase (SA-β-Gal) Stain**

To determine the proportion of senescent cells within the fibroblast monolayers, cells were first stained with the SA-β-Gal staining kit (#9860, Cell Signaling Technologies) according to the manufacturer's protocol, then rinsed twice with PBS and counterstained and cured overnight at room temperature using ProLong® Gold Antifade Mountant with DAPI (P36931, ThermoFisher). Cells were then imaged using a QImaging MicroPublisher 3.3 RTV camera with channels for brightfield illumination and DAPI (~330-380 nm). The number of blue-stained cells under brightfield illumination were considered positive for senescence (if selected by ImageJ thresholds) and the number of DAPI-stained particles (i.e. nuclei) was used to represent the total cell population, thus the percentage of dead cells was calculated as $= 100 * (N_{SA.\beta.Gal}/N_{DAPI})$.

**Alpha-Smooth Muscle Actin (αSMA) Immunocytochemistry Stain**

To determine the proportion of myofibroblasts within the fibroblast monolayers, cells were first washed twice with PBS, fixed with 200 µl of 4% paraformaldehyde for 20min at room temp, then washed twice again with PBS. Cells were permeabilized with 0.1% v/v Triton-X100/PBS for 10 minutes, washed four times with 0.1% Tween-20/PBS (PBST) for 5min each, then blocked with 200 µl of 5% Bovine Serum Albumin/PBST (BSA/PBST) for 1 hour at room temperature. Blocked cells were incubated with 200 µl of a 1:400 dilution of anti-αSMA monoclonal mouse antibodies (#A2547, Sigma) within BSA/PBST overnight at 4°C. Primary antibody-tagged cells were washed thrice with PBS for 5min each then incubated with 200 µl of a 1:2000 dilution of anti-mouse IgG (H+L) polyclonal goat antibodies conjugated with Alexa Flour 488 fluorophores (#A-11001, ThermoFisher) for 2 hours in the dark at room temperature. Secondary antibody-stained cells were rinsed thrice with PBS for 5 minutes each, counterstained and cured overnight with ProLong® Gold Antifade Mountant with DAPI (P36931, ThermoFisher), then imaged using a QImaging EXi Blue fluorescence microscopy camera with FITC and DAPI channels. All DAPI-stained particles that colocalized within stained regions of αSMA fibers determined with the ImageJ plugin JACoP [123] were considered positively-tagged myofibroblasts, while the total number of DAPI-stained particles was used to represent the total cell population, thus the percentage of myofibroblasts was calculated as

$$= 100 * (N_{colocal(DAPI+aSMA)} / N_{DAPI}).$$

**Statistical Analyses**

Scratch assays were analyzed using two-way ANOVAs with repeated measures and Holm-Sidak post-hoc tests for multiple comparisons to evaluate differences among paired time-points between cell lines (i.e. NHLF vs DHLF) and treatment medias (i.e. FBM, FGM and 50 µg/ml CSC) across groups within time-points or within groups across time. Scratch assay analyses were performed for an overall view (i.e. 0, 12 and 24 hours).

MTT and CCK-8 assays were analyzed using two-way ANOVAs with Holm-Sidak post-hoc tests for multiple comparisons to evaluate differences between treatment medias (i.e. FBM, FGM, and titrations of CSC or DMSO) and unpaired time-points.

Staining assays (i.e. SA-β-Gal, Viability, and αSMA) were also analyzed using two-way ANOVAs with Holm-Sidak post-hoc tests for multiple comparisons to evaluate differences between treatment medias (i.e. FBM, FGM and 0.125% CSC) and unpaired time-points.

All data were collected and pre-processed within Excel; all statistics were performed within GraphPad Prism 6 software. Differences with p-values $< 0.05$ were considered significant. Unless otherwise noted, all experiments were performed with a minimum of $N = 3$ biological repeats in triplicate.

## *In Silico* **Methods**

Fundamentally, this agent based model is designed to simulate fibroblasts within the context of an *in vitro* scratch wound healing assay in order to characterize their time-dependent response in terms of the population's proportions of inactive, active, myofibroblast and senescent states along with their mean rates of migration, proliferation and death. The model operates on NetLogo version 5.3.1. The *in vitro* environment is represented by a two dimensional lattice network of square patch units, fibroblasts are represented by mobile agents, and the model rules are applied each tick to represent their activity in 20 minute steps. Agents interact with other nearby agents and the Moore's neighborhood of patches below them, consisting of the central patch beneath the agent's center and the eight surrounding patches, through a series of rules and procedures designed to model the scratch closure behavior of fibroblasts *in vitro*. Simulations to find calibrated parameter-sets for the *in vitro* datasets and analyze parameter sensitivities were performed using the BehaviorSpace tool with 10 simulation runs per parameter-set evaluated.

**Model Setup**

The model world consists of 101x101 patch units representing the 2.8123 mm$^2$ area evaluated in the *in vitro* scratch assays. Each patch (*XY*) has a unit length equivalent to 16.6040 μm. This lattice has a periodic boundary, so a fibroblast agent moving beyond one

edge is reintroduced at the opposite edge. While they are displayed with various shapes, each of the *N* fibroblast agents is modeled as a circle and assigned attributes associated with one of the following states that a fibroblast may exhibit *in vitro*: 1) Inactivated Fibroblasts (*IFibs*) represent immobile, inactive fibroblasts that have not yet been activated by the tissue culture plastic beneath them; 2) Activated Fibroblasts (*AFibs*) represent mobile, αSMA-negative fibroblasts (i.e. proto-myofibroblasts); 3) Myofibroblasts (*MFibs*) represent mobile, αSMA-expressing fibroblasts; 4) Senescent Fibroblasts (*SFibs*) represent non-proliferating, apoptosis-resistant fibroblasts that have lost their contact inhibition; and dead cells (*DFibs*) interact with nothing. Each of these agent states (*F*) has a defined size ($S_{(F)}$), migration rate ($M_{(F)}$), resistance to apoptosis ($R_{(F)}$), and proliferation rate ($D_{(F,N)}$). Each agent also has their own rate of senescence due to replication based on the Hayflick limit ($T_{SENESCE(F,N)}$), sensitivity to stimulatory signaling ($Z_{(N)}$), level of stimulation ($stim_{(N)}$), and set of stimulation-dependent transition probabilities governing changes between agent states. All fibroblasts are capable of dying or becoming senescent due to stimulation; however *IFibs* can also activate into *AFibs*, and *AFibs* can also deactivate back into *IFibs* or become *MFibs* through further activation signaling. The model parameters for mean migration rate ($M_0$) and mean division interval ($T_{DIVIDE}$) are attributed to active fibroblasts and used as baselines for the other states. More details on these attributes and other variables – including values, calculations and citations – are available in Appendix B.

**Initial Conditions & Agent Preconditioning**

Fibroblast agents are generated at random locations within the model world with the same percentages of senescent cells, myofibroblasts, and dead cells as were measured *in vitro* among NHLF in FGM incubated for 6 hours post-seeding, when cells first attached to and flattened out on the plate (data not shown). All remaining agents are generated as *AFibs* to model the *in vitro* activation response of fibroblasts attached to tissue culture plastic (TCP). As shown in the top row of Figure 3.1, the agents are capable of deactivating into *IFibs* within the model, however the stimulation threshold which controls this state transition is set at such a low level that *AFibs* do not deactivate beyond the first few steps to mimic fibroblasts becoming fully attached to and stimulated by the non-physiologic stiffness of the tissue culture plastic to which they're attached after 6-8 hours in culture. These initial agents are generated with a population (*Pop_t00*) equal to the seeding density used *in vitro* (*Pop_t00* = 400,000 cells/well = 416.67 cells/mm$^2$). The precondition procedure runs the model a number of steps equivalent to the *in vitro* time interval between the seeding and the scratching of wells during a scratch assay (*Time_seed-scratch* = 8 hours) using the parameter-set calibrated to *in vitro* data for NHLF treated with FGM (Table 4.1). This step is necessary to initialize their spatial distribution, stimulation levels *stim$_{(N)}$*, division counters *D$_{(F,N)}$*, and replicative senescence counters *T$_{SENESCE(F,N)}$*. At the end of the precondition step, parameter values are switched to the parameter-set associated with the scratch closure response, and the associated agent variables governing stimulation sensitivity (*Z$_{(N)}$*) and division interval (*D$_{(F,N)}$*) are averaged

together to represent an agent's memory of past exposures and prevent artifact shifts in the agent states.

**Scratch Implementation & Closure Measurement**

To model the scratch, all agents within the defined *Scratch Region* are removed to simulate a monolayer of fibroblasts being scratched *in vitro*. Dead agents are also removed regardless of their location to simulate the *in vitro* post-scratch wash step, adjusted such that 8.05% of the resulting agent population consists of *DFibs* to mimic the percentage of dead cells found *in vitro* 0 hours after the scratch. The *Scratch Region* extends vertically down the model world, centered on the y-axis, and its ratio of patches within the model world is equivalent to the *in vitro* ratio of scratched to non-scratched areas within a square-cropped image centered on the scratch. This is shown in the bottom row of Figure 3.1.

Every patch possesses two variables accounting for the relative coverage of neighboring patches by agents, termed "*Void Scores*," that are used to measure the current cell coverage of the *Scratch Region* (*Healed Region*) and model the *in vitro* contact inhibition of migrating and proliferating fibroblasts (i.e. Rules #1 & #2 detailed below; also illustrated in Figure 3.2). Each time step, each patch (*XY*) calculates the *Primary Void Score* ($V1_{(XY)}$) as the averaged count of patches within its Moore neighborhood, e.g. the bold-edged patches in Figure 3.2), not including itself, that are devoid of any live fibroblast agents. Then the model calculates a *Secondary Void Score* ($V2_{(XY)}$) as the average $V1_{(XY)}$ of the same neighboring patches. Any patch within the *Scratch Region* with a $V1_{(XY)}$ or $V2_{(XY)}$ less than 0.5 is considered to contain a fibroblast and is included as part of the *Healed*

*Region* (e.g. the green-filled patches in Figure 3.2).The percentage of the scratch region

which is also part of the healed region (*%Healed*) is used as an output parameter for

comparison to percentage healed data from *in vitro* scratch assays.

| **T = seed** | **T = seed + 1** | **T = pre-scratch** |
|---|---|---|
| **T = scratch + 0** | **T = scratch + 12** | **T = scratch + 24** |
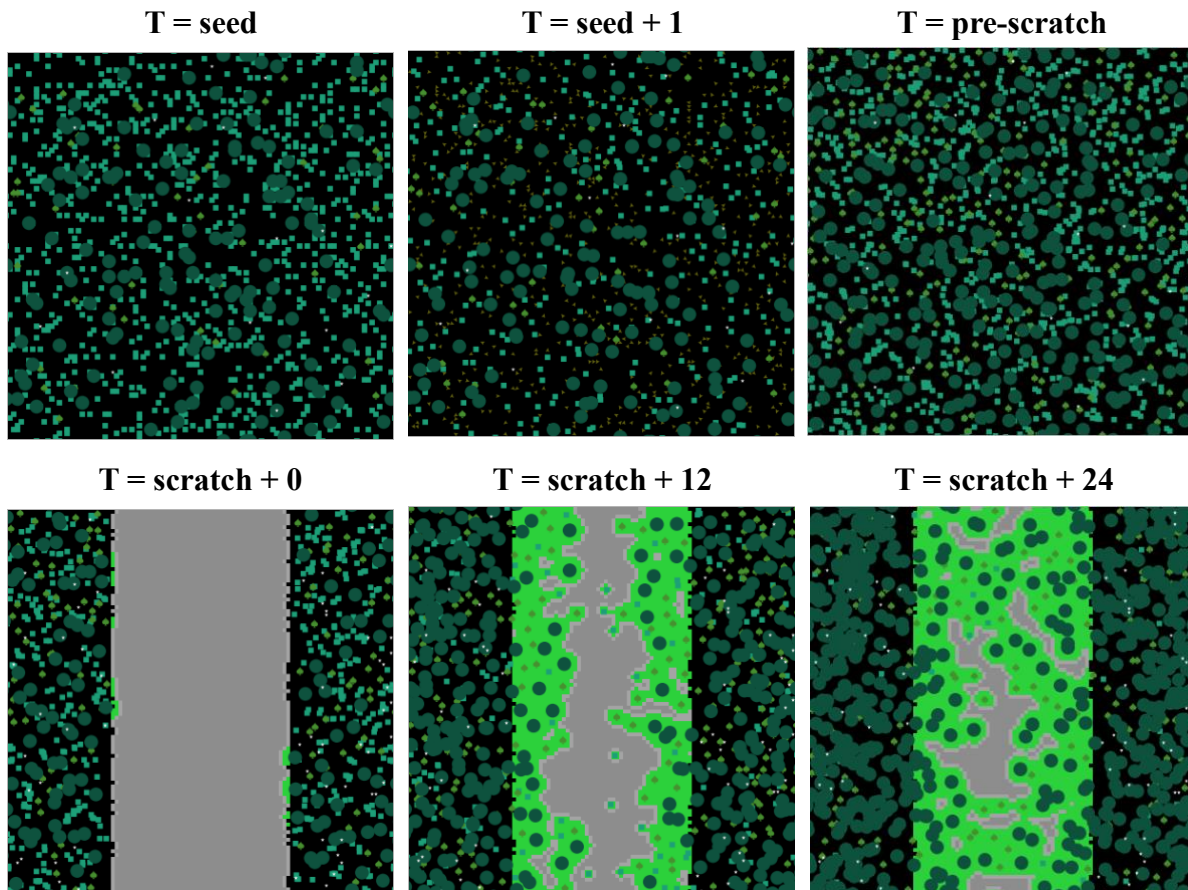


**Figure 3.1** – Representative simulation of fibroblast agents closing a scratch. Time-points are shown during the pre-scratch and post-scratch intervals when agents are initially seeded (top left), one step after seeding (top middle), immediately prior to being scratched after 8 hours of growth (top right), and after being scratched for 0, 12 or 24 simulated hours (bottom row). *Unscratched* patches are colored black, *Scratched* patches are grey, *Healed* patches are lime green, and *Unhealed Edge* patches are light grey. *IFibs* are displayed as yellow triangles, *AFibs* as teal squares, *MFibs* as green clovers, and *SFibs* as dark green circles. All agents are modeled to scale as circles but not displayed as such.

The length of the border between the *Healed Region* and the rest of the *Scratch Region*, relative to its length when the scratch was created (*Relative Unhealed Edge Length*), is used to quantify the amount of disorder in the fibroblasts' invasion of the scratch region. The relative unhealed edge length is also used as an output parameter for comparison to relative scratch edge length data from *in vitro* scratch assays; however this was not used to calibrate parameter-sets of the model.
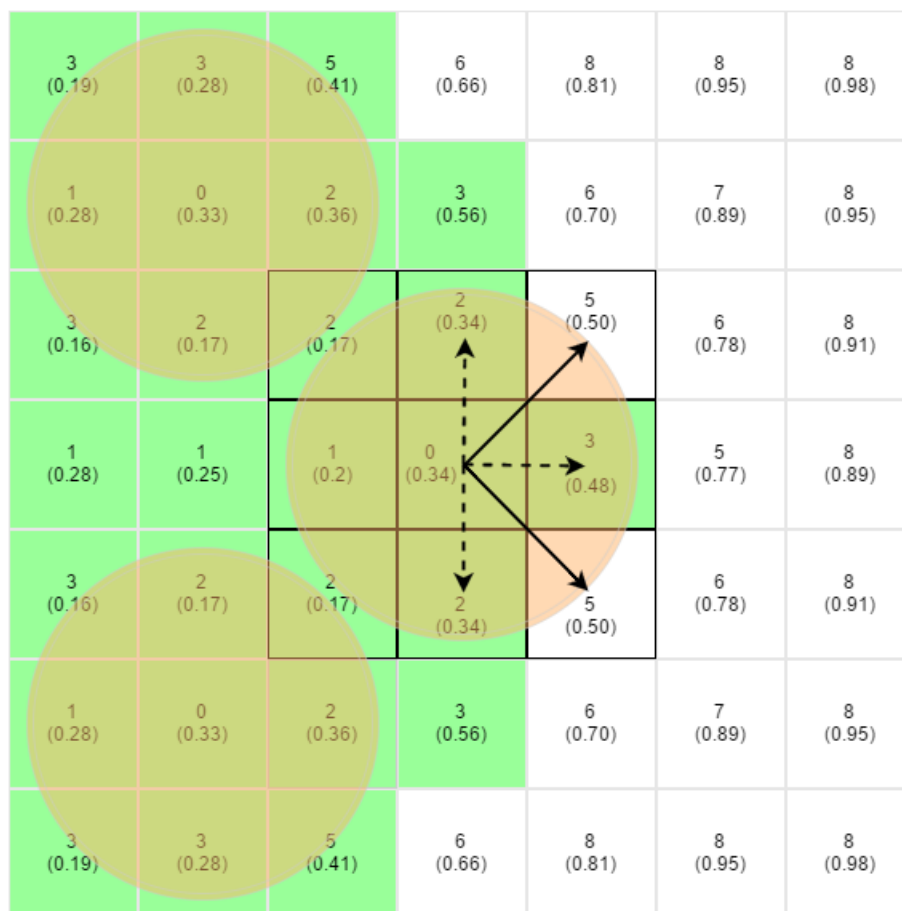


**Figure 3.2** – Patch diagram displaying how *Void Scores* are calculated and used. This method measures the *Healed Region* and guides the navigation of circular fibroblast agents as described in Rule #1. The bold-outlined patches represent the Moore's neighborhood for the fibroblast agent in the center; the whole number within each patch is the patch's $V1_{(XY)}$ score while the value in parenthesis is its $V2_{(XY)}$ score.

**Model Rules**

The dynamics of fibroblast migration, proliferation, senescence, myofibroblast activation and death within the model presented are controlled by the following rules. These are implemented each time step to generate scratch closure as seen in Figure 3.1.

**Rule #1a:** A non-senescent fibroblast having any neighboring patches with a $V2_{(XY)}$ above 0.5 will migrate $M_{(F)}$ distance towards the neighboring patch with the greatest $V2_{(XY)}$ with a standard deviation of 15°.

This mechanism of agent navigation is intended to mimic the migratory contact inhibition exhibited by non-senescent fibroblasts *in vitro,* whereby those which come into contact tend to migrate away from each other [87–90]. In contrast, senescent fibroblasts have been reported to lose this contact inhibition [63,124]. Directional migration is reported to be dependent upon phosphorylation of calveolin-1 to inhibit Rho signaling and increase activity of Rac1 and Cdc42 to reorient the actomyosin machinery polarization [125]. Additionally, caveolin-1 is required for α5β1-integrin endocytosis crucial for migration [126]. Since senescent cells exhibit upregulated caveolin-1 along with high activation of Rac1 and Cdc42 [127–129], that's reversible along with the senescent phenotype when Caveolin-1 status is decreased [129], we model senescent cell migration with a random walk.

**Rule #1b:** A senescent fibroblast migrates $M_{(S)}$ distance in a random direction, regardless of its patch neighbors' *Void Scores*.

**Rule #2a:** A non-senescent fibroblast may divide after growing for $D_{(F,N)}$ hours, if and only if a patch in the Moore neighborhood of the patch beneath it has a $V2_{(XY)}$ score above 0.5. $D_{(F,N)}$ is randomly generated for each agent when it is introduced to the model world and each time it divides from a normal distribution with a mean of $T_{DIVIDE}$, adjusted for each agent state $F$ (see Figure 3.3), with a standard deviation of one third this value.

**Rule#2b:** Senescent cells do not divide. This is the definition of senescence [35,40,64,130,131].

Both daughter cells inherit the parent cell's $stim_{(N)}$ level to model the even splitting of cellular contents between daughter cells that conserves the parent cell's proportions of receptors to ligands. Daughter cells also maintain the parent cell's activity state and $T_{SENESCE}$ counter value (see Rule #3) to model the conservation of their parent cell's expression profile and division history (i.e. telomere length), respectively. One daughter cell remains on the patch below the parent cell, while the other moves into the patch with the greatest $V2_{(XY)}$ in its neighborhood. This method of cell division is intended to model the contact inhibition of proliferation among cells *in vitro* – whereby a population's rate of division decreases in proportion to increasing population density [93,94,100,132] and "new" cells are preferentially added within the plane of the monolayer, rather than atop or beneath the "parent" cells [103]. All agents have their $D_{(F,N)}$ value reassigned at the time of the scratch and averaged with its pre-scratch value to model a cell's memory of previous exposures within a two-hit exposure system.

**Rule #3:** A non-senescent fibroblast becomes senescent after $T_{SENESCE}$ time steps, where $T_{SENESCE}$ is stochastically assigned to agents during model initialization from a normal distribution with a mean of $40 * D_{(F)}$ and a standard deviation of $40 * T_{DIVIDE} / 3$. This counter models the replication induced senescence reported to occur in all cells after $50\pm10$ population doublings, known as the Hayflick limit [63,124]; however we limited agents to 40 divisions to account for presumably shorter telomeres among our cells, derived from an adult population, versus the embryological cells used by Hayflick.
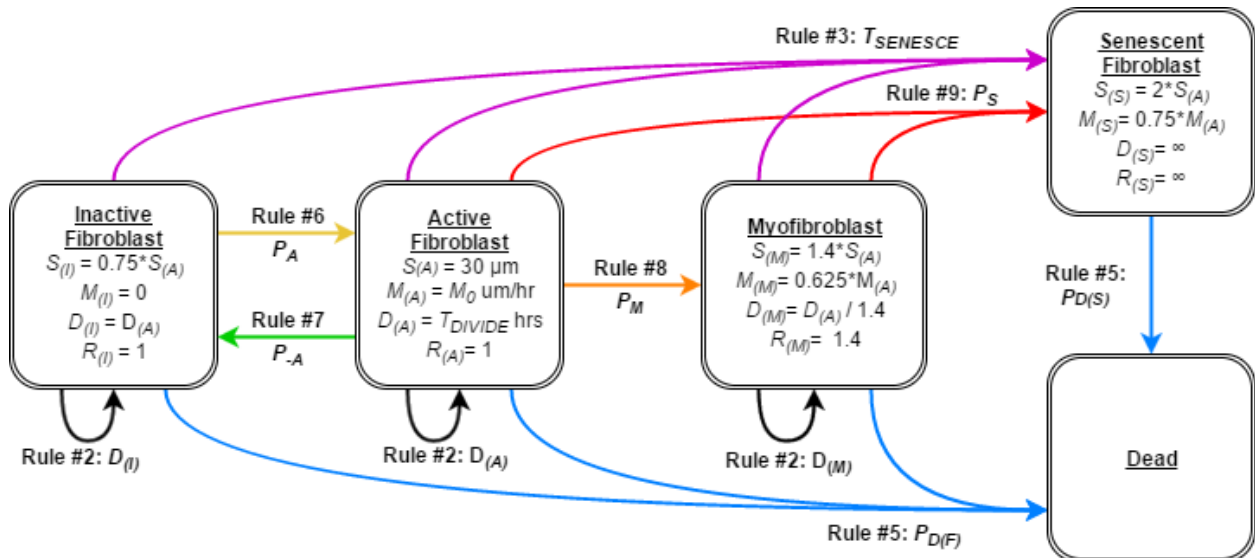


**Figure 3.3** – Flow diagram of fibroblast agent states, characteristics and associated rules. Each fibroblast phenotype (*F*) has characteristic values describing each state's size ($S_{(F)}$), migration rate ($M_{(F)}$), mean division interval ($D_{(F)}$), and death resistance ($R_{(F)}$). The corresponding rate or probability regarding proliferation (Rule #2; black), replicative senescence (Rule #3; purple), cell death (Rule #5; blue) and stimulation-induced state transitions (Rules #6-9; green-red gradient) are described in the text; color-legend regarding Rules #5-9 correlate with Figure 3.4.

**Rule #4:** Each time step, every agent increases their internal level of stimulation, $stim_{(N)}$, by the product of their sensitivity to stimulation ($Z_{(N)}$) and the magnitude of environmental stimuli ($\mu_{STIM}$). Agents are assigned a sensitivity to stimulation $Z_{(N)}$ from a normal distribution with a mean of 1 and standard deviation of $\sigma_{STIM}$, and this $Z_{(N)}$ value is preserved among daughter cells when a fibroblast divides. All agents have their $Z_{(N)}$ value reassigned at the time of the scratch and averaged with its pre-scratch value to model a cell's memory of previous exposures within a two-hit exposure system. The $stim_{(N)}$ level for each fibroblast represents the sum of activity among all intracellular signaling pathways that can induce activation, senescence, or apoptosis (e.g. NOX4, SMADs, p21, p16, p53, etc.). The $\mu_{STIM}$ parameter represents the magnitude of the sum of all stimuli within the *in vitro* environment that can induce fibroblast activation and senescence (e.g. substrate stiffness, CSC, ROS, FGFβ, TGFβ, PGE2); whereas the $\sigma_{STIM}$ parameter represents the variation in sensitivity to these stimuli among individual cells in a population to model a heterogeneous response to stimuli among the cell population and prevent all of the agents from transitioning simultaneously.
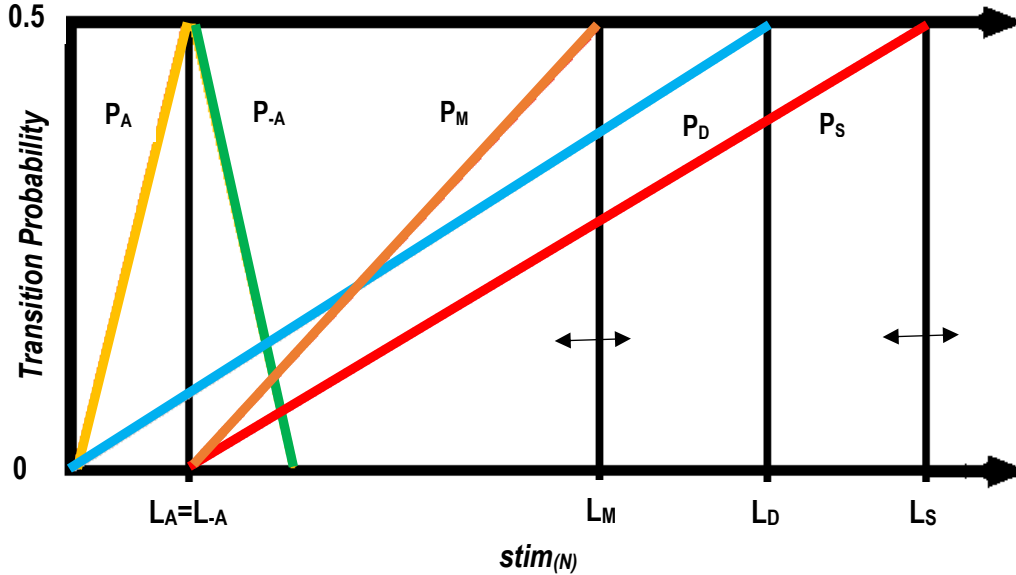
**Figure 3.4 –** Plot of the probabilities governing agent transitions between states. Each agent's transition probabilities (colored lines) depend upon their $stim_{(N)}$ and the population's transition thresholds (horizontal black bars); representing the mean values associated with a 50% probability for each state transition ($L_{(F)}$; black bars). Fibroblasts continually increase their $stim_{(N)}$ (Rule#4), which directly and linearly increase their probability for each state transition (Rules #5-9). Both $L_{(M)}$ and $L_{(S)}$ (bars with arrows) serve as parameters that directly control the transition probabilities and subpopulations of myofibroblasts and senescent cells, respectively. Color-codes for each transition probability are consistent with Figure 3.3.

**Rule #5:** Each time step, all living agents have a $P_{D(F,N)}$ probability of death due to stimuli, such that:

$$P_{D(F,N)} = \frac{stim_{(N)}}{2L_D R_{(F)}}$$

where $R_{(F)}$ represents the resistance to apoptosis for each fibroblast state or phenotype, $F$.

The damage level at which a fibroblast is 50% likely to die ($L_D$) is arbitrarily set to 1 $stim$ in order to give the stimulation parameters a reference value. The line associated with this probability is plotted in Figure 3.4 in yellow.

**Rule #6:** Each time step, all inactive agents have a $P_{A(N)}$ probability of activation, such that:

$$P_{A(N)} = \frac{stim_{(N)}}{2L_A}$$

**Rule #7:** Each time step, all active agents have a $P_{-A(N)}$ probability of deactivation, such that:

$$P_{-A(N)} = \frac{2L_A - stim_{(N)}}{2L_{-A}} = 1 - \frac{stim_{(N)}}{2L_A}$$

The stimulation limits for governing an agent's transition to an activated or inactivated state, $L_A$ or $L_{-A}$, respectively, are set equal to each other in order to allow an *AFib* the chance to transition back into an *IFib* if their $stim_{(N)}$ level is low enough. These shared stimulation limits for activation represent the average $stim_{(N)}$ level at which fibroblasts are 50% likely to be inactivated or activated. This functionality is designed to model fibroblasts' tendency to remain inactivated in the absence of stimuli along with their ability to deactivate once activated if their internal level of stimulation is resolved.

**Rule #8:** Each time step, all active agents have a $P_{M(N)}$ probability of becoming myofibroblasts, such that:

$$P_{M(N)} = \frac{stim_{(N)} - L_A}{2(L_M - L_A)}$$

where the model parameter $L_M$ is the *stim* limit representing the average $stim_{(N)}$ level at which an activated fibroblast is 50% likely to become an αSMA-expressing myofibroblast.

**Rule #9:** Each time step, all active agents have a $P_{S(N)}$ probability of becoming senescent due to stimuli, such that:

$$P_{S(N)} = \frac{stim_{(N)} - L_A}{2(L_S - L_A)}$$

where the model parameter $L_S$ is the *stim* limit representing the average $stim_{(N)}$ level at which an activated fibroblast or myofibroblast is 50% likely to become senescent.

The effect of these $L_F$ given in Rules #5-9 is such that a histogram of the fibroblast population's $stim_{(N)}$ levels superimposed upon Figure 4 produces a skewed bell curve of *stim* levels traveling to the right of this graph with respect to time, causing progressively more agents to become *AFibs*, then *MFibs*, *SFibs* or dead agents.

# Results

## Metabolic Response

To increase the physiological relevance of our model and facilitate the incorporation of an epithelial layer within future iterations, we wished to use a dosage of CSC which would allow us to view an effect in both lung fibroblast and epithelial cells without killing too many cells. Previous studies have tested the effects of CSC in both fibroblasts and epithelial cells with dosages ranging from below 1 µg/ml [133,134] to over 1 mg/ml [135]; however to our knowledge it had not been tested on NHLF or DHLF in vitro. To evaluate the effect of CSC on NHLF metabolism and screen for dosage to use with the rest of our experiments, we performed MTT assays and chose 50 µg/ml (0.125% v/v) CSC for all future experiments since this dosage produced the largest increase in cell metabolism without inducing cell death (data not shown). On a log scale, this dosage sits at the midpoint of dosages evaluated across both cell types in the literature and corresponds with values tested among both fibroblasts [15] and epithelial cells [136–138]. However, this was the lowest dosage used on lung fibroblasts in the literature [15,33,66,135,139]. This dosage was diluted within serum-free FBM and termed cigarette smoke media (CSM). To evaluate the effect of each of our treatment medias on NHLF metabolism and ensure that the effect of CSM was not due to its DMSO content, we performed a CCK8 assay (Figure 4.1). Overall, metabolic changes were modest; yet a statistically significant difference was found

between FGM and CSM at 24 hours. Given the absence of statistical differences between

CSM and either of its vehicle controls, we concluded CSM was not mimicking DMSO

exposure.
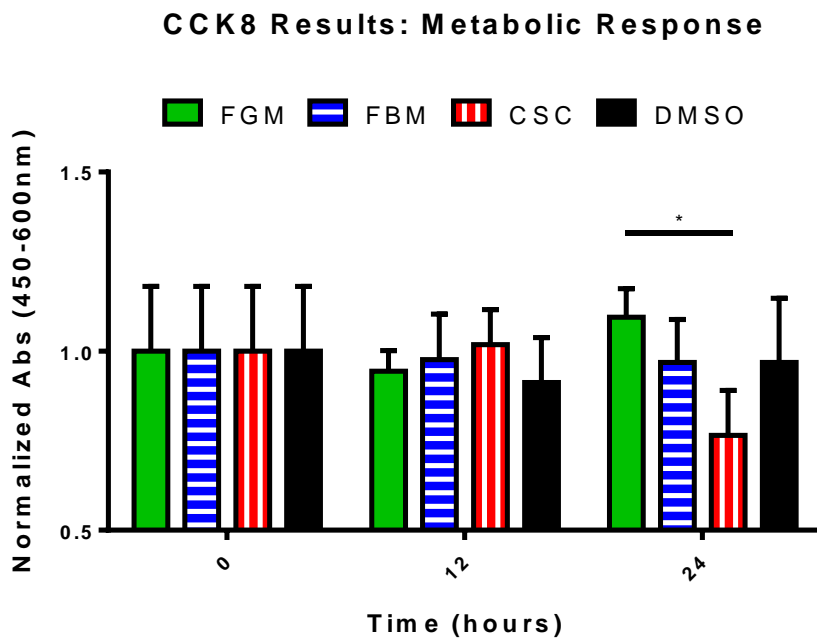


**Figure 4.1** – Metabolic responses of normal human lung fibroblasts exposed to either FGM, FBM, CSM or 0.125% DMSO over 24 hours. Data is shown as the mean ± SD of sextuplicate wells. Significant statistical differences are noted with * where p<0.05. Within-group comparisons with baseline (time = 0) are indicated above the error bar and between-group comparisons within each time-point are indicated with a horizontal line.

**Scratch Wound Closure**

To evaluate the wound healing response of lung fibroblasts *in vitro*, NHLF and

DHLF were grown to a confluent monolayer then scratched to mimic a tissue injury and

observed as the cells invaded and re-covered the denuded region over 24 hours (Figure

4.2). In general, fibroblasts made statistically significant progress after 12 hours in all

conditions except for DHLF treated with CSM. NHLF under all conditions also made

statistically significant progress between 12 and 24 hours post-scratch, however DHLF's

progress was less significant. NHLF treated with FGM often achieved 90% closure after

24 hours; however, at all time-points this rate of healing was significantly impaired when

fibroblasts were deprived of serum, exposed to CSM, and/or derived from COPD patients.

A significant difference was also found between FBM and CSM exposures after 24 hours

among NHLF, but not DHLF, indicating that DHLF could be resistant to 50 µg/ml CSC
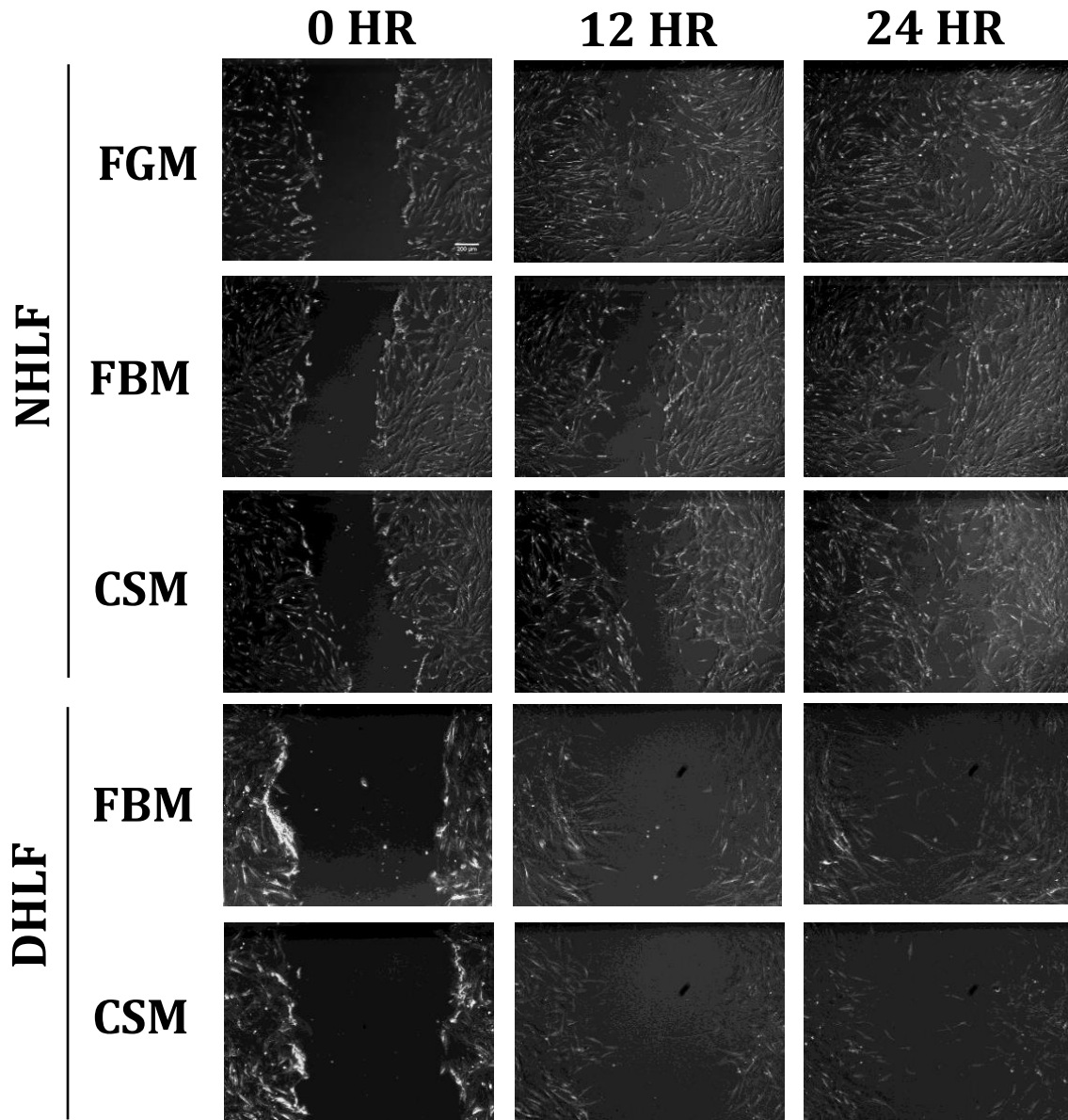
(Figure 4.3).

**Figure 4.2** – Phase contrast images of NHLF and DHLF closing a scratched monolayer over 24 hours while exposed to either FGM, FBM or CSM *in vitro*. Scale bar = 200 µm.
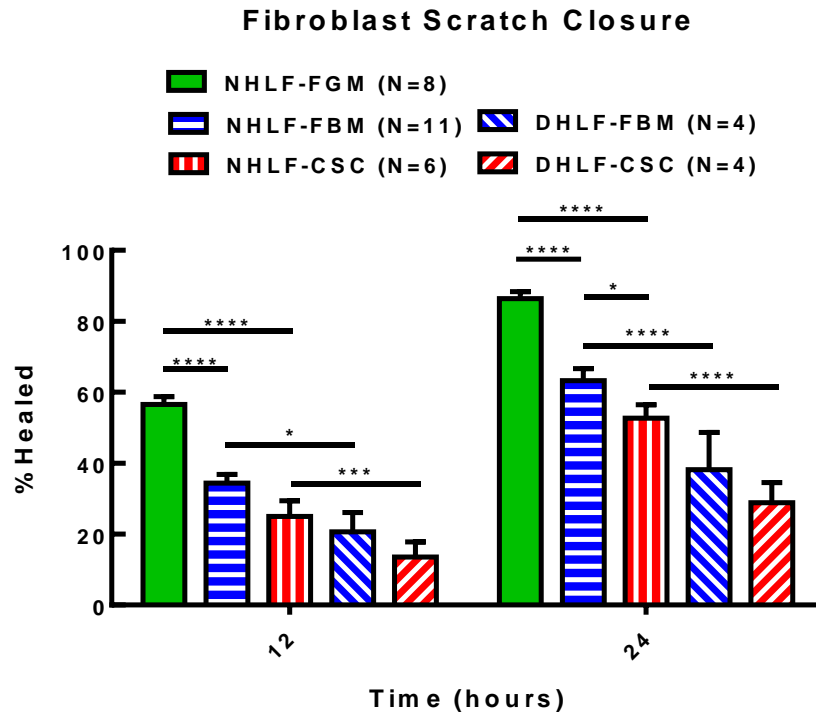
**Figure 4.3** – *In vitro* scratch closure data of NHLF or DHLF monolayers exposed to FGM, FBM or CSM over 24 hours. Data is expressed as the percentage of the initial scratched area re-covered by cells (%Healed); shown as the mean ± SEM of N ≥ 4 biological repeats. Significant statistical differences are noted with * where p<0.005, *** where p<0.005 and **** where p<0.0001. Between-group comparisons within each time-point are indicated with a horizontal line.

The calibrated parameter-sets were found to fit within two standard deviations of the *in vitro* mean scratch closure at every time-point measured, even though the model was not being evaluated with the 4 hour time-point (Figure 4.4). The parameter-sets also fit within one standard deviation of the mean at most time-points for most groups (data not shown); such was the case for NHLF treated with FBM or CSM at all time-points – as well as NHLF treated with FGM, or DHLF treated with FBM, at all time-points after 8 hours.
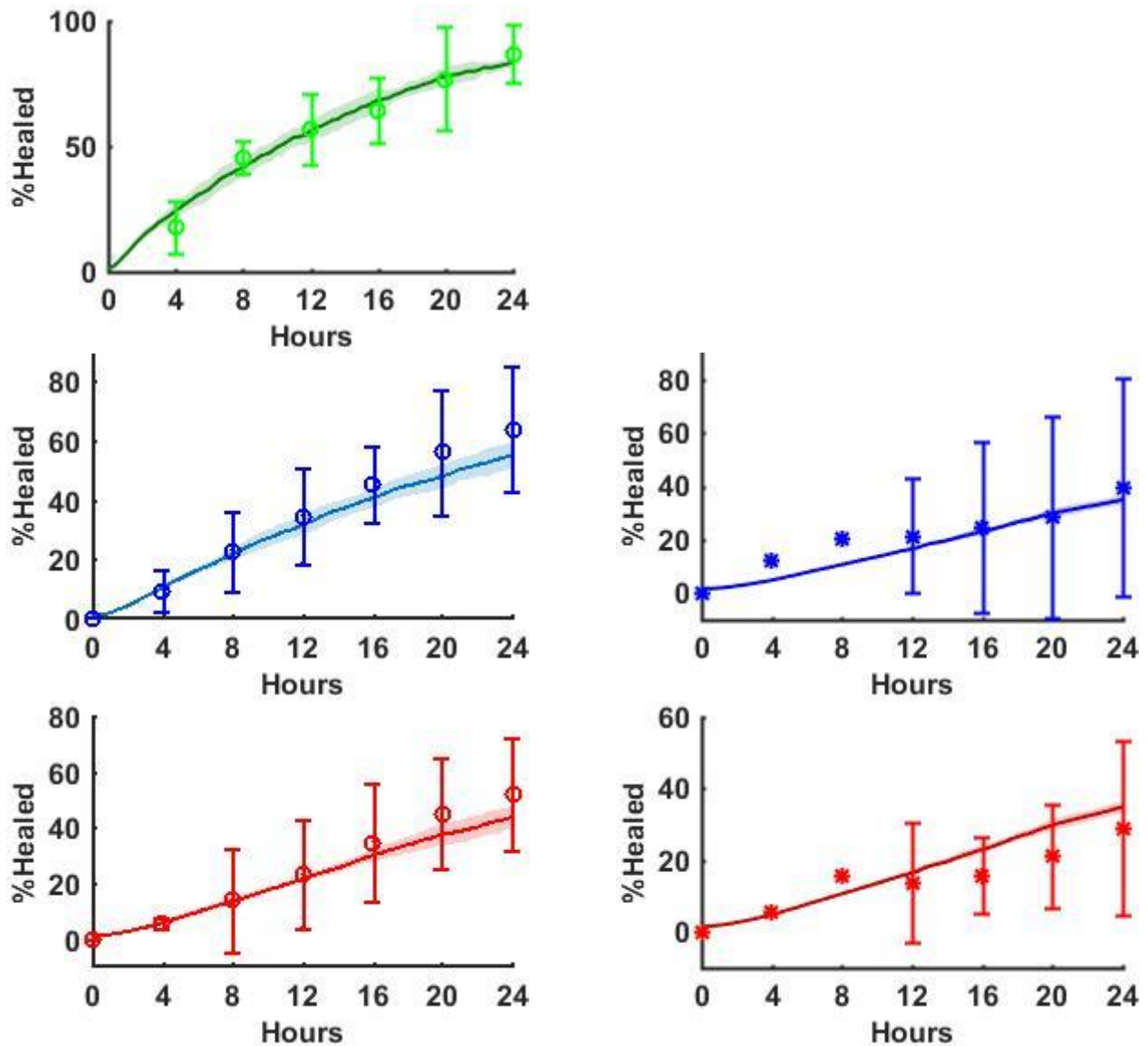
**Figure 4.4** – Simulated transients and *in vitro* scratch closure data of NHLF and DHLF. Shown are NHLF (circles, left column; N = 3-11) or DHLF (stars, right column; N = 1-4) responses to FGM (green), FBM (blue) or CSM (red) while closing a scratched monolayer over 24 hours; expressed as the percentage of the initial scratched area re-covered by cells (%Healed). *In vitro* data (markers with error bars) is shown as mean ± 2SD of N biological repeats. Simulated transients were calculated by taking the mean and standard deviation of 10 simulations using the same initial conditions and parameter-set calibrated for each cell type and media exposure (Table 4.1); means are plotted with a solid curve and standard deviations are depicted by a shaded region around the mean curves.

**Total Population**

To evaluate NHLF proliferation during a scratch assay with each treatment *in vitro* and generate a dataset representing cell population to fit against the model, the total cell population measured in each *in vitro* cell stain assay was pooled together after first being normalized. The average cell count data was first normalized by $(1677 \ \mu m)^2$ to account for differences in cell count between the different areas measured by the two cameras and the model area, then this was normalized to the baseline cell density at the start of either the pre-scratch or post-scratch interval to account for differences between the *in vitro* seeding densities for the scratch assays and stain assays.

Overall, changes in the cell density data were modest over the 24 hours post-scratch, with only NHLF treated with FGM showing a significant difference from baseline after 24 hours, at which point it was also significantly different from the other treatments (Figure 4.5). There was a large amount of error within this dataset that may have masked other differences being revealed, and this may have also undercut its use as a dataset to fit the model against. The calibrated parameter-set for NHLF treated with FGM was able to fit the *in vitro* data within one standard deviation of the mean in both the pre-scratch and post-scratch intervals until 24 hours post-scratch, which still fell within two standard deviations. The other calibrated parameter-sets fit within one standard deviation of their *in vitro* means (Figure 4.6).

**Pooled Stain Results:**
**Cell Density per $(1677\ um)^2$**
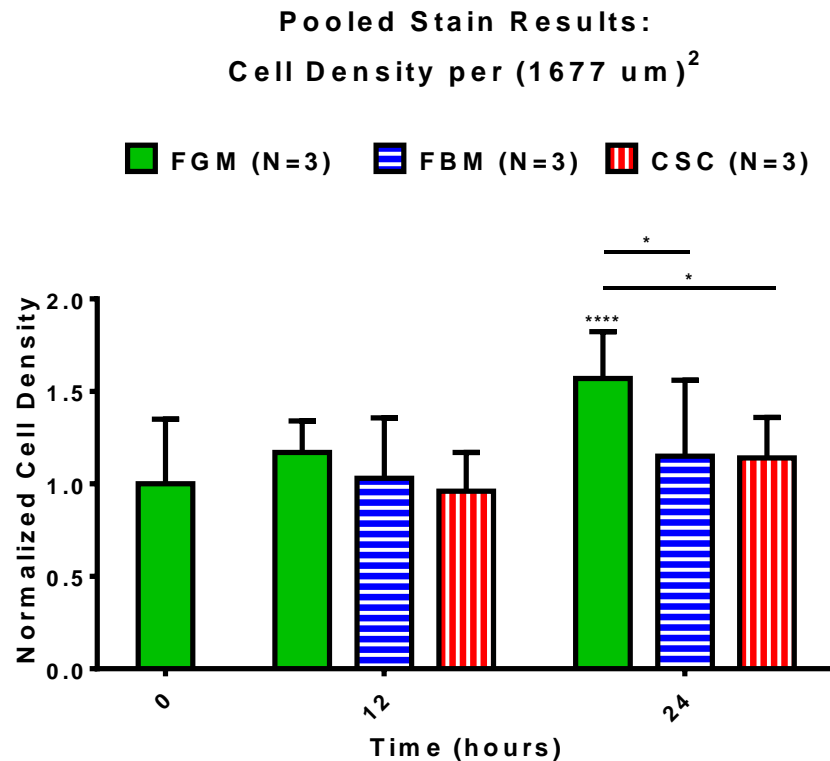
**Figure 4.5** – *In vitro* cell density among NHLF exposed to FGM, FBM or CSM while closing a scratched monolayer over 24 hours. Data is expressed as the number of cells per $(1677\ \mu m)^2$; shown as the mean $\pm$ SD of three independent assays normalized to baseline. Significant statistical differences are noted with * where $p<0.05$ and **** where $p<0.001$. Within-group comparisons with baseline (time = 0) are indicated above the error bar and between-group comparisons within each time-point are indicated with a horizontal line.

### Cell Death & Viable Subpopulation

To determine the percentage of cell death among NHLF during a scratch assay with each treatment *in vitro* and generate datasets to fit the model against, cell monolayers were scratched and subsequently stained with fluorescent dyes to mark live and dead cells (Figure 4.7). Surprisingly, the ratio of dead cells significantly decreased from baseline after only 12 hours post-scratch in all conditions, at which point the percentage of cell death was below 5% of the population and showed no differences between treatments (Figure 4.8).
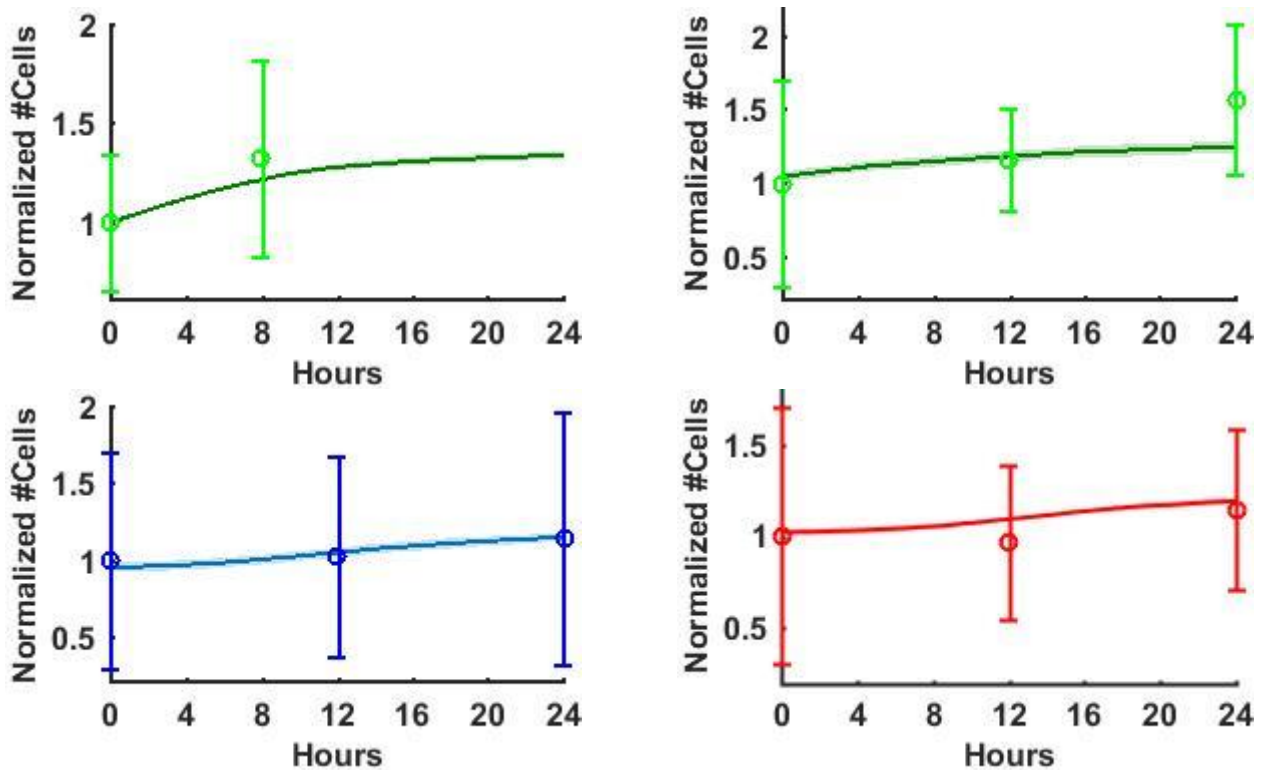
**Figure 4.6** – Simulated transients and *in vitro* cell density data among NHLF. Shown are responses to FGM (green), FBM (blue) or CSM (red) during the 8 hour pre-scratch interval (top left plot) or while closing a scratched monolayer over 24 hours (top right and bottom plots); expressed as the number of cells per $(1677 \ \mu m)^2$. *In vitro* data (markers with error bars) is normalized to baseline and shown as the mean $\pm$ 2SD of 3 independent experiments. Simulated transients were calculated by taking the mean and standard deviation of 10 simulations using the same initial conditions and parameter-set calibrated for each cell type and media exposure (Table 4.1); means are plotted with a solid curve and standard deviations are depicted by a shaded region around the mean curves.

Due to the negligibly low percentage of cell death, inability of the model to fit this viability data along with the proliferation data (not shown), and lack of a direct method to reduce the percentage of dead cells, this data was excluded as a calibration-set for the model.
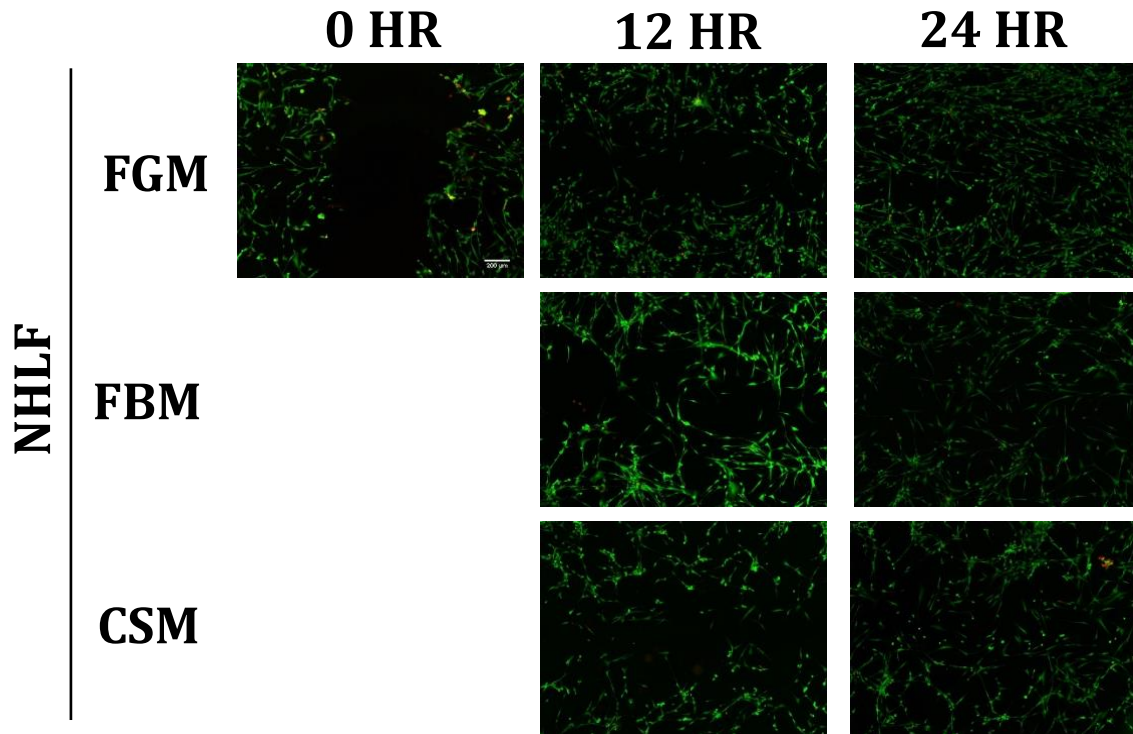
**Figure 4.7** – Fluorescent stain of live (green) and dead (red) NHLF exposed to FGM, FBM or CSM while closing a scratched monolayer over 24 hours *in vitro*. Scale bar = 200 µm.

**Senescent Subpopulation**

To determine the percentage of cell senescence among NHLF during a scratch assay with each treatment *in vitro* and generate datasets to fit the model against, cell monolayers were scratched and subsequently stained with chromogenic SA-β-Gal and fluorescent DAPI to mark senescent cells among all the cell nuclei (Figure 4.9). As expected, the ratio of senescent cells increased over the first 12 hours post-scratch; however we were surprised to find the percentage returned to baseline levels over the following 12 hours. After 12 hours, the percentage of senescence was significantly increased over 2.5 among NHLF treated with FGM and nearly 2-fold with FBM treatment,

but showed no change with respect to baseline when treated with CSM. However,

treatment with CSM did show more error in the data, potentially indicating a masked effect

that may be uncovered with repeated experiments. This was reflected in the statistically

significant differences found between FGM and both other treatments at 12 hours post-

scratch when no difference was found between FBM and CSM treatments (Figure 4.10).
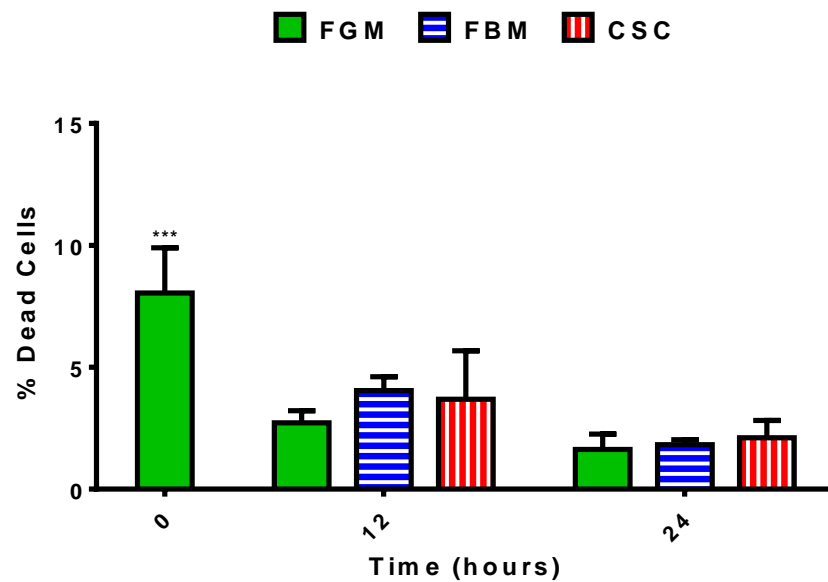


**Figure 4.8** – *In vitro* percentage of dead cells among NHLF exposed to either FGM, FBM or CSM while closing a scratched monolayer over 24 hours. Data is expressed as the percentage of dead cells among all living and dead cells; shown as the mean ± SD of quadruplicate wells. Significant statistical differences with all other groups are noted above the error bar with *** where p<0.0005.
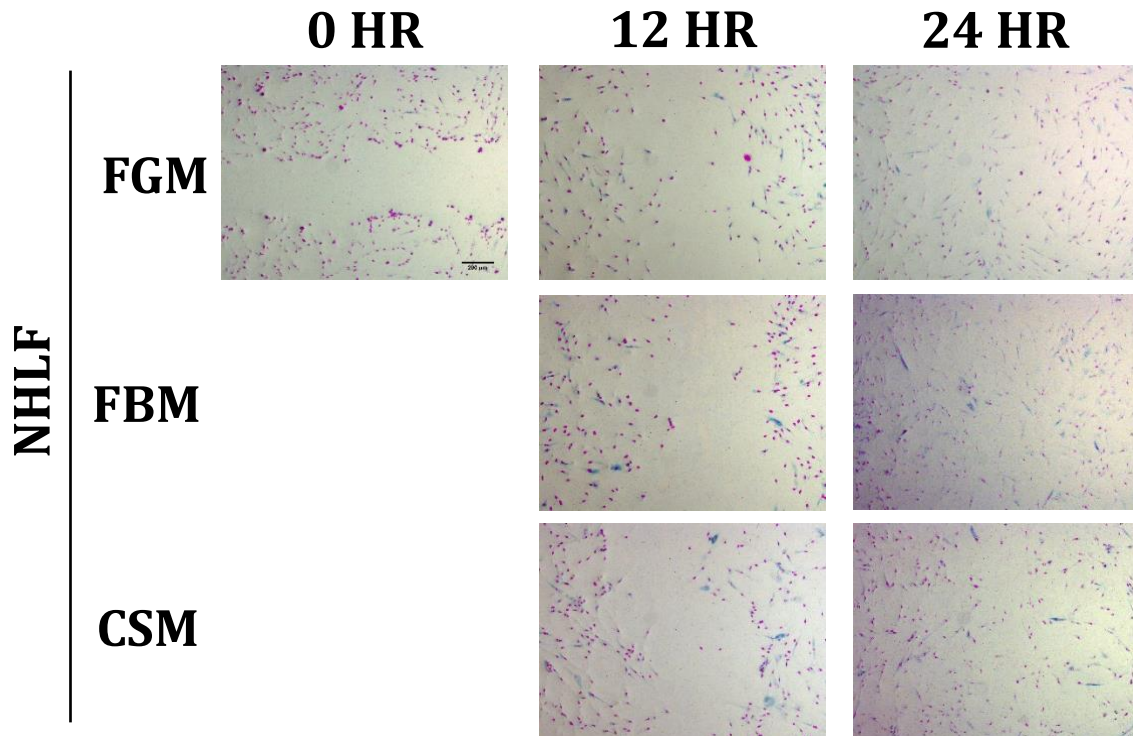
**Figure 4.9** – Superimposed channels of chromogenic SA-β-Gal (cyan) and fluorescent DAPI (magenta) stained NHLF exposed to FGM, FBM or CSM while closing a scratched monolayer over 24 hours *in vitro*. Scale bar = 200 µm.

Due to the lack of evidence in the literature supporting reversible senescence and the inability of the model to decrease the level of senescence outside of cell death (shown above to be negligible), the 24 hour time-point was excluded from the dataset used to calibrate the model. The calibrated parameter-set for NHLF treated with FGM was able to fit the *in vitro* data within one standard deviation of the mean except for the 8 hour time-point in the pre-scratch interval, which still fell within two standard deviations. The calibrated parameter-sets for NHLF fit within one standard deviation of the *in vitro* means for CSM treatment, but only fit within two standard deviations for FBM treatment, in part due to the relatively large error within the *in vitro* data for CSM treatment (Figure 4.11).
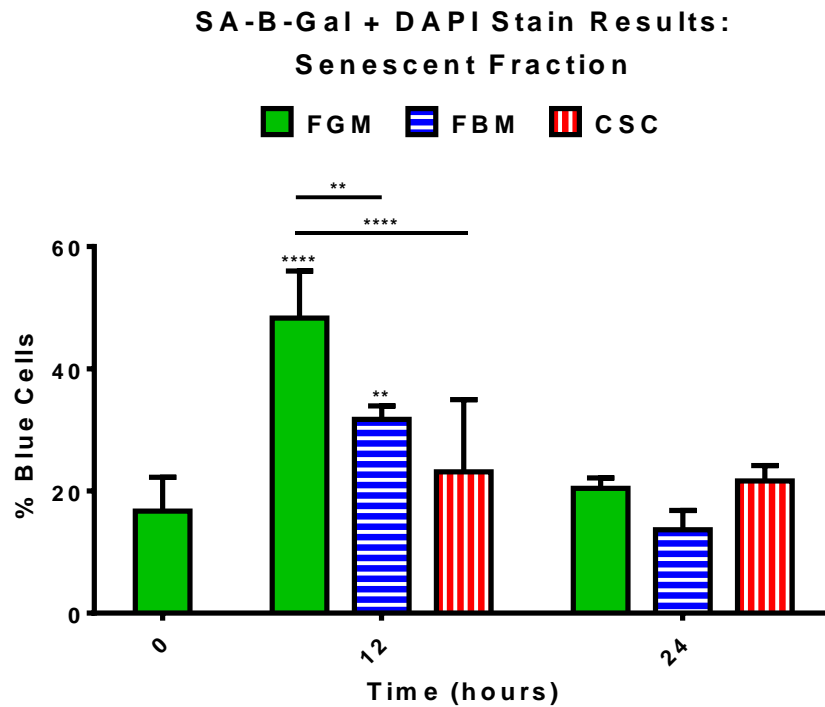
**Figure 4.10** – *In vitro* percentage of senescent cells among NHLF exposed to either FGM, FBM or CSM while closing a scratched monolayer over 24 hours. Data is expressed as the percentage of SA-β-Gal stained cytoplasms among DAPI stained nuclei; shown as the mean ± SD of quadruplicate wells. Significant statistical differences are noted with ** where $p<0.01$ and **** where $p<0.001$. Within-group comparisons with baseline (time = 0) are indicated above the error bar and between-group comparisons within each time-point are indicated with a horizontal line.

**Myofibroblast Subpopulation**

To determine the percentage of myofibroblasts among NHLF during a scratch

assay with each treatment *in vitro* and generate datasets to fit the model against, cell

monolayers were scratched and subsequently stained with fluorescent anti-αSMA

immunocytochemistry and DAPI to mark myofibroblast cytoskeletons among all cell

nuclei (Figure 4.12). The percentage of myofibroblasts remained consistent with baseline

at 10-20% when treated with FGM or FBM over 24 hours, however CSM treatment was

found to induce a statistically-significant, approximately 3-fold increase of myofibroblasts that returned to baseline by 24 hours (Figure 4.13).
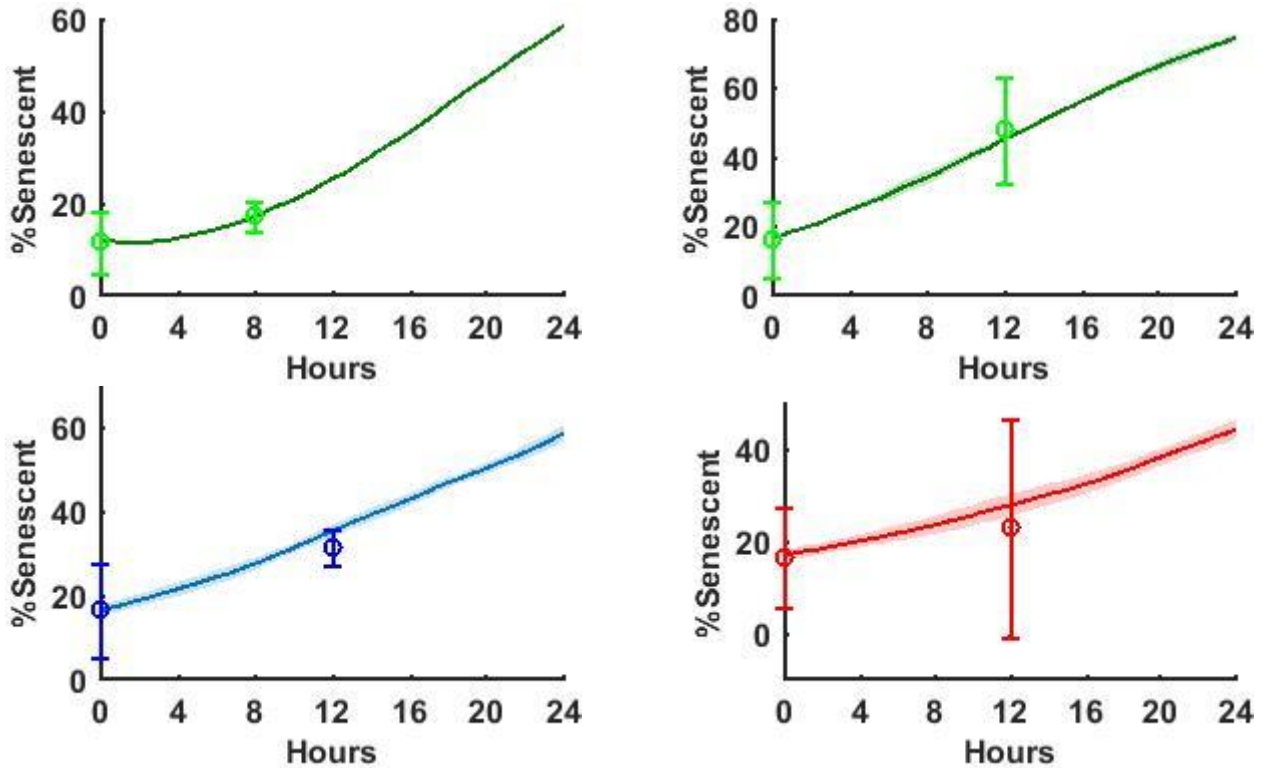


**Figure 4.11** – Simulated transients and *in vitro* senescence data among NHLF. Shown are responses to FGM (green), FBM (blue) or CSM (red) during the 8 hour pre-scratch interval (top left plot) or while closing a scratched monolayer over 24 hours (top right and bottom plots). *In vitro* data (markers with error bars) is shown as the mean ± 2SD of quadruplicate wells. Simulated transients were calculated by taking the mean and standard deviation of 10 simulations using the same initial conditions and parameter-set calibrated for each cell type and media exposure (Table 4.1); means are plotted with a solid curve and standard deviations are depicted by a shaded region around the mean curves.

The calibrated parameter-set for NHLF treated with FGM was able to fit the *in vitro* data within two standard deviation of the mean percentage of myofibroblasts in both the pre-scratch and post-scratch intervals at all time-points, even falling within one

standard deviation after 12 and 24 hours post-scratch. The other calibrated parameter-sets

fit within two standard deviations of their *in vitro* means, except for the 12 hour post-

scratch time-point for FBM parameter-set (Figure 4.14).
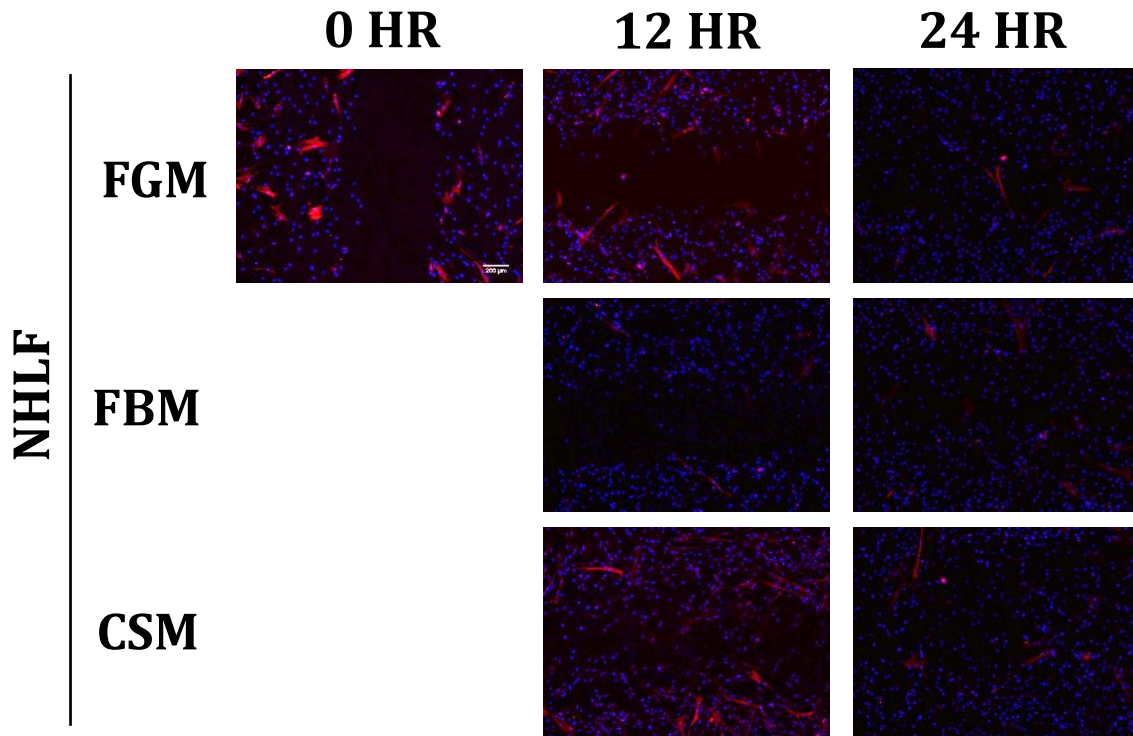


**Figure 4.12** – Superimposed fluorescent channels of αSMA (red) and DAPI (blue) stained
NHLF exposed to FGM, FBM or CSM while closing a scratched monolayer over 24 hours
*in vitro.* Scale bar = 200 µm.

Among the parameter-sets screened, parameter-sets which fit the 12 hour time-

point of the FBM *in vitro* data were not also able to fit the 24 hour time-point because the

transients that fit either time-point took opposing trajectories that excluded the other. All of

the transients initialize with approximately 15% myofibroblasts due the preconditioning

step and the overall trend of the *in vitro* data for FBM treatment had a downward

trajectory, so the calibrated parameter-set for FBM was chosen from parameter-sets which

fit the 24 hour time-point with a downward trajectory as opposed to the 12 hour time-point

with an upward trajectory (Figure 4.14).
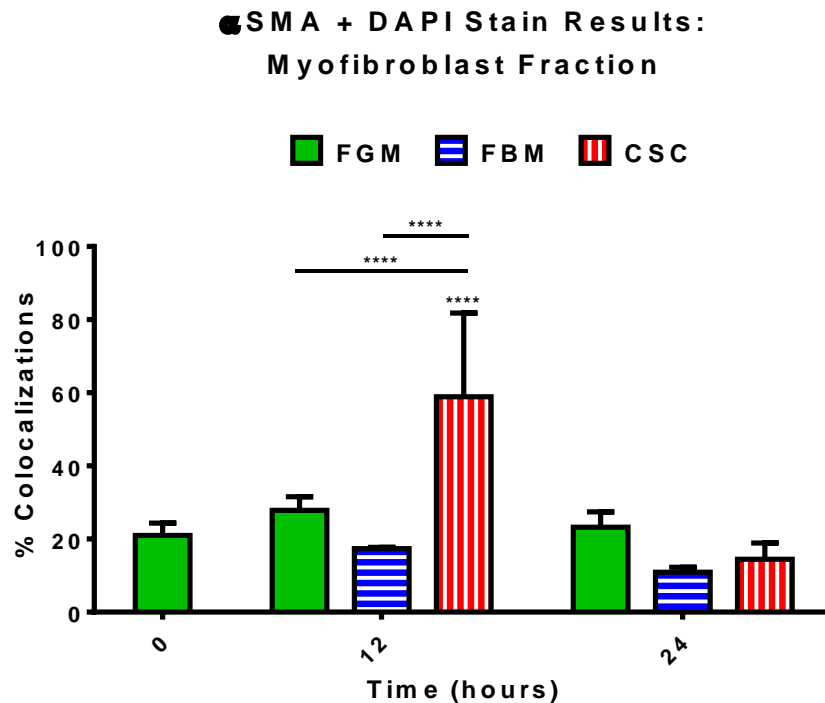


**Figure 4.13** – *In vitro* percentage of myofibroblasts among NHLF exposed to either FGM, FBM or CSM while closing a scratched monolayer over 24 hours. Data is expressed as the percentage of DAPI-stained nuclei co-localized with αSMA-stained cytoskeletons among all DAPI-stained nuclei and shown as the mean ± SD of quadruplicate wells. Significant statistical differences are noted with **** where $p < 0.001$. Within-group comparisons with baseline (time = 0) are indicated above the error bar and between-group comparisons within each time-point are indicated with a horizontal line.

**Superimposed Subpopulations**

Taken all together, our evaluation of NHLF subpopulations show a spike in either

myofibroblasts and/or senescent cells that returns to baseline or below by 24 hours, and that

the overarching difference between treatment groups are represented by the magnitude and relative composition of this spike. Cell death primarily occurred peri-scratch, ostensibly due to the scratch itself, and was otherwise negligible. Cell proliferation was also found to be negligible over 24 hours, with the exception of FGM treatment at the end of the 24 hour period evaluated.
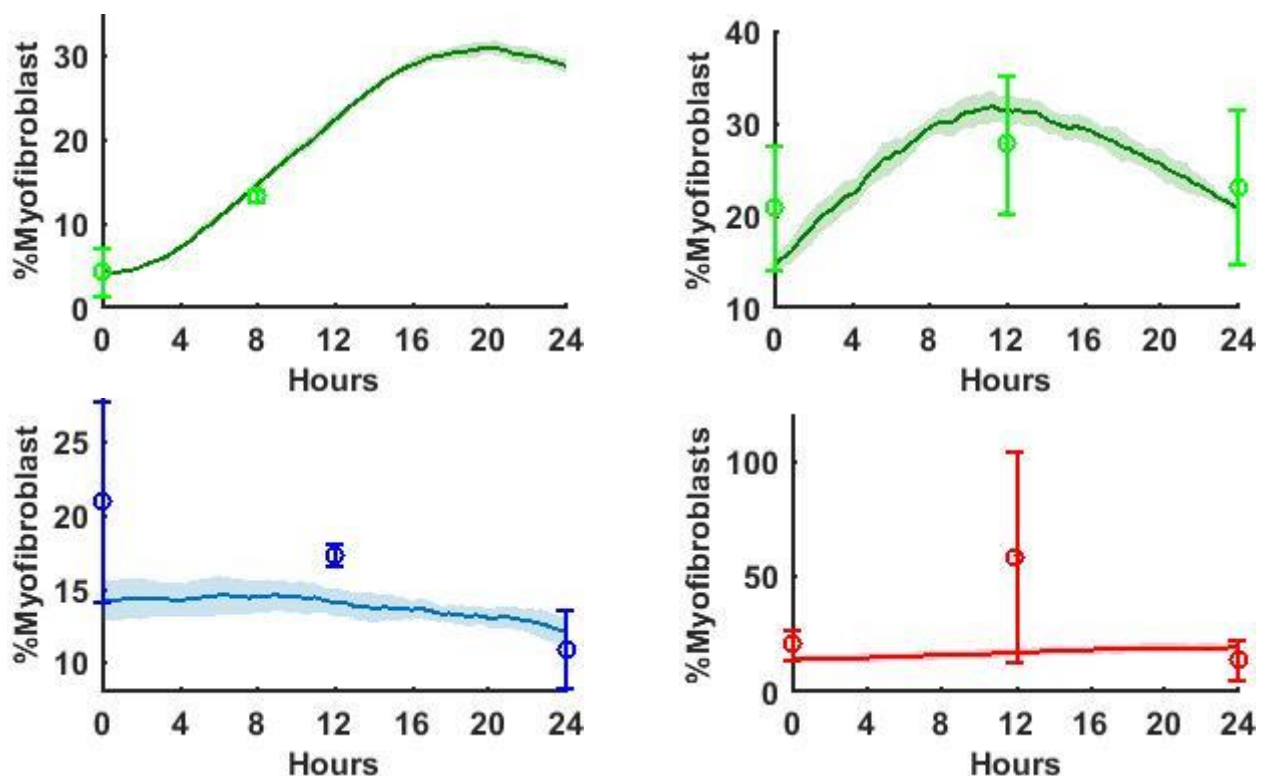


**Figure 4.14** – Simulated transients and *in vitro* myofibroblast data among NHLF. Shown are responses to FGM (green), FBM (blue) or CSM (red) during the 8 hour pre-scratch interval (top left plot) while closing a scratched monolayer over 24 hours (top right and bottom plots). *In vitro* data (markers with error bars) is shown as the mean ± 2SD of quadruplicate wells. Simulated transients were calculated by taking the mean and standard deviation of 10 simulations using the same initial conditions and parameter-set calibrated for each cell type and media exposure (Table 4.1); means are plotted with a solid curve and standard deviations are depicted by a shaded region around the mean curves.
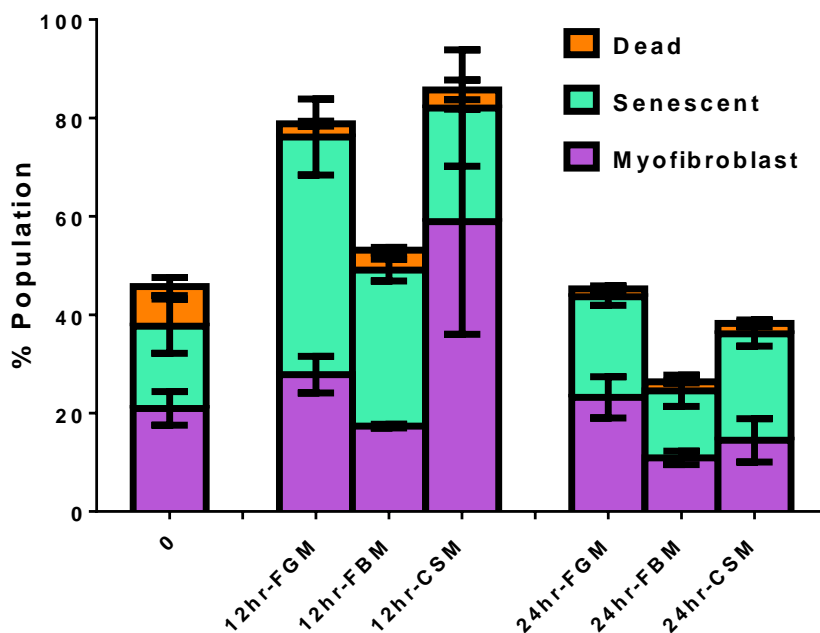
**Figure 4.15** – Superimposed percentages of myofibroblasts, senescent cells and dead cells among NHLF exposed to FGM, FBM or CSM during scratch closure. Data is expressed as the mean ± SD of quadruplicate wells.

At baseline, approximately 40% of cells were either myofibroblasts or senescent. While FGM and CSM treatments returned to this level by 24 hours, treatment with FBM decreased to approximately 30% myofibroblasts or senescent cells. During the spike in subpopulations found 12 hours post-scratch, FBM treatment subtly increased the percentage of senescence and myofibroblasts to approximately 50% of cells with a significant increase in the percentage of senescent cells (Figure 4.10) paired with an insignificant decrease in the myofibroblast percentage. However, treatment with either

FGM or CSM increased the baseline percentage of myofibroblasts and senescent cells approximately 2-fold during this 12 hour spike. We also found that while FGM treatment achieves this through an increase in the senescent subpopulation with negligible change in myofibroblasts, CSM treatment achieves this through an increase of myofibroblasts with minor changes in the senescent subpopulation (Figure 4.15).

**Calibrated Parameter-Sets**

The fibroblast wound healing model was evaluated through the analysis of 3000 distinct parameter-sets which produced a pattern of parameter-sets that fit the *in vitro* data for total population, percentage of myofibroblasts and percentage of senescent cells, but not scratch closure. Analysis of a further 100 parameter-sets with varied migration and proliferation rates found 50 parameter-sets that fit within two standard deviation of all the *in vitro* data for NHLF treated with FGM in both pre-scratch and post-scratch intervals, however only one of these fit most of the *in vitro* data within one standard deviation when evaluated with 10 simulations per parameter-set (data not shown). Therefore, this parameter-set was chosen to represent NHLF treated with FGM and used to calibrate the pre-scratch interval of the model by preconditioning the agents' variables since all of the *in vitro* scratch assays the model is fit against were incubated in FGM during the seed-scratch interval. These are the parameters that govern the preconditioning of agent subpopulations, stimulation levels and division rates during the pre-scratch interval. Another 256 parameter-sets were subsequently evaluated to find fits for the remaining experimental groups (Table 4.1). All of the calibrated parameter-sets were found to share the same

values for the magnitude of environmental stimulation ($A_M = 2*10^{-4}$ stim/hour) and distribution of the fibroblast population's sensitivity to stimuli ($A_S = 0.3$). The parameter-sets that fit the *in vitro* data for NHLF treated with CSM also shared the same stimulation thresholds for myofibroblast and senescent transitions ($L_M = 0.5$ and $L_S = 0.3$) as DHLF in either condition.

**Table 4.1 – Calibrated Parameter-Sets of the Fibroblast Responses.**

| Parameter | NHLF | | | DHLF | |
|:---:|:---:|:---:|:---:|:---:|:---:|
| | FGM | FBM | CSM | FBM | CSM |
| **M** | 65 | 24 | 16 | 12 | 12 |
| **P** | 27 | 24 | 30 | 42 | 42 |
| **Ls** | 0.1 | 0.17 | 0.3 | 0.3 | 0.3 |
| **Lm** | 0.06 | 0.58 | 0.5 | 0.5 | 0.5 |
| **Am** | 2.00E-04 | | | | |
| **As** | 0.3 | | | | |

Table 4.1 caption – Calibrated parameter-sets which fit the *in vitro* responses of NHLF and DHLF exposed to FGM, FBM, or CSM while closing a scratched monolayer over 24 hours. Simulated outputs were calculated by taking the mean and standard deviation of 10 simulations with the same initial conditions for each parameter-set. Simulated means within two standard deviations of the *in vitro* mean were considered a fit for that output.

Overall, it was found that the experimental groups with slower scratch closure rates had lower values of *M*, and higher values of *P*, $L_M$ and $L_S$. In particular, lower ratios of parameters *M:P* reliably produced slower closure rates. As expected from the model design, lower values of $L_M$ were associated with more myofibroblasts, lower values of $L_S$

were associated with more senescent cells, and lower ratios of $L_M$:$L_S$ were associated with a sharper spike in the percentage of myofibroblasts (Figures 4.11 & 4.14).

**Parameter Sensitivity Analysis**

To evaluate the sensitivity of parameter modulations around each calibrated parameter-set on the model outputs, we independently modulated each parameter by +/- 10% and calculated the percentage difference in each model output. As seen in Table 4.2, up to 2 or 3-fold change in model outputs per unit change in model parameters could be achieved for scratch closure, the percentage of senescent cells, and the percentage of myofibroblasts. Sensitivity analysis results for other outputs are shown in Appendix C. Notably, model responses were largely insensitive to modulations in the stimulation parameters $A_M$ or $A_S$ within any of the calibrated-sets, with adjustments in the model responses largely following the overall trend of adjustments due to modulations in the other parameters.

As expected due to the low probability of death due to stimulation within the model, modulating the parameters had minimal effect on the percentage of dead cells, with a maximum increase of 7% cell death when the proliferation interval was increased with the calibrated-set for NHLF treated with FGM. The large majority of parameter modulations increased cell death, and this effect decreased among sets with slower scratch closure rates. Increasing the division interval or decreasing the migration rate generated the largest increase in cell death among all of the calibrated-sets, and this was almost always associated with a concomitant decrease in the total population.

Also as expected due to the relatively short time interval evaluated with respect to the division intervals (parameter $P$) for these parameter-sets, modulating the parameters produced $\leq 12.5\%$ difference from the calibrated-sets' total populations among all of the calibrated-sets' parameter modulations. However it was somewhat surprising to find that most parameter modulations had a negative effect on the cell population, with the largest increase of 5.1% more cells after 24 hours among the DHLF parameter-set attributed to increasing the senescence threshold (Appendix C), which decreases the rate of senescence within the model.

As expected from the model design and calibrated parameter-sets, increasing the parameters for migration rate increased the scratch closure rate more than any other parameter alone. As expected due to the robust healing response of NHLF treated with FGM, differences in scratch closure due to parameter modulations within this calibrated-set skewed negative; and those differences among calibrated-sets associated with lower rates of scratch closure skewed increasingly positive. Many of the parameter modulations were also found to produce differences in scratch closure 12 hours post-scratch that were partially lost by 24 hours.

In general, the percentage of senescent cells and myofibroblasts were found to increase more, or decrease less, with lower values of $L_S$ and $L_M$, respectively; although lower values of $L_S$ were also consistently correlated with a decrease in myofibroblasts. Further illustrating the interdependence of these subpopulations within the model, modulations in the calibrated-sets' parameters that decreased the percentage of senescent cells generally also increased the percentage of myofibroblasts and vice versa. Strikingly,

modulations of any parameter in either direction within the calibrated parameter-set for

NHLF treated with FBM increased the senescent population by 20-30% at both 12 and 24

hours post-scratch while the myofibroblasts lost 0-10% and 15-25% of their population

after 12 and 24 hours, respectively. This also illustrates clearly how a spike in the

percentage of myofibroblasts can be created by adjusting the parameters such that more

myofibroblasts are formed at earlier time-points which subsequently become senescent by

the end of 24 hours (e.g. necessary to fit the calibrated-set for NHLF treated with FGM;

Figure 4.14), and how this effect can be used to adjust the time dynamics of the scratch

closure rates in a nonlinear manner.

Among the calibrated parameter-sets, NHLF treated with FGM was the least

sensitive to modulations in the parameters and showed a generally negative skew in the

scratch closure output accompanied with a proportionate boost in the percentage of

senescent cells and a flatter spike in the percentage of myofibroblasts 12 hours post-

scratch. The calibrated-set for NHLF with FBM also produced modest modulations in the

scratch closure rate, but these showed a consistent time-dynamic; parameter modulations

around this set typically increased scratch closure by 12 hours post-scratch, but this boost

was lost or reversed by 24 hours. As stated earlier, this mild boom-bust response in the

scratch closure rate due to parameter modulations was also accompanied with a large static

boost in the percentage of senescent cells along with a decrease in the percentage of

myofibroblasts that intensified with time. Taking into consideration the inability of the

calibrated-set for NHLF with FBM to fit both the 12 and 24 hour time-points of the *in vitro*

data for the percentage of myofibroblasts (Figure 4.14), the negative skew in the model's

myofibroblasts output indicates that up to ±10% modulation in any parameter would not be able to fit this 12 hour time-point, all due to the same downward trend in myofibroblasts.

The calibrated-sets for either NHLF treated with CSM or DHLF were much more sensitive to changes in the parameters, with the most drastic boost on the scratch closure output being produced by increases in the migration parameter. Interestingly, the calibrated-set for DHLF was found to be insensitive to the proliferation and transition limit parameters while the calibrated-set for NHLF treated with CSC was found to be relatively sensitive to these terms, despite these sets sharing the same values of $L_M$ and $L_S$. This illustrates how the values of some parameters (e.g. $M$, $P$) can influence the sensitivity of the model outputs to the other parameters (e.g. $L_M$, $L_S$). Additionally, it was found that the ratio of these parameters were as important as their raw values to find parameter-sets whose outputs matched a given dataset; where the ratio of $M{:}P$ had more of an effect on the scratch closure rate while the ratio of $L_M{:}L_S$ had more of an effect on the subpopulation levels and nonlinearity of scratch closure.

**Simulated Treatments for Smoke Exposure & COPD Fibroblasts**

Since the results of our sensitivity analysis indicated an increase in the migration rate would result in a faster rate of scratch closure among either cell line treated with CSM, we performed simulations of these calibrated-sets with up to 3-fold higher migration rates to represent potential treatments for these fibroblasts that could recover the scratch closure response of NHLF in FBM (Figure 4.16). Although modulating other parameters were

found to increase the scratch closure rate within the sensitivity analysis, intensifying these

modulations failed to increase the closure rate further (data not shown).
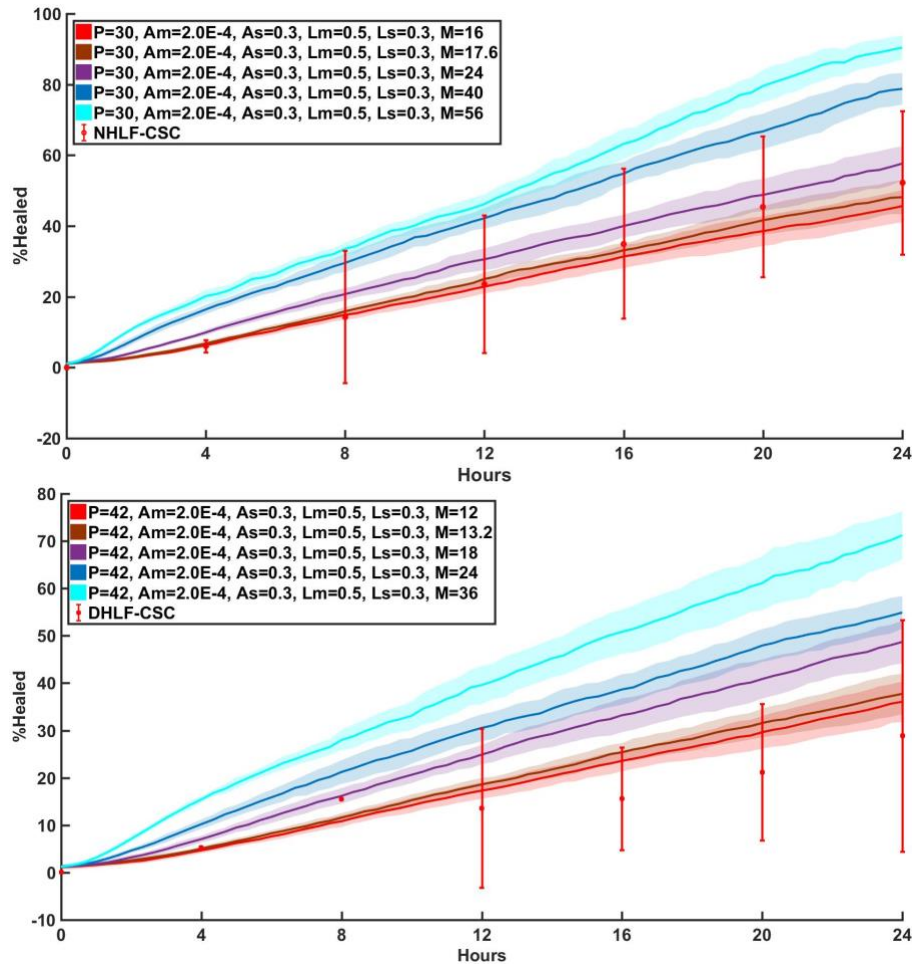


**Figure 4.16** – Simulated treatments for NHLF and DHLF exposed to smoke. Transients of parameter modulations around the calibrated-set (red) for NHLF (top) or DHLF (bottom) treated with CSM that increase scratch closure (*%Healed*; brown-blue gradient). Transients are juxtaposed with *in vitro* scratch closure data of NHLF (N = 3-6) or DHLF (N = 1-4) exposed to CSM, shown as the mean ± 2SD of N biological repeats. Simulated transients were calculated by taking the mean and standard deviation of 10 simulations using the same parameter-set and initial conditions.

**Table 4.2 – Heat-map of each calibrated-set's sensitivity to parameter changes.**

| Group | Parameter Modulation | | %Healed | | %Senescent Cells | | %Myofibroblasts | |
|---|---|---|---|---|---|---|---|---|
| | | | 12 HR | 24 HR | 12 HR | 24 HR | 12 HR | 24 HR |
| NHLF FGM | M | + | 0.4 | 0.8 | 2.4 | 1.0 | -0.9 | 2.2 |
| | | - | -6.6 | -5.4 | 2.5 | 1.3 | -1.6 | -0.2 |
| | P | + | -1.8 | -1.0 | 0.6 | 0.4 | -1.0 | 1.3 |
| | | - | -3.3 | -5.5 | 1.7 | -0.2 | 0.5 | 5.3 |
| | $L_M$ | + | -3.1 | -1.5 | 2.1 | 1.2 | -4.3 | -2.6 |
| | | - | -2.4 | -3.3 | 1.3 | 1.2 | 2.8 | 3.4 |
| | $L_S$ | + | -2.6 | 0.5 | -3.6 | -3.7 | 3.4 | 16.1 |
| | | - | -2.9 | -5.1 | 5.1 | 4.2 | -2.6 | -9.8 |
| | $A_M$ | + | 0.7 | -3.1 | 4.9 | 3.1 | -0.5 | -4.6 |
| | | - | -7.3 | -3.6 | -0.1 | -2.6 | -3.5 | 9.9 |
| | $A_S$ | + | -0.3 | -0.8 | 2.2 | 0.8 | -0.4 | 2.9 |
| | | - | -3.1 | -4.3 | 2.8 | 0.4 | -2.4 | 2.2 |
| NHLF FBM | M | + | 8.8 | 0.9 | 21.7 | 22.9 | -2.7 | -19.9 |
| | | - | -1.5 | -9.1 | 23.5 | 25.0 | -0.6 | -20.2 |
| | P | + | 4.9 | -1.5 | 24.7 | 26.0 | -5.1 | -21.7 |
| | | - | 7.6 | 2.4 | 24.9 | 25.2 | -7.6 | -24.9 |
| | $L_M$ | + | 2.1 | -0.7 | 19.9 | 23.6 | -8.4 | -24.8 |
| | | - | 9.4 | -2.8 | 25.6 | 25.9 | -0.2 | -16.9 |
| | $L_S$ | + | 6.8 | -1.8 | 19.4 | 18.4 | -0.9 | -15.8 |
| | | - | 2.3 | -5.1 | 28.6 | 30.9 | -5.4 | -26.6 |
| | $A_M$ | + | 3.6 | -2.8 | 26.9 | 28.8 | -5.8 | -21.9 |
| | | - | 5.4 | -0.1 | 21.6 | 19.3 | -8.4 | -18.8 |
| | $A_S$ | + | 1.1 | -4.7 | 21.7 | 21.8 | 0.0 | -18.5 |
| | | - | 6.7 | -1.2 | 23.2 | 23.6 | -8.8 | -25.3 |
| NHLF CSM | M | + | 16.8 | 9.6 | 4.6 | 1.2 | -5.9 | -4.4 |
| | | - | -3.7 | -3.7 | 1.0 | -0.5 | -4.8 | -2.4 |
| | P | + | 4.6 | -0.1 | 4.8 | 1.8 | -5.2 | -4.6 |
| | | - | 9.4 | 8.4 | -0.1 | -1.5 | -3.3 | -1.1 |
| | $L_M$ | + | -1.6 | -0.4 | 4.2 | 1.5 | -9.8 | -9.4 |
| | | - | 7.4 | 5.2 | 1.7 | 0.7 | -3.3 | -1.2 |
| | $L_S$ | + | 7.6 | 5.8 | -4.9 | -7.7 | -3.7 | -0.1 |
| | | - | 5.3 | 2.5 | 8.2 | 6.5 | -5.1 | -10.8 |
| | $A_M$ | + | 8.0 | 6.7 | 1.9 | 3.0 | -1.6 | -3.1 |
| | | - | 9.8 | 6.0 | -1.1 | -2.4 | -6.1 | -6.4 |
| | $A_S$ | + | 4.0 | -0.5 | 0.8 | 0.1 | -6.8 | -4.5 |
| | | - | 9.0 | 0.3 | -0.9 | -1.5 | 0.0 | 1.8 |
| DHLF | M | + | 19.5 | 11.9 | -2.0 | 1.7 | 3.3 | -1.3 |
| | | - | -2.7 | -3.3 | -2.2 | 1.1 | -2.4 | -1.8 |
| | P | + | 3.3 | 0.4 | -0.8 | -0.4 | -2.7 | -0.5 |
| | | - | 1.9 | -0.3 | -2.0 | -0.4 | 2.0 | 4.9 |
| | $L_M$ | + | 3.7 | 1.5 | -4.2 | 0.1 | -2.6 | -3.4 |
| | | - | -1.8 | -5.6 | 1.2 | 2.8 | 2.7 | 6.0 |
| | $L_S$ | + | -1.0 | 2.6 | -5.2 | -5.0 | 2.0 | 8.5 |
| | | - | 4.7 | 1.9 | -0.1 | 4.7 | 1.7 | -1.6 |
| | $A_M$ | + | 2.0 | 5.1 | -3.9 | 0.5 | 4.8 | 3.3 |
| | | - | 10.2 | 8.7 | -6.0 | -5.4 | -1.2 | 3.7 |
| | $A_S$ | + | 3.5 | -0.2 | 0.3 | 3.3 | -1.7 | -2.8 |
| | | - | 7.6 | 7.2 | -3.0 | 0.7 | 2.0 | 1.6 |

Table 4.2 caption (previous page): sensitivity of model outputs to parameter modulations with respect to each calibrated parameter-set are expressed as the percentage difference from the calibrated parameter-set's mean output when each parameter is independently modulated by ± 10%. Model outputs are shown for the percentage of scratch closure (*%Healed*) and the percentage of senescent cells or myofibroblasts after 12 or 24 hours. Parameter-set mean outputs were calculated from 10 simulations with the same conditions. A blue-red gradient was applied across all outputs and parameter modulations within each experimental group.

## Discussion

**Differences among Normal Fibroblast Exposures**

We selected a dosage of 50 µg/ml CSC within our CSM treatment media because dosages of 250 and 1000 µg/ml were found to cause 50-80% decrease in metabolism by MTT assay (N = 1-2; not shown), which we interpreted as cell death and aimed to avoid within our experiments in order to evaluate CSC's effect on fibroblast functions, rather than its effect on apoptosis; and we confirmed a significant difference between NHLF treated with FGM versus CSM by CCK8 assay (Figure 4.1). However, considering that both of these assays depend on NADH/NAD metabolism and CSC is also known to induce oxidative stress associated with elevated NADH/NAD ratios, we had to confirm we were avoiding cell death using a non-metabolic assay.

Our avoidance of large drops in metabolism is likely why we found ≤ 10% dead cells at any of the time-points we evaluated in our cell stain experiments; however it was surprising to find that the percentage of cell death decreased over time at a rate which we were unable to match with the model while also fitting the population data for NHLF treated with FGM (not shown), indicating that the percentage of dead cells *in vitro* were being decreased directly. Upon re-evaluating the literature to confirm this result, we found reports that fibroblasts participate in efferocytosis to clear dead cells and debris during wound closure as one of their many roles in tissue maintenance [140,141]. Since our *in vitro*

data contained negligibly low levels of cell death, we simply left this out of our model; however, future iterations of the model that aim to evaluate fibroblast responses involving more cell death than this iteration should include a rule for this functionality to ensure this model output is relevant to *in vitro* measurements to which it's fit.

While intriguing, any conclusions drawn from interpretations of this *in vitro* population data are unfortunately limited by the lack of biological repeats. Also, the senescence and myofibroblasts assays each suffered from limitations in their measurement that likewise limits the confidence in conclusions drawn from them. The SA-β-Gal assay used to evaluate the percentage of senescent cells can induce a false positive among quiescent cells, particularly fibroblasts in confluent monolayers such as those used within the scratch assays. Thus, the seeding density of all the cell stain experiments were lowered in order to minimize the probability of false positives within the senescence assay and perform these experiments with the same conditions to preserve the cells' level of contact inhibition within the stain experiments; and this adjustment in the seeding density may have compromised our assessment of the subpopulations within the scratch closure experiments. Also analyzing the DAPI stain for senescence-associated heterochromatic foci could have served as a control against quiescent cells [130], however the large degree of background fluorescence within this stain limited our ability to do this analysis. The immunocytochemistry assay of αSMA expression also suffered from pervasive background fluorescence that limited the image contrast available for image processing, such that the percentage of myofibroblasts may have been systematically over-reported. These limitations are highlighted by our observation of less cell senescence following a spike in

senescence 12-hours post-scratch among NHLF treated with FGM; while anecdotal reports of reversible senescence exist [142], these have not yet passed peer review. As mentioned earlier, the model was not required to match a decrease in cell senescence at the 24 hour time-points for this reason. Despite any concerns regarding the accuracy of the *in vitro* subpopulation data, calibrated parameter-sets were able to match both the percentage of myofibroblasts and senescent cells along with scratch closure rates with few exceptions (Figure 4.14).

Our scratch wound closure assays revealed that NHLF exposed to each media type produced a significantly different scratch closure rate from the others 24 hours post-scratch, and each of these closure responses was characterized by a unique dynamic in the cell subpopulations that was supported by the calibrated parameter-sets for these groups. The relatively short time evaluated by the model with respect to these cell types mean division intervals (parameter $P$) limits our ability to find significant differences in this parameter between experimental groups. Additionally, we found that regardless of cell type of media exposure, all experimental groups were associated with calibrated-sets containing the same values for the parameters governing the magnitude of environmental stimulation (parameter $A_M$) and heterogeneity of individual responses to a given type or level of stimulation among the population of fibroblast (parameter $A_S$).

With respect to the calibrated parameter-set for NHLF treated with FBM, treatment with FGM was associated with a 2.4-fold increase in migration rate paired with a 9.7-fold higher rate of myofibroblast activation compensated by a 1.7-fold higher rate of senescence. Despite the spike in senescence associated with negligible myofibroblast

increase that we found *in vitro* and matched *in silico*, this calibrated-set still indicates a

drastic enhancement of migration and myofibroblast activation due to the inclusion of

serum, bFGF and insulin to their media – which makes sense considering these ingredients

are included in FGM to enhance fibroblast migration, proliferation and activation via the

Wnt/β-catenin pathway [143] or Akt1, myocardin and serum response factor [144] . Notably,

bFGF has also been found to deactivate myofibroblasts when stimulated by TGFβ, both

mediated by Akt1 [144], which supports our in vitro finding of mildly elevated

myofibroblasts that returned to baseline over 24 hours.

With respect to the calibrated parameter-set for NHLF treated with FBM, treatment

with CSM was associated with a 33% drop in migration rate paired with a 16% higher rate

of myofibroblast activation compensated by a 44% lower rate of senescence. This indicates

an inhibition of NHLF migration rate independent to the loss in migration rate expected

from the concomitant increase in myofibroblasts with less senescent cells; however, this

calibrated-set was nearly 2 standard deviations from the mean of the *in vitro* data for the

percentage of myofibroblast, so the independent decrease in migration rate found in this

calibrated-set may be compensating for this lack of myofibroblast activation in order to fit

the scratch data. This is supported by reports showing that fibroblast activation is

stimulated by oxidative stress, such as is found within cigarette smoke [60].

**Differences between Normal & COPD Fibroblasts:**

Many aspects of this project were influenced by the limited availability of DHLF, as they only maintained log-growth for one or two passages; so one of the main goals of the project was to use the model and *in vitro* scratch closure data for this cell line to evaluate how DHLF functions may differ from NHLF and inform future investigations into this cell line. For this reason, dosages of CSC were not tested among DHLF to ensure the chosen dose produced an effect within both cell lines – which may have prevented us from evaluating how DHLF responses to CSC differ from NHLF – however, our *in vitro* scratch results show that DHLF is resistant to CSC relative to NHLF. In support of this finding, the calibrated-set for DHLF was found to fit the DHLF *in vitro* data when exposed to either FBM or CSM.

The limited availability of *in vitro* datasets of DHLF population responses to fit the model against – or of DHLF exposed to FGM – also produced two problems. First, this required the model's preconditioning parameters for both cell lines to be calibrated using *in vitro* data of NHLF and created an unlikely assumption within the model that DHLF responses to FGM were the same as NHLF during the pre-scratch interval. Second, there were many more parameter-sets that could have been classified as a calibrated-set among DHLF since there were less datasets available to filter out sets that were not biologically relevant to this cell line. Therefore, in order to use this forced assumption as a tool in our comparison of these groups and help guide our selection of the calibrated-sets for DHLF, we fit the model to both of these groups while maintaining the $L_M$ and $L_S$ parameters between these sets and the calibrated-set for NHLF treated with CSM. This allowed us to

use the calibrated-set for NHLF treated with CSM as a reference parameter-set that assumed no difference between these cell lines' subpopulation responses and limited the variation between these sets to the migration and proliferation parameters.

Since the scratch closure response showed some sensitivity to all of the parameters while the population levels were relatively insensitive to the migration and proliferation parameters (Table 4.2) – and since the different subpopulations exhibit different migration and proliferation rates (Figure 3.4) – variations in these parameters between the calibrated-sets for DHLF and NHLF exposed to CSM suggest how the subpopulation levels may change between these groups. Both the migration rate and proliferation rate were found to be lower among DHLF calibrated-sets relative to NHLF treated with CSM, which may indicate either (A) these cells migrate and proliferate less due to a fundamental (e.g. genetic, epigenetic) difference between these cell lines, (B) there are more myofibroblasts, (C) there are more senescent cells, or (D) some combination of these. It is impossible to speculate upon the likelihood of genetic differences among DHLF using this analysis of the model, as these kinds differences may produce a relative increase in myofibroblasts or cell senescence; however, we can infer from the relatively equal decrease in migration and proliferation parameters – down to 72-75% of the values for the set calibrated to NHLF treated with CSM – that this difference is likely due to an increase in the percentage of myofibroblasts rather than senescent cells. Since senescent cells lose the ability to proliferate or migrate in a directed manner, we would expect more of a decrease in both of these terms, particularly the proliferation rate; however future simulations repeating this analysis while holding the migration and proliferation parameters constant, or letting them

all vary together, could be used to test this hypothesis *in silico* prior to *in vitro* investigations.

Taking these findings into consideration with the years of smoke exposure typically needed to produce COPD symptoms, a more holistic interpretation of DHLF's significant decrease from NHLF closure rates, insensitivity to CSM *in vitro* and *in silico*, and relative decrease in migration and proliferation rates *in silico* suggest that DHLF represents a subpopulation of NHLF that had survived a selection process for resistance to cigarette smoke and upregulated the percentage of myofibroblasts. This interpretation is supported by our *in vitro* finding that NHLF exposure to CSM induced a spike in the percentage of myofibroblasts after 12 hours.

Since *in vivo* wound healing and homeostasis is an orchestrated process requiring a balance of multiple native cell types, our interpretation that COPD pathogenesis is at least in part due to an upregulation of fibroblasts relative to other cell types due to selective pressures of oxidative stress caused by chronic smoke exposure is supported by the distribution of tissue degradation and fibrosis within COPD. Elevated proportions of epithelial and endothelial cells to native fibroblasts within parenchymal regions relative to the bronchioles among normal lungs, paired with a chronically elevated rate of mesenchymal transitions, would be expected to result in the pattern of tissue loss and fibrosis seen in each respective region among COPD lungs. Luckily, the autoflourescence of NADH may be used as a biomarker of oxidative stress and metabolic health in future studies of this mechanism [145].

**Simulated Treatments for Smoke Exposure & COPD Fibroblasts**

Our sensitivity analysis and following simulations of increasing modulations of individual parameters around the calibrated-sets for DHLF and NHLF treated with CSM found that an increase in the migration parameter alone would continue to increase the scratch closure rate the more it was elevated (Figure 4.16), but increasing modulations in the other parameters alone had practically no effect (data not shown). It is unlikely that a potential *in vitro* treatment would affect migration rate without also affecting other pathways due to the degree of crosstalk among cellular signaling pathways; however, since the model is sensitive to modulations in ratios of parameters more than individual parameters, further simulations of parameter modulations of multiple parameters around these calibrated-sets are likely to reveal more potential treatments for these groups. Regardless, increasing fibroblast migration rates should be achievable in vitro through several means (Table 5.1). Increased migration should be achievable by drugs which increase actin expression, actin treadmilling, microtubule stabilization, Rho/Rac signaling or inhibition of contractility. Additionally, increased migration via decreased contractility could be achieved with less myofibroblasts, which in itself would be achievable by treatments which limit their activation, induce their deactivation, or induce senescence – once such mechanism to accomplish this would be to supplement with bFGF to induce deactivation and promote senescence as was seen in our *in vitro* experiments among NHLF treated with FGM. Counteracting the cigarette smoke induced oxidative stress to prevent the associated increase in myofibroblasts may also represent a valid strategy – this could be achieved directly through supplementation with an antioxidant such as vitamin C, and

potentially protected against if cell-native antioxidants are primed prior to smoke exposure. Likewise, caloric restriction or drugs which mimic this (e.g. glycolysis inhibitors, glutaminolysis inhibitors, etc.) could be used to buffer NADH/NAD levels to minimize the effect of oxidative signaling on downstream targets; and these downstream targets (i.e. SIRT-1 and HIF-1α) can be inhibited directly to prevent upregulation of mesenchymal marker genes (e.g. αSMA) or senescence. Finally, a recent review indicates various interleukin inhibitors as another promising method to treat COPD by targeting the NLRP3 inflammasome theorized to drive the autoinflammatory processes observed in COPD [16].

**Additional Functionality & Future Directions for the Model:**

The aspects of the model explored here are not comprehensive. Our results may be expanded upon with the model through a thorough evaluation of the parameter space that fits each cell type and media exposure to judge if another parameter-set may represent a better fit for the *in vitro* data than those presented, or to evaluate if modulations of more than one parameter may produce synergy to improve scratch closure. However, high performance computing resources are recommended for more intensive analyses or models due to the number of simulations required, paired with NetLogo's computational inefficiency compared to other ABM platforms [114,115]. Additionally, while this model was weakly validated when it was found to fit the 4 hour time-point of the scratch closure data, *in vitro* data sets of the DHLF subpopulations or of scratch closure to 48 hours post-scratch could validate if our model and calibrated parameter-sets have predictive value.

The availability of *in vitro* data sets from other fibroblast lines, media exposures or other types of collective migration experiments would allow this model to be applied towards additional questions. While we present here a model of fibroblast scratch closure, the scratch and non-scratch regions could easily be switched to model a barrier removal assay to evaluate differences in contact inhibition among the cell types and exposures with less influence from cytokines released from damaged cells or the population of cells across the scratch. Migration following cytokine gradients were not modeled, so different values in the migration parameter required to fit data for these *in vitro* experiment types may reveal the presence of such gradients and if DHLF and/or CSM responses are less sensitive to these gradients. Additionally, data from migration assays for other cell lines (e.g. IPF-fibroblasts, mesenchymal stem cells, cancer-associated fibroblasts) or exposures (e.g. E-cigarettes, H2O2, TGFβ) would allow the model to evaluate differences in those cell types or exposure responses. Assays of these fibroblasts exposed to conditioned media from normal or COPD-derived epithelial cells or macrophages would create parameter-sets representing fibroblast responses to paracrine signaling from these cell types. Similarly, assays of these fibroblasts on polyacrylamide gels of lung-relevant stiffnesses coated with ECM from normal and COPD lungs could be used to generate parameter-sets representing fibroblast responses to these substrate properties and vice versa. These parameter-sets would allow differences in paracrine and cell-substrate signaling mechanisms within the lung during smoking or COPD to be evaluated and would inform future model iterations that include these cell types and mechanical features. For example, ECM composition and stiffness could be modeled as patch variables that the fibroblast agents can interact with

and differentially modulate based on their breed – this data could be fit against in vitro data of fibril formation during the in vitro assays of fibroblasts on ECM-coated polyacrylamide gels, or simulated from other models of fibril formation [146] or fibrosis [113] – while another layer of patches and breed of agents could be included to model interactions with a layer of epithelial cells and patrolling macrophages [112], respectively. However, these would take exponentially more time to simulate with the number of patches or agents, so a modular approach, high performance computing resources and/or more computationally efficient modeling platforms are recommended [115,118].

**Table 5.1 – Potential Treatment Strategies for COPD and Smoke Exposure.**

| Treatment Strategy | Method | Therapy/Drug | Citation |
|---|---|---|---|
| Increase Migration | Stabilize microtubules & cell polarity | Paclitaxel | [147] |
| | ↑ Actin content | Glucocorticoids | [84,148] |
| | ↑ Actin dynamics | Heat, CalyculinA | [84] |
| | ↑ Adhesion dynamics (via ROCK) | Fasudil, Y27632 | [149] |
| | ↓ Senescent induction | Fasudil, Y27632, Rapamycin, Rapalogs | [29,100,149] |
| | ↓ Senescent population (senolytics) | Dasatinib, Quercetin, Fisetin, Navitoclax, Venetoclax, | [150] |
| | ↓ Contractility & myofibroblasts | Roflumilast, Piclamilast, Aclidinium, SMIFH2, NOX4 inhibitors | [42,60,147,151–154] |
| Inhibit Myofibroblasts | ↓ Activation | anti-Akt | [144] |
| | ↑ Deactivation | bFGF | [144] |
| Inhibit Inflammation | anti IL-1beta | Canakinumab | [16] |
| | anti IL-1Ralpha | Anakinra | [16] |
| | IL-1 trap (mock receptor) | Rilonacept | [16] |
| Counter CSC & ROS | ↑ antioxidants | Vitamin C | [29,60,155,156] |
| | caloric restriction | 2DG (anti-glycolysis) | [29,157,158] |
| | ↑ SIRT1 / ↓ HIF-1α | SRT2172, SRT1720 | [29,159,160] |
| | | Reservatrol | [29,159,160] |
| | | Metformin | [29,160] |

Table 5.1 caption – Potential strategies, methods and specific therapeutics that may achieve increased scratch closure among DHLF or NHLF exposed to cigarette smoke. Our model suggests scratch closure will be most improved with increased migration rates, which can be also accomplished by decreasing levels of senescence and myofibroblasts. Lower levels of these cells may also be achieved through inhibition NLRP3-mediated inflammation or countering the effects of oxidative stress from cigarette smoke.

## Conclusions

We designed a model that captured the dynamics of fibroblast scratch closure due to changes in myofibroblast activation and cell senescence and calibrated parameter-sets to in vitro data for human lung fibroblasts exposed to cigarette smoke. Our in vitro results and calibrated parameter-sets recapitulated findings of increased myofibroblast activation and senescence among lung fibroblasts exposed to smoke or when derived from COPD. Calibrated-sets for this model could be fit to in vitro data of other fibroblast lines or exposures to evaluate their effects on scratch closure to investigate other diseases, paracrine signaling with other cell types, potential toxins like E-cigarette vapor, or therapeutics. Future iterations addressing COPD should work towards evaluating the dynamics of myofibroblast activation on regulation of the ECM during wound healing through traction forces and protease/antiprotease secretion mediated by oxidative stress.

**<u>Literature Cited</u>**

Literature Cited

1. Kochanek, K. D., Murphy, S. L., Xu, J. & Tejada-Vera, B. *Deaths: Final Data for 2014. National vital statistics reports : from the Centers for Disease Control and Prevention, National Center for Health Statistics, National Vital Statistics System* **65,** (2016).

2. Vestbo, J. *et al.* Global Strategy for the Diagnosis, Managment, and Prevention of Chronic Obstructive Pulmonary Disease (Updated 2014). in *Global Initiative for Chronic Obstructive Lung Disease* 1–80 (Global Initiative for Chronic Obstructive Lung Disease, Inc., 2014).

3. Szilasi, M., Dolinay, T., Nemes, Z. & Strausz, J. Pathology of chronic obstructive pulmonary disease. *Pathol. Oncol. Res.* **12,** 52–60 (2006).

4. Barreiro, E. & Criner, G. J. Update in chronic obstructive pulmonary disease 2013. *Am. J. Respir. Crit. Care Med.* **189,** 1337–44 (2014).

5. Barnes, P. J. *et al.* Chronic obstructive pulmonary disease. *Nat. Rev. Dis. Prim.* **1,** 15076 (2015).

6. Yoshida, T. & Tuder, R. M. Pathobiology of cigarette smoke-induced chronic obstructive pulmonary disease. *Physiol. Rev.* **87,** 1047–82 (2007).

7. Molfino, N. a & Jeffery, P. K. Chronic obstructive pulmonary disease: histopathology, inflammation and potential therapies. *Pulm. Pharmacol. Ther.* **20,** 462–72 (2007).

8. Jeffery, P. K. Remodeling in asthma and chronic obstructive lung disease. *Am. J. Respir. Crit. Care Med.* **164,** S28-38 (2001).

9. Togo, S. *et al.* Lung fibroblast repair functions in patients with chronic obstructive pulmonary disease are altered by multiple mechanisms. *Am. J. Respir. Crit. Care Med.* **178,** 248–60 (2008).

10. Barnes, P. J. Chronic Obstructive Pulmonary Disease. *N. Engl. J. Med.* **343,** 269–280 (2000).

11. Suki, B. *et al.* Emphysema and mechanical stress-induced lung remodeling. *Physiology (Bethesda).* **28,** 404–13 (2013).

12. National Organization for Rare Disorders (NORD). Alpha-1 Antitrypsin Deficiency. (2017). Available at: https://rarediseases.org/rare-diseases/alpha-1-antitrypsin-deficiency/. (Accessed: 25th April 2018)

13. Lokke, A., Lange, P., Scharling, H., Fabricius, P. & Vestbo, J. Developing COPD: a 25 year follow up study of the general population. *Thorax* **61,** 935–939 (2006).

14. Barnes, P. J. Mediators of chronic obstructive pulmonary disease. *Pharmacol. Rev.* **56,** 515–48 (2004).

15. NOBUKUNI, S. *et al.* Cigarette smoke inhibits the growth of lung fibroblasts from patients with pulmonary emphysema. *Respirology* **7,** 217–23 (2002).

16. Scambler, T., Holbrook, J., Savic, S., McDermott, M. F. & Peckham, D. Autoinflammatory Disease in the Lung. *Immunology* (2018). doi:10.1111/imm.12937

17. Lonza Group. Fibroblasts Instructions for Use. *Clonetics ᵀᴹ Human Fibroblast Cell Systems* 1–4 (2010).

18. Dagouassat, M. *et al.* The cyclooxygenase-2-prostaglandin E2 pathway maintains senescence of chronic obstructive pulmonary disease fibroblasts. *Am. J. Respir. Crit. Care Med.* **187,** 703–14 (2013).

19. Kumar, M., Seeger, W. & Voswinckel, R. Senescence-associated secretory phenotype and its possible role in chronic obstructive pulmonary disease. *Am. J. Respir. Cell Mol. Biol.* **51,** 323–33 (2014).

20. Zhang, J. *et al.* Pro-inflammatory phenotype of COPD fibroblasts not compatible with repair in COPD lung. *J. Cell. Mol. Med.* **16,** 1522–32 (2012).

21. Huang, S., Wettlaufer, S. H., Hogaboam, C., Aronoff, D. M. & Peters-Golden, M. Prostaglandin E(2) inhibits collagen expression and proliferation in patient-derived normal lung fibroblasts via E prostanoid 2 receptor and cAMP signaling. *Am. J. Physiol. Lung Cell. Mol. Physiol.* **292,** L405-13 (2007).

22. Hallgren, O. *et al.* Enhanced ROCK1 dependent contractility in fibroblast from chronic obstructive pulmonary disease patients. *J. Transl. Med.* **10,** 171 (2012).

23. Fujita, Y. *et al.* Suppression of autophagy by extracellular vesicles promotes myofibroblast differentiation in COPD pathogenesis. *J. Extracell. Vesicles* **4,** 1–12 (2015).

24. Okunishi, K., DeGraaf, A. J., Zasłona, Z. & Peters-Golden, M. Inhibition of protein translation as a novel mechanism for prostaglandin E2 regulation of cell functions.

*FASEB J.* **28,** 56–66 (2014).

25. Selige, J., Tenor, H., Hatzelmann, A. & Dunkern, T. Cytokine-dependent balance of mitogenic effects in primary human lung fibroblasts related to cyclic AMP signaling and phosphodiesterase 4 inhibition. *J. Cell. Physiol.* **223,** 317–26 (2010).

26. Liu, X. *et al.* Vitamin D Modulates PGE2 Synthesis and Degradation in Human Lung Fibroblasts. *Am. J. Respir. Cell Mol. Biol.* **50,** 130813135401001 (2013).

27. Huang, S. K., Wettlaufer, S. H., Chung, J. & Peters-Golden, M. Prostaglandin E2 inhibits specific lung fibroblast functions via selective actions of PKA and Epac-1. *Am. J. Respir. Cell Mol. Biol.* **39,** 482–9 (2008).

28. Müller, K. *et al.* Lung fibroblasts from patients with emphysema show markers of senescence in vitro. *Respir. Res.* **7,** 32 (2006).

29. Barnes, P. J. Senescence in COPD and Its Comorbidities. *Annu. Rev. Physiol.* **79,** 517–539 (2017).

30. Barnes, P. Identifying Molecular Targets for New Drug Development for Chronic Obstructive Pulmonary Disease: What Does the Future Hold? *Semin. Respir. Crit. Care Med.* **36,** 508–522 (2015).

31. National Organization of Rare Disorders (NORD). Idiopathic Pulmonary Fibrosis - NORD (National Organization for Rare Disorders). (2017). Available at: https://rarediseases.org/rare-diseases/idiopathic-pulmonary-fibrosis/. (Accessed: 25th April 2018)

32. Aoshiba, K. & Nagai, A. Senescence hypothesis for the pathogenetic mechanism of chronic obstructive pulmonary disease. *Proc. Am. Thorac. Soc.* **6,** 596–601 (2009).

33. Nyunoya, T. *et al.* Cigarette smoke induces cellular senescence. *Am. J. Respir. Cell Mol. Biol.* **35,** 681–8 (2006).

34. Coppé, J.-P., Desprez, P.-Y., Krtolica, A. & Campisi, J. The senescence-associated secretory phenotype: the dark side of tumor suppression. *Annu. Rev. Pathol.* **5,** 99–118 (2010).

35. Rodier, F. & Campisi, J. Four faces of cellular senescence. *J. Cell Biol.* **192,** 547–56 (2011).

36. Jun, J.-I. & Lau, L. F. Cellular senescence controls fibrosis in wound healing. *Aging (Albany. NY).* **2,** 627–31 (2010).

37. Burton, D. G. a & Krizhanovsky, V. Physiological and pathological consequences

of cellular senescence. *Cell. Mol. Life Sci.* **71,** 4373–86 (2014).

38. van Deursen, J. M. The role of senescent cells in ageing. *Nature* **509,** 439–46 (2014).

39. Tchkonia, T., Zhu, Y., van Deursen, J., Campisi, J. & Kirkland, J. L. Cellular senescence and the senescent secretory phenotype: therapeutic opportunities. *J. Clin. Invest.* **123,** 966–972 (2013).

40. Campisi, J. & d'Adda di Fagagna, F. Cellular senescence: when bad things happen to good cells. *Nat. Rev. Mol. Cell Biol.* **8,** 729–40 (2007).

41. Eurlings, I. M. J. *et al.* Cigarette Smoke Extract Induces a Phenotypic Shift in Epithelial Cells; Involvement of HIF1α in Mesenchymal Transition. *PLoS One* **9,** e107757 (2014).

42. Milara, J., Peiró, T., Serrano, A. & Cortijo, J. Epithelial to mesenchymal transition is increased in patients with COPD and induced by cigarette smoke. *Thorax* **68,** 410–420 (2013).

43. Laurent, G. J. Regulation of Lung Collagen Production During Wound Healing. *CHEST J.* **99,** 67–69 (1991).

44. Dee, K. C., Puleo, D. A. & Bizios, R. Wound Healing. in *Tissue-Biomaterial Interactions* 127–47 (John Wiley & Sons, Inc., 2002).

45. Micallef, L. *et al.* The myofibroblast, multiple origins for major roles in normal and pathological tissue repair. *Fibrogenesis Tissue Repair* **5,** S5 (2012).

46. Darby, I. a & Hewitson, T. D. Fibroblast differentiation in wound healing and fibrosis. *Int. Rev. Cytol.* **257,** 143–79 (2007).

47. Gardner, A., Borthwick, L. A. & Fisher, A. J. Lung epithelial wound healing in health and disease. *Expert Rev. Respir. Med.* **4,** 647–660 (2010).

48. Akamatsu, T. *et al.* Direct isolation of myofibroblasts and fibroblasts from bleomycin-injured lungs reveals their functional similarities and differences. *Fibrogenesis Tissue Repair* **6,** 15 (2013).

49. Hinz, B. *et al.* The Myofibroblast. *Am. J. Pathol.* **170,** 1807–1816 (2007).

50. Hinz, B. The myofibroblast: Paradigm for a mechanically active cell. *J. Biomech.* **43,** 146–155 (2010).

51. Frankel, S. K. *et al.* TNF-alpha sensitizes normal and fibrotic human lung

fibroblasts to Fas-induced apoptosis. *Am. J. Respir. Cell Mol. Biol.* **34,** 293–304 (2006).

52. White, E. S. Lung extracellular matrix and fibroblast function. *Ann. Am. Thorac. Soc.* **12 Suppl 1,** S30-3 (2015).

53. Hinz, B. *et al.* Recent developments in myofibroblast biology: paradigms for connective tissue remodeling. *Am. J. Pathol.* **180,** 1340–55 (2012).

54. Phan, S. H. Genesis of the myofibroblast in lung injury and fibrosis. *Proc. Am. Thorac. Soc.* **9,** 148–52 (2012).

55. Malmström, J. *et al.* Transforming growth factor-beta 1 specifically induce proteins involved in the myofibroblast contractile apparatus. *Mol. Cell. Proteomics* **3,** 466–77 (2004).

56. Eickelberg, O. *et al.* Transforming Growth Factor- 1 Induces Interleukin-6 Expression via Activating Protein-1 Consisting of JunD Homodimers in Primary Human Lung Fibroblasts. *J. Biol. Chem.* **274,** 12933–12938 (1999).

57. Malmstrom, J. *et al.* Proteome Annotations and Identifications of the Human Pulmonary research articles. *J. Proteome Res.* **3,** 525–537 (2004).

58. Ng, C. P., Hinz, B. & Swartz, M. a. Interstitial fluid flow induces myofibroblast differentiation and collagen alignment in vitro. *J. Cell Sci.* **118,** 4731–9 (2005).

59. Barnes, T. C., Anderson, M. E. & Moots, R. J. The many faces of interleukin-6: the role of IL-6 in inflammation, vasculopathy, and fibrosis in systemic sclerosis. *Int. J. Rheumatol.* **2011,** 721608 (2011).

60. Sampson, N., Berger, P. & Zenzmaier, C. Therapeutic Targeting of Redox Signaling in Myofibroblast Differentiation and Age-Related Fibrotic Disease. *Oxid. Med. Cell. Longev.* **2012,** 1–15 (2012).

61. Ramos, C. *et al.* Fibroblasts from Idiopathic Pulmonary Fibrosis and Normal Lungs Differ in Growth Rate, Apoptosis, and Tissue Inhibitor of Metalloproteinases Expression. *Am. J. Respir. Cell Mol. Biol.* **24,** 591–598 (2001).

62. Beauséjour, C. M. *et al.* Reversal of human cellular senescence: roles of the p53 and p16 pathways. *Eur. Mol. Biol. Organ. J.* **22,** 4212–22 (2003).

63. Naylor, R. M., Baker, D. J. & van Deursen, J. M. Senescent cells: a novel therapeutic target for aging and age-related diseases. *Clin. Pharmacol. Ther.* **93,** 105–16 (2013).

64. Campisi, J. Senescent cells, tumor suppression, and organismal aging: good citizens, bad neighbors. *Cell* **120,** 513–22 (2005).

65. Takahashi, A., Aoshiba, K. & Nagai, A. Apoptosis of wound fibroblasts induced by oxidative stress. *Exp. Lung Res.* **28,** 275–284 (2002).

66. Deslee, G. *et al.* Cigarette smoke induces nucleic-acid oxidation in lung fibroblasts. *Am. J. Respir. Cell Mol. Biol.* **43,** 576–84 (2010).

67. van der Vaart, H., Postma, D. S., Timens, W. & ten Hacken, N. H. T. Acute effects of cigarette smoke on inflammation and oxidative stress: a review. *Thorax* **59,** 713–21 (2004).

68. Lemmon, C. a & Romer, L. H. A predictive model of cell traction forces based on cell geometry. *Biophys. J.* **99,** L78-80 (2010).

69. Tan, J. L. *et al.* Cells lying on a bed of microneedles: an approach to isolate mechanical force. *Proc. Natl. Acad. Sci. U. S. A.* **100,** 1484–9 (2003).

70. Hakim, V. & Silberzan, P. Collective cell migration: a physics perspective. *Reports Prog. Phys.* **80,** 076601 (2017).

71. Sepúlveda, N. *et al.* Collective Cell Motion in an Epithelial Sheet Can Be Quantitatively Described by a Stochastic Interacting Particle Model. *PLoS Comput. Biol.* **9,** e1002944 (2013).

72. Dyer, J. M. *et al.* Tracking Shallow Chemical Gradients by Actin-Driven Wandering of the Polarization Site. *Curr. Biol.* **23,** 32–41 (2013).

73. Caballero, D., Voituriez, R. & Riveline, D. Protrusion Fluctuations Direct Cell Motion. *Biophys. J.* **107,** 34–42 (2014).

74. Comelles, J. *et al.* Cells as Active Particles in Asymmetric Potentials: Motility under External Gradients. *Biophys. J.* **107,** 1513–1522 (2014).

75. Ghibaudo, M. *et al.* Substrate Topography Induces a Crossover from 2D to 3D Behavior in Fibroblast Migration. *Biophys. J.* **97,** 357–368 (2009).

76. Ruprecht, V. *et al.* Cortical Contractility Triggers a Stochastic Switch to Fast Amoeboid Cell Motility. *Cell* **160,** 673–685 (2015).

77. Chi, Q. *et al.* Rear actomyosin contractility-driven directional cell migration in three-dimensional matrices: a mechano-chemical coupling mechanism. *J. R. Soc. Interface* **11,** 20131072–20131072 (2014).

78.  Friedl, P. & Wolf, K. Plasticity of cell migration: a multiscale tuning model. *J. Cell Biol.* **188,** 11–19 (2010).

79.  Zegers, M. M. & Friedl, P. Rho GTPases in collective cell migration. *Small GTPases* **5,** e983869 (2014).

80.  Haeger, A., Wolf, K., Zegers, M. M. & Friedl, P. Collective cell migration: Guidance principles and hierarchies. *Trends in Cell Biology* **25,** 556–566 (2015).

81.  Schwarz, U. S., Nelson, C. M. & Silberzan, P. Proteins, cells, and tissues in patterned environments. *Soft Matter* **10,** 2337 (2014).

82.  Wilson, C. A. *et al.* Myosin II contributes to cell-scale actin network treadmilling through network disassembly. *Nature* **465,** 373–377 (2010).

83.  Roycroft, A. & Mayor, R. Molecular basis of contact inhibition of locomotion. *Cell. Mol. Life Sci.* **73,** 1119–1130 (2016).

84.  Barnhart, E., Lee, K.-C., Allen, G. M., Theriot, J. A. & Mogilner, A. Balance between cell−substrate adhesion and myosin contraction determines the frequency of motility initiation in fish keratocytes. *Proc. Natl. Acad. Sci.* **112,** 5045–5050 (2015).

85.  Barnhart, E. L., Lee, K.-C., Keren, K., Mogilner, A. & Theriot, J. A. An Adhesion-Dependent Switch between Mechanisms That Determine Motile Cell Shape. *PLoS Biol.* **9,** e1001059 (2011).

86.  Keren, K. *et al.* Mechanism of shape determination in motile cells. *Nature* **453,** 475–480 (2008).

87.  Abercrombie, M. & Heaysman, J. E. M. OBSERVATIONS ON THE SOCIAL BEHAVIOUR OF CELLS IN TISSUE CULTURE II. 'Monolayering' of Fibroblasts. *Exp. Cell Res.* **6,** 293–306 (1954).

88.  Abercrombie, M., Heaysman, J. E. M. & Pegrum, S. M. THE LOCOMOTION OF FIBROBLASTS IN CULTURE I. Movements of the Leading Edge. *Exp. Cell Res.* **59,** 393–398 (1970).

89.  Abercrombie, M., Heaysman, J. E. M. & Pegrum, S. M. THE LOCOMOTION OF FIBROBLASTS IN CULTURE II. 'Ruffling'. *Exp. Cell Res.* **60,** 437–444 (1970).

90.  Abercrombie, M., Heaysman, J. E. M. & Pegrum, S. M. The locomotion of fibroblasts in culture. III. Movements of particles on the dorsal surface of the leading lamella. *Exp. Cell Res.* **62,** 389–398 (1970).

91. Petitjean, L. *et al.* Velocity fields in a collectively migrating epithelium. *Biophys. J.* **98,** 1790–1800 (2010).

92. Mayor, R. & Etienne-Manneville, S. The front and rear of collective cell migration. *Nat. Rev. Mol. Cell Biol.* **17,** 97–109 (2016).

93. STOKER, M. G. P. & RUBIN, H. Density Dependent Inhibition of Cell Growth in Culture. *Nature* **215,** 171–172 (1967).

94. Takai, Y., Miyoshi, J., Ikeda, W. & Ogita, H. Nectins and nectin-like molecules: roles in contact inhibition of cell movement and proliferation. *Nat. Rev. Mol. Cell Biol.* **9,** 603–615 (2008).

95. Garcia, S. *et al.* Physics of active jamming during collective cellular motion in a monolayer. *Proc. Natl. Acad. Sci.* **112,** 15314–15319 (2015).

96. Farooqui, R. & Fenteany, G. Multiple rows of cells behind an epithelial wound edge extend cryptic lamellipodia to collectively drive cell-sheet movement. *J. Cell Sci.* **118,** 51–63 (2005).

97. Tambe, D. T. *et al.* Collective cell guidance by cooperative intercellular forces. *Nat. Mater.* **10,** 469–75 (2011).

98. Loeb, L. AMOEBOID MOVEMENT, TISSUE FORMATION AND CONSISTENCY OF PROTOPLASM. *Science (80-. ).* **53,** 261–262 (1921).

99. Camley, B. A. & Rappel, W.-J. Physical models of collective cell motility: from cell to tissue. *J. Phys. D. Appl. Phys.* **50,** 113002 (2017).

100. Leontieva, O. V., Demidenko, Z. N. & Blagosklonny, M. V. Contact inhibition and high cell density deactivate the mammalian target of rapamycin pathway, thus suppressing the senescence program. *Proc. Natl. Acad. Sci.* **111,** 8832–8837 (2014).

101. Seluanov, A. *et al.* Hypersensitivity to contact inhibition provides a clue to cancer resistance of naked mole-rat. *Proc. Natl. Acad. Sci.* **106,** 19352–19357 (2009).

102. Duclos, G., Garcia, S., Yevick, H. G. & Silberzan, P. Perfect nematic order in confined monolayers of spindle-shaped cells. *Soft Matter* **10,** 2346–2353 (2014).

103. Deforet, M., Hakim, V., Yevick, H. G., Duclos, G. & Silberzan, P. Emergence of collective modes and tri-dimensional structures from epithelial confinement. *Nat. Commun.* **5,** 3747 (2014).

104. Buganza Tepole, A. & Kuhl, E. Systems-based approaches toward wound healing. *Pediatr. Res.* **73,** 553–563 (2013).

105. Buganza-Tepole, A., Steinberg, J. P., Kuhl, E. & Gosain, A. K. Application of Finite Element Modeling to Optimize Flap Design with Tissue Expansion. *Plast. Reconstr. Surg.* **134,** 785–792 (2014).

106. Cai, A. Q., Landman, K. A. & Hughes, B. D. Multi-scale modeling of a wound-healing cell migration assay. *J. Theor. Biol.* **245,** 576–594 (2007).

107. Holmes, W. R., Park, J., Levchenko, A. & Edelstein-Keshet, L. A mathematical model coupling polarity signaling to cell adhesion explains diverse cell migration patterns. *PLOS Comput. Biol.* **13,** e1005524 (2016).

108. Ramaswamy, S. The Mechanics and Statistics of Active Matter. *Annu. Rev. Condens. Matter Phys.* **1,** 323–345 (2010).

109. Ben Amar, M. & Wu, M. Re-epithelialization: advancing epithelium frontier during wound healing. *J. R. Soc. Interface* **11,** 20131038–20131038 (2014).

110. Javierre, E., Vermolen, F. J., Vuik, C. & van der Zwaag, S. A mathematical analysis of physiological and morphological aspects of wound closure. *J. Math. Biol.* **59,** 605–630 (2009).

111. Garzón-Alvarado, D. A., Cárdenas Sandoval, R. P. & Vanegas Acosta, J. C. A mathematical model of medial collateral ligament repair: migration, fibroblast proliferation and collagen formation. *Comput. Methods Biomech. Biomed. Engin.* **15,** 571–583 (2012).

112. Reynolds, A., Koombua, K., Pidaparti, R. M. & Ward, K. R. Cellular automata modeling of pulmonary inflammation. *Mol. Cell. Biomech.* **9,** 141–56 (2012).

113. Brown, B. N. *et al.* An agent-based model of inflammation and fibrosis following particulate exposure in the lung. *Math. Biosci.* **231,** 186–96 (2011).

114. An, G., Mi, Q., Dutta-Moscato, J. & Vodovotz, Y. Agent-based models in translational systems biology. *Wiley Interdiscip. Rev. Syst. Biol. Med.* **1,** 159–171 (2009).

115. Chiacchio, F., Pennisi, M., Russo, G., Motta, S. & Pappalardo, F. Agent-based modeling of the immune system: NetLogo, a promising framework. *Biomed Res. Int.* **2014,** 907171 (2014).

116. Vodovotz, Y. *et al.* Mechanistic simulations of inflammation: Current state and future prospects. *Math. Biosci.* **217,** 1–10 (2009).

117. Nikolai, C. & Madey, G. Tools of the Trade: A Survey of Various Agent Based Modeling Platforms. *J. Artif. Soc. Soc. Simul.* **12,** (2009).

118. An, G. Introduction of an agent-based multi-scale modular architecture for dynamic knowledge representation of acute inflammation. *Theor. Biol. Med. Model.* **5,** 11 (2008).

119. Wilensky, U. NetLogo. (1999).

120. González-Valverde, I. & García-Aznar, J. M. Mechanical modeling of collective cell migration: An agent-based and continuum material approach. *Comput. Methods Appl. Mech. Eng.* **337,** 246–262 (2018).

121. Rueden, C. T. *et al.* ImageJ2: ImageJ for the next generation of scientific image data. *BMC Bioinformatics* **18,** 529 (2017).

122. Schindelin, J. *et al.* Fiji: an open-source platform for biological-image analysis. *Nat. Methods* **9,** 676–682 (2012).

123. BOLTE, S. & CORDELIÈRES, F. P. A guided tour into subcellular colocalization analysis in light microscopy. *J. Microsc.* **224,** 213–232 (2006).

124. HAYFLICK, L. & MOORHEAD, P. S. The serial cultivation of human diploid cell strains. *Exp. Cell Res.* **25,** 585–621 (1961).

125. Petrie, R. J., Doyle, A. D. & Yamada, K. M. Random versus directionally persistent cell migration. *Nat. Rev. Mol. Cell Biol.* **10,** 538–549 (2009).

126. Bass, M. D. *et al.* A Syndecan-4 Hair Trigger Initiates Wound Healing through Caveolin- and RhoG-Regulated Integrin Endocytosis. *Dev. Cell* **21,** 681–693 (2011).

127. Zou, H., Stoppani, E., Volonte, D. & Galbiati, F. Caveolin-1, cellular senescence and age-related diseases. *Mech. Ageing Dev.* **132,** 533–542 (2011).

128. Volonte, D. *et al.* Oxidative Stress-induced Inhibition of Sirt1 by Caveolin-1 Promotes p53-dependent Premature Senescence and Stimulates the Secretion of Interleukin 6 (IL-6). *J. Biol. Chem.* **290,** 4202–4214 (2015).

129. Cho, K. A. *et al.* Morphological Adjustment of Senescent Cells by Modulating Caveolin-1 Status. *J. Biol. Chem.* **279,** 42270–42278 (2004).

130. Debacq-Chainiaux, F., Erusalimsky, J. D., Campisi, J. & Toussaint, O. Protocols to detect senescence-associated beta-galactosidase (SA-betagal) activity, a biomarker of senescent cells in culture and in vivo. *Nat. Protoc.* **4,** 1798–806 (2009).

131. Orjalo, A. V., Bhaumik, D., Gengler, B. K., Scott, G. K. & Campisi, J. Cell surface-bound IL-1 is an upstream regulator of the senescence-associated IL-6/IL-8 cytokine network. *Proc. Natl. Acad. Sci.* **106,** 17031–17036 (2009).

132. Dietrich, C., Wallenfang, K., Oesch, F. & Wieser, R. Differences in the mechanisms of growth control in contact-inhibited and serum-deprived human fibroblasts. *Oncogene* **15,** 2743–2747 (1997).

133. Hellermann, G. R., Nagy, S. B., Kong, X., Lockey, R. F. & Mohapatra, S. S. Mechanism of cigarette smoke condensate-induced acute inflammatory response in human bronchial epithelial cells. *Respir. Res.* **3,** 22 (2002).

134. Anto, R. J., Mukhopadhyay, A., Shishodia, S., Gairola, C. G. & Aggarwal, B. B. Cigarette smoke condensate activates nuclear transcription factor-kappaB through phosphorylation and degradation of IkappaB(alpha): correlation with induction of cyclooxygenase-2. *Carcinogenesis* **23,** 1511–1518 (2002).

135. Nakamura, Y. *et al.* Cigarette smoke inhibits lung fibroblast proliferation and chemotaxis. *Am. J. Respir. Crit. Care Med.* **151,** 1497–503 (1995).

136. Pierson, T., Learmonth-Pierson, S., Pinto, D. & van Hoek, M. L. Cigarette smoke extract induces differential expression levels of beta-defensin peptides in human alveolar epithelial cells. *Tob. Induc. Dis.* **11,** 10 (2013).

137. Pace, E. *et al.* Cigarette smoke increases Toll-like receptor 4 and modifies lipopolysaccharide-mediated responses in airway epithelial cells. *Immunology* **124,** 401–411 (2008).

138. Kulkarni, R. *et al.* Cigarette Smoke Inhibits Airway Epithelial Cell Innate Immune Responses to Bacteria. *Infect. Immun.* **78,** 2146–2152 (2010).

139. Ning, W. *et al.* Cigarette smoke stimulates matrix metalloproteinase-2 activity via EGR-1 in human lung fibroblasts. *Am. J. Respir. Cell Mol. Biol.* **36,** 480–90 (2007).

140. Vandivier, R. W., Henson, P. M. & Douglas, I. S. Burying the Dead. *Chest* **129,** 1673–1682 (2006).

141. McCubbrey, A. L. & Curtis, J. L. Efferocytosis and Lung Disease. *Chest* **143,** 1750–1757 (2013).

142. Saleh, T. *et al.* Reversibility of chemotherapy-induced senescence is independent of autophagy and a potential model for tumor dormancy and cancer recurrence. *bioRxiv* (2017). doi:https://doi.org/10.1101/099812

143. Wang, X. *et al.* Feedback Activation of Basic Fibroblast Growth Factor Signaling via the Wnt/β-Catenin Pathway in Skin Fibroblasts. *Front. Pharmacol.* **08,** 32 (2017).

144. Abdalla, M., Goc, A., Segar, L. & Somanath, P. R. Akt1 Mediates α-Smooth Muscle

Actin Expression and Myofibroblast Differentiation via Myocardin and Serum Response Factor. *J. Biol. Chem.* **288,** 33483–33493 (2013).

145. Alfveby, J. Native NADH As A Biomarker For Oxidative Stress In Living Cells. (University of Minnesota, 2014).

146. Weinberg, S. H., Mair, D. B. & Lemmon, C. A. Mechanotransduction Dynamics at the Cell-Matrix Interface. *Biophys. J.* **112,** 1962–1974 (2017).

147. Sandbo, N. *et al.* Control of myofibroblast differentiation by microtubule dynamics through a regulated localization of mDia2. *J. Biol. Chem.* **288,** 15466–15473 (2013).

148. Miki, H. *et al.* Glucocorticoid-induced contractility and F-actin content of human lung fibroblasts in three-dimensional culture. *Am. J. Physiol. Cell. Mol. Physiol.* **278,** L13–L18 (2000).

149. Park, J. T. *et al.* A crucial role of ROCK for alleviation of senescence-associated phenotype. *Exp. Gerontol.* **106,** 8–15 (2018).

150. Schafer, M. J., Haak, A. J., Tschumperlin, D. J. & LeBrasseur, N. K. Targeting Senescent Cells in Fibrosis: Pathology, Paradox, and Practical Considerations. *Curr. Rheumatol. Rep.* **20,** 3 (2018).

151. Vogelmeier, C. F. *et al.* Global Strategy for the Diagnosis, Management, and Prevention of Chronic Obstructive Lung Disease 2017 Report. GOLD Executive Summary. *Am. J. Respir. Crit. Care Med.* **195,** 557–582 (2017).

152. Dunkern, T. R., Feurstein, D., Rossi, G. A., Sabatini, F. & Hatzelmann, A. Inhibition of TGF-β induced lung fibroblast to myofibroblast conversion by phosphodiesterase inhibiting drugs and activators of soluble guanylyl cyclase. *Eur. J. Pharmacol.* **572,** 12–22 (2007).

153. Roth, M. Airway and Lung Remodelling in Chronic Pulmonary Obstructive Disease: A Role for Muscarinic Receptor Antagonists? *Drugs* **75,** 1–8 (2015).

154. Milara, J. *et al.* Aclidinium inhibits cigarette smoke-induced lung fibroblast-to-myofibroblast transition. *Eur. Respir. J.* **41,** 1264–1274 (2013).

155. Chen, Y. *et al.* Vitamin C Mitigates Oxidative Stress and Tumor Necrosis Factor-Alpha in Severe Community-Acquired Pneumonia and LPS-Induced Macrophages. *Mediators Inflamm.* **2014,** (2014).

156. Mohammed, B. M. *et al.* Vitamin C promotes wound healing through novel pleiotropic mechanisms. *Int. Wound J.* **13,** 572–584 (2016).

157. Lim, J.-H. *et al.* Sirtuin 1 Modulates Cellular Responses to Hypoxia by Deacetylating Hypoxia-Inducible Factor 1α. *Mol. Cell* **38,** 864–878 (2010).

158. Edatt, L., Maurya, A. K., Raji, G., Kunhiraman, H. & Kumar, S. V. B. MicroRNA106a regulates matrix metalloprotease 9 in a sirtuin-1 dependent mechanism. *J. Cell. Physiol.* **233,** 238–248 (2018).

159. Nakamaru, Y. *et al.* A protein deacetylase SIRT1 is a negative regulator of metalloproteinase-9. *FASEB J.* **23,** 2810–2819 (2009).

160. Rahman, I., Kinnula, V. L., Gorbunova, V. & Yao, H. SIRT1 as a therapeutic target in inflammaging of the pulmonary disease. *Prev. Med. (Baltim).* **54,** S20–S28 (2012).

# **APPENDIX A**

```
;; NETLOGO MODEL FOR IN VITRO FIBROBLAST WOUND HEALING
;; VERSION 1.2 - updated 03/23/2018
;; BY JAMES ALEX RATTI


;=============================================================|
;; VARIABLE & CONSTANT DEFINITIONS

globals [
 Iheight ; in vitro image height
 maxC    ; modeled world's max coordinate (sets resolution)
 ds      ; patch length (=image size/101)
         ; { Patch Area = (101)^2 patches, due to origin + axes }
         ; { correlates to cropped image size of 1677x1677 um   }
 dt      ; step interval (arbitrary)
         ; { model functions in step intervals = dt * tick      }
         ; { such that there will be '1/dt' steps per tick.     }
         ; { tick units = hours (arbitrary)                     }
         ; { b/c model timer only counts ticks in whole numbers }

 time_SS ; in vitro seed-scratch time for scratch assays
         ; { mean+/-sd of in vitro seed-scratch times = 14+/-   }
 I_AR    ; in vitro image area (frm 2244.6x1677.0 for square dim.)
 Rs_AR   ; in vitro mean scratch area @ t=0, from all assays
 Rc_AR   ; in vitro cell-covered area
 %s_AR   ; in vitro ratio of scratched area to cropped image area
 Vs_AR   ; virtual scratch size [patches]
 Scratch_width    ; num. full rows per side (excluding center)
 Scratch_center   ; num. patches in filled rows
 Scratch_edges    ; num. patches in unfilled rows (ragged edge)
 Scratch ; virtual initial scratched region (patch-set)
 Healed  ; virtual healed region (patch-set)
 UnHealed; vitrual unhealed region (patch-set)
 UnHealed_edge    ; virtual unhealed region's border (patch-set)
 Edge_length_t0   ; unhealed region's est. border length @t=0 [um]
 Cell_AR ; individual cell area (assumed circular)
```

N_diam  ; in vitro diameter for NHLF
        ; selected* to fit cells w/ and w/o aSMA, within 1SD
        ; { *lit. avg    = 35.8+/-7.0 um (with aSMA)       }
        ; {                = 25.7+/-5.8 um (without aSMA)     }


Pop_Sm  ; initial agent population, der. from seeding density
        ; { derived from in vitro seeding density for MTTs    }
        ; { Pop_S = Pop_S*(IPop_S + APop_S + SPop_S)          }
Pop_Ss  ; initial agent population, der. from seeding density
        ; { derived from in vitro seeding density for scratches}
        ; { Pop_S = Pop_S*(IPop_S + APop_S + SPop_S)          }
Pop_Ss6 ; agent population at t=seed+6
IPop_S  ; initial population ratio of inactive fibs @t=seed+6
APop_S  ; initial population ratio of activated fibs @t=seed+6
MPop_S  ; initial population ratio of myo-fibs @t=seed+6
SPop_S  ; initial population ratio of senescent fibs @t=seed+6
DPop_S  ; initial population ratio of dead fibs @ t=seed+6
Pop_A   ; initial agent population, der. from cell areas
        ; { derived from approx. confluency and cell diameter  }
        ; { Pop_A = Pop_A*(IPop_A + APop_A + SPop_A)          }
IPop_A  ; initial population ratio of inactive fibs @confluency
APop_A  ; initial population ratio of activated fibs @confluency
MPop_A  ; initial population ratio of myo-fibs @confluency
SPop_A  ; initial population ratio of senescent fibs @confluency
Pop_t00 ; initial seeded cell population, from Pop_S or Pop_A
Pop_t00I; initial population of inactive fibs
Pop_t00A; initial population of active fibs
Pop_t00M; initial population of myo-fibs
Pop_t00S; initial population of senescent fibs
Pop_t0  ; initial cell population on non-scratch areas, estimated

stim_max; 'stimulation' maximum (for scaling reference)
stim_Ta ; 'stimulation' threshold w 50% fibroblast activation per hr
stim_T-a; 'stimulation' threshold w 50% fib deactivation per hr
stim_Tm ; 'stimulation' treshold w 50% AFib->MFib transition per hr
stim_Ts ; 'stimulation' threshold w 50% fibroblast senescence per hr
Alpha_Z ; size coefficient for inactivate fibs
Alpha_M ; migration coefficient for inactivate fibs
Alpha_P ; prolif. coefficient for inactivate fibs
Alpha_D ; death coefficient for inactivate fibs
Beta_Z  ; size coefficient for activated (proto-myo-)fibs
Beta_M  ; migration coefficient for activated (proto-myo-) fibs

Beta_P  ; prolif. coefficient for activated (proto-myo-)fibs
Beta_D  ; death coefficient for activated (proto-myo-)fibs
Gamma_Z ; size coefficient for myo-fibs
Gamma_M ; migration coefficient for myo-fibs
Gamma_P ; prolif. coefficient for myo-fibs
Gamma_D ; death coefficient for myo-fibs
Omega_Z ; size coefficient for senescent fibs
Omega_M ; migration coefficient for senescent fibs
Omega_P ; prolif. coefficient for senescent fibs
Omega_D ; death coefficient for senescent fibs

Fsize   ; baseline fib diameter [patches]
IFsize  ; IFib diameter [patches]
AFsize  ; AFib diameter [patches]
MFsize  ; MFib diameter [patches]
SFsize  ; SFib diameter [patches]
IFsplit ; dist. req. for IFibs to divide (fnx. of diameter)
AFsplit ; dist. req. for AFibs to divide (fnx. of diameter)
MFsplit ; dist. req. for MFibs to divide (fnx. of diameter)
SFsplit ; dist. req. for SFibs to divide (fnx. of diameter)
IFmove  ; dist. req. for IFibs to move (fnx. of diameter)
AFmove  ; dist. req. for AFibs to move (fnx. of diameter)
MFmove  ; dist. req. for MFibs to move (fnx. of diameter)
SFmove  ; dist. req. for SFibs to move (fnx. of diameter)

Fstep   ; baseline fib step size (ref = IFibs)        = Migration_rate*dt/ds
IFspeed ; IFib step size [patch/tick]         = Fspeed*Alpha_Z
AFspeed ; AFib step size [patch/tick]          = Fspeed*Beta_M
MFspeed ; MFib step size [patch/tick]           = Fspeed*Gamma_M
SFspeed ; SFib step size [patch/tick]          = Fspeed*Omega_M
t_life  ; agent lifespan mean                = Death_rate
sd_life ; agent lifespan std dev              = t_life/3
t_div   ; agent doubling time mean             = Prolif_rate
sd_div  ; agent doubling time std dev            = t_div/3
        ; {mean+-sd = 33.2 +- 10.4 hrs (for NHLF in FGM) }
        ; {lit. source: [Mio et al. 1992]            }
m_stim  ; agent stimulation rate mean            = Stim_mean
]

patches-own [
 V1_score  ; ratio of neighbors without an agent (excluding Apops) present (max=1)
 V2_score  ; average of neighbors' V1_scores (max=1)
 ]

```
turtles-own [
  Fspeed    ; step size for fibroblast
  fission   ; countdown to fibroblast division (divide @ fission<=0)
  life      ; countdown to fibroblast rep-senescence (sen @ life<=0)
  Zsense    ; factor for sensitivity to stimuli
  stim      ; counter for fibroblast stimulation (min=0, max=1)
  P_die     ; probability of fibroblast death
  P_senesce ; probability for fibroblasts to senesce due to stimuli
  ]

breed [ IFibs IFib ] ; INACTIVE FIBROBLASTS  (mobile; solid/hollow triangles)
IFibs-own [
  P_activate       ; probability for inactivated fibroblasts to activate
  ]

breed [ AFibs AFib ] ; ACTIVE PROTO-MYO-FIBROBLASTS (mobile; solid/hollow
squares)
AFibs-own [
  P_deactivate      ; probability for activated fibroblasts to deactivate
  P_transmyo        ; probability for activated fibroblasts to become myofibroblasts
  ]

breed [ MFibs MFib ] ; MYO-FIBROBLASTS    (mobile; spade/club card symbols)

breed [ SFibs SFib ] ; SENESCENT FIBROBLASTS (mobile; g/b/r, solid/hollow circles)

breed [ Apops Apop ] ; DEAD CELLS / APOPTOTIC BODIES (immobile markers; white
stars)
```

```
;================================================================|
;; MODEL INITIATION
to setup
  clear-all

  ; SETS CONSTANTS FOR TIME/SPACE RESOLUTION
  set maxC 50              ; sets world's max coordinate   = 50     patches
  resize-world (-1 * maxC) maxC (-1 * maxC) maxC ; world size   = 101*101 patches
  set Iheight 1677         ; in vitro image height       = 1677   um
  set ds Iheight / world-height ; patch length             = 16.604  um/patch
  set dt 20 / 60           ; step interval               =[ 20    min/step]
  set N_diam 30            ; NHLF diameter               = 30     um

  ; SETS CONSTANTS FOR SCRATCH DIMENSIONS
  set I_AR Iheight ^ 2         ; in vitro image area         = 2812329 um^2
  set Rs_AR 1296089.3932       ; in vitro scratch area        = 1296089 um^2
  set %s_AR Rs_AR / I_AR       ; scratch area as ratio        = 0.4609
  set Vs_AR round (%s_AR * world-height ^ 2); virt. scratch area = 4701    patches
  set Rc_AR (I_AR - Rs_AR)     ; in vitro cell-covered area    = 1516240 um^2
  set time_SS time_seed-scratch / dt ; in vitro seed-scratch time= 42      steps

  ; SETS CONSTANTS FOR STIM. FUNCTION & CELL-STATE TRANSITIONS
  set stim_max 1              ; stim maximum per hr
  set stim_Ta 0.0001          ; stim threshold(a)  = lvl w 50% activation/hr
  set stim_T-a stim_Ta        ; stim threshold(-a) = lvl w 50% deactivation/hr
  set stim_Tm 0.06            ; myofib stim threshold
  set stim_Ts 0.1             ; senescence stim threshold
  set Alpha_Z 0.75            ; Inactive fib size coeff.
  set Alpha_M 0               ; Inactive fib speed coeff.
  set Alpha_P 1               ; Inactive fib proliferation period coeff.
  set Alpha_D 1               ; Inactive fib death period coeff.
  set Beta_Z 1                ; Activated fib size coeff.
  set Beta_M 1                ; Activated fib speed coeff.
  set Beta_P 1                ; Activated fib proliferation period coeff.
  set Beta_D 1                ; Activated fib death period coeff.
  set Gamma_Z 1.4             ; Myo- fib size coeff.
  set Gamma_M .625            ; Myo- fib speed coeff.
  set Gamma_P 1.4             ; Myo- fib proliferation period coeff.
  set Gamma_D 1.4             ; Myo- fib death period coeff.
  set Omega_Z 2               ; Senescent fib size coeff.
  set Omega_M .75             ; Senescent fib speed coeff.
  set Omega_P 1000            ; Senescent fib proliferation period coeff.
  set Omega_D 1000            ; Senescent fib death period coeff.
```

```
; SETS CONSTANTS FOR CELL LINES AND MEDIA TREATMENTS
set-default-shape Apops "star"
set-default-shape IFibs "default"   ; IFib shape
set-default-shape AFibs "square"    ; AFib shape
set-default-shape MFibs "suit spade"; MFib shape
set-default-shape SFibs "circle"    ; SFib shape
set Fsize (N_diam / ds)          ; baseline diameter    = 1.8068  patches
set IFsize (Fsize * Alpha_Z)      ; IFib diameter       = 1.8068  patches
set AFsize (Fsize * Beta_Z)       ; AFib diameter       =       patches
set MFsize (Fsize * Gamma_Z)      ; MFib diameter       =       patches
set SFsize (Fsize * Omega_Z)      ; SFib diameter       =       patches
set Cell_AR (pi * (N_diam / 2)^ 2) ; NHLF cell area     = 706.86  um^2
set IPop_A 0.00             ; Inactive fib ratio @ confl.  = 0
set APop_A 0.74             ; Active fib ratio @ confl.    = 0.74
set MPop_A 0.15             ; Active fib ratio @ confl.    = 0.15
set SPop_A 0.11             ; Senescent fib ratio @ confl. = 0.11
set IPop_S 0               ; Inactive fib ratio @ t=seed+6  =
set MPop_S 0.0435           ; Myo-fib ratio @ t=seed+6      =
set SPop_S 0.1191           ; Senescent fib ratio @ t=seed+6 =
set DPop_S 0.0148           ; Dead fib ratio @ t=seed+6
set APop_S (1 - Ipop_S - MPop_S - SPop_S - DPop_S);Active fib ratio @t=seed+6


; SETS PARAMS FOR MIGRATION, DIVISION, DEATH & STIM COUNTERS
set Fstep (65 * dt / ds)   ; baseline fib speed  = {NHLF*FGM} FOR PRE-COND.
set IFspeed Fstep * Alpha_M       ; IFib speed
set AFspeed Fstep * Beta_M        ; AFib speed
set MFspeed Fstep * Gamma_M        ; MFib speed
set SFspeed Fstep * Omega_M        ; SFib speed

set t_div 27 / dt        ; division rate mean
set sd_div t_div / 3            ; division rate st.dev.  = {P}   hrs

set t_life 40 * t_div          ; base lifespan mean     = 40*{P} hrs
set sd_life 40 * sd_div          ; base lifespan st.dev.  = 40*{P} hrs

set m_stim 0.0002 * dt     ; 'stimulation' rate mean = {NHLF*FGM} FOR PRE-COND.

; INITIATES ("SEEDS") FIBROBLASTS
set Pop_A round (I_AR / Cell_AR)     ; agent pop. @100%confl. = 3979  agents
set Pop_Ss round (4E5 * I_AR / 9.6E8); IV-det agent pop.($cr) = 1172  agents
set Pop_Sm round (2E4 * I_AR / 3.2E7); IV-det agent pop.(MTT) = 1758  agents
```

```
if Seed_Density = "Max Confluency" [ ; seeds fibs @100%confl. ignoring overlaps
  set Pop_t00 Pop_A
  set Pop_t00I round(Pop_t00 * IPop_A)
  set Pop_t00A round(Pop_t00 * APop_A)
  set Pop_t00M round(Pop_t00 * MPop_A)
  set Pop_t00S round(Pop_t00 * SPop_A)
 ]
if Seed_Density = "In Vitro" [      ; seeds fibs @ in vitro seeding density:
  if Experiment_Type = "Culture Cond." [    ; sets seeding density for 96wells
    ifelse Seed_IFibs_Only? = true [set Pop_t00 Pop_Ss][
      set Pop_t00 Pop_Ss
    ]
  ]
  if Experiment_Type = "Scratch Healing" [  ; sets seeding density for 6wells
    ifelse Seed_IFibs_Only? = true  [set Pop_t00 Pop_Ss][
      set Pop_t00 Pop_Ss
    ]
  ]
  if Experiment_Type = "Barrier Removal" [  ; sets seeding density for 6wells
    ifelse Seed_IFibs_Only? = true  [set Pop_t00 Pop_Ss][
      set Pop_t00 Pop_Ss
    ]
  ]
  set Pop_t00I round(Pop_t00 * IPop_S)
  set Pop_t00A round(Pop_t00 * APop_S)
  set Pop_t00M round(Pop_t00 * MPop_S)
  set Pop_t00S round(Pop_t00 * SPop_S)
 ]
ifelse Seed_IFibs_Only? = true [     ; seeds all agents in inactive state
  ask n-of Pop_t00 patches  [ sprout-IFibs 1 [ train_IFib ] ]
  ask turtles [ set fission ((random-float 1) * t_div) ]
  ask turtles [ set Zsense random-normal 1 0.3 ]
  ][                               ; seeds agent states by proportions
  ask n-of Pop_t00I patches [ sprout-IFibs 1 [ train_IFib ] ]
  ask n-of Pop_t00A patches [ sprout-AFibs 1 [ train_AFib ] ]
  ask n-of Pop_t00M patches [ sprout-MFibs 1 [ train_MFib ] ]
  ask n-of Pop_t00S patches [ sprout-SFibs 1 [ train_SFib ] ]
  ask n-of round(Pop_t00 * DPop_S) patches [ Fib_apoptose ]
  ask turtles [ set fission ((random-float 1) * t_div) ]
  ask turtles [ set Zsense random-normal 1 0.3 ]    ; {NHLF*FGM} for Pre-conditioning
  ]
```

```
; INITIATES AGENTS AND VARIABLES (PRECONDITIONING)
 ifelse Precondition? = true [ Precondition_Fibs
     ; re-initializing parameters to simulate post-scratch interval
   set Fstep (Migrate_rate * dt / ds)  ; baseline fib speed     = {M} patches/step
   set IFspeed Fstep * Alpha_M        ; IFib speed
   set AFspeed Fstep * Beta_M         ; AFib speed
   set MFspeed Fstep * Gamma_M          ; MFib speed
   set SFspeed Fstep * Omega_M          ; SFib speed
   ask IFibs [set Fspeed IFspeed] ; re-sets IFib speed for post-scratch conditions
   ask AFibs [set Fspeed AFspeed] ; re-sets AFib speed for post-scratch conditions
   ask MFibs [set Fspeed MFspeed] ; re-sets MFib speed for post-scratch conditions
   ask SFibs [set Fspeed SFspeed] ; re-sets SFib speed for post-scratch conditions
   set t_div Prolife_rate / dt          ; division rate mean     = {P}   hrs
   set sd_div t_div / 3              ; division rate st.dev.  = {P}   hrs
     ; averages pre+post-interval fission rates (ie cells fully adjust w next cell cycle)
   ask turtles [ set fission ((fission + ((random-float 1) * t_div)) / 2) ]
   set m_stim Stim_rate * dt            ; 'stimulation' rate mean    = {}    stim/step
     ; averages pre+post-interval Zsense dist. to sim degrees of signalling overlap
   ask turtles [ set Zsense ((Zsense + (random-normal 1 Stim_sense)) / 2) ]
   set stim_Tm T_myo                ; stim threshold(m)  = lvl w 50% fib myo-trans. per hr
   set stim_Ts T_sen                ; stim threshold(s)  = lvl w 50% fib senescence per hr
 ] [ ]


; INITIATES WORLD AND SCRATCH AREA (CENTERED AROUND Y-AXIS)
if Experiment_Type = "Culture Cond." [  ; NO CHANGE W/ CULTURE CONDITIONS
   set Scratch_width 0
   set Scratch_center 0
   set Scratch_edges 0
   set Scratch patch-set nobody
   set Pop_t0 count turtles
   ]
if Experiment_Type = "Scratch Healing" [ Scratch_Cells ] ; CREATE SCRATCH
if Experiment_Type = "Barrier Removal" [ Remove_Barrier ]; REMOVE BOUNDARY

 calc_Vscores     ; initiates void scores for plot initialization and model operation
 Measure_Healed   ; initiates/labels Healed and Unhealed Edge regions for reporters
 set Edge_length_t0 Edge_length ; sets initial Unhealed Edge Length for reporters

 reset-ticks      ; sets tick counter to 0 and sets/updates all plots
 setup-plots      ; initiates plots (req. with "tick-advance" notation)
end
```

```
;===============================================================|
;; MODEL OPERATION

to go

  react          ; Fibroblast stim (ticker) + hetero response (stoch. Xforms)
  age            ; Fibroblast replicative senesence (counter)
  divide         ; Fibroblast proliferation (counter)
  migrate        ; Fibroblast migration (see below for mode descriptions)

  calc_Vscores    ; updates void scores for plot updates and model operation
  Measure_Healed   ; updates/labels Healed and UnHealed Edge regions for reporters

  tick-advance dt  ; moves model forward by 1 step = "dt" ticks
  update-plots     ; updates plots with each step (req. with "tick-advance" notation)

  if ticks >= t_end [        ; time limit for the model (slider, default = 24 hrs)
    stop
    repeat 2 [beep wait 1.6]] ; emits 2 beeps spaced 1.6s apart
end


;===============================================================|
;; SHORTCUT TO PRECONDITION AGENT VARIABLES

to Precondition_Fibs

  repeat time_SS [ ; Runs the "go" procedure from below for time_ss iterations
      react         ; Fibroblast stim (ticker) + hetero respone (stoch. Xforms)
      age           ; Fibroblast replicative senesence (counter)
      divide        ; Fibroblast proliferation (counter)
      migrate       ; Fibroblast migration (see below for mode descriptions)
      calc_Vscores   ; Calculates void scores
      ]
end
```

```
;=========================================================|
;; SHORTCUT TO SCRATCH CELL MONOLAYER

to Scratch_Cells
  set Scratch_width floor((Vs_AR - world-height) / (2 * world-height))
     ; scratch width, excluding center and edges [rows/side]  = 45    rows/side
   set Scratch_center (world-height + ((2 * world-height) * Scratch_width))
      ; number of patches in filled rows, including center    = 4545   patches
    set Scratch_edges  Vs_AR - Scratch_center
      ; number of patches in the scratch's "ragged" edge      = 156    patches
    set Scratch ( patch-set
     patches with [ pxcor <= Scratch_width and pxcor >= (-1 * Scratch_width) ]
      n-of Scratch_edges patches with [
       pxcor = (Scratch_width + 1) or pxcor = (-1 * Scratch_width - 1)
       ] )
    ask Scratch [set pcolor grey]          ; tags scratch patches
    ask turtles-on patches with [          ; clears cells from the scratch area & edges
    (pxcor <= (Scratch_width + 2) and pxcor >= (-1 * Scratch_width - 2))
    and (not member? self Apops) ][ die ]
    ifelse Seed_IFibs_Only? [              ; clears 'excess' dead cells
     ask Apops [die] ][
     let dead_pctIV14s round(.0805 * count turtles)
     ifelse count Apops = dead_pctIV14s [][
      if count Apops > dead_pctIV14s [
        ask n-of (count Apops - dead_pctIV14s ) Apops [die] ]
      if count Apops < dead_pctIV14s [
        ask n-of (dead_pctIV14s - count Apops) turtles with [
         not member? self Apops] [
         ask patch-here [Fib_apoptose] die ]]
    ]
    ]
   set Pop_t0 count turtles              ; counts remaining cells for calculations
end
```

;================================================================|
;; SHORTCUT TO REMOVE BARRIER (NOT A TRUE BARRIER REMOVAL)

```
to Remove_Barrier
   set Scratch_width floor((Vs_AR - world-height) / (2 * world-height))
     ; scratch width, excluding center and edges [rows/side]   = 45    rows/side
   set Scratch_center (world-height + ((2 * world-height) * Scratch_width))
     ; number of patches in filled rows, including center      = 4545   patches
   set Scratch_edges  Vs_AR - Scratch_center
     ; number of patches in the scratch's "ragged" edge        = 156    patches
   let Not_Scratch ( patch-set
    patches with [ pxcor <= Scratch_width and pxcor >= (-1 * Scratch_width) ]
    n-of Scratch_edges patches with [
      pxcor = (Scratch_width + 1) or pxcor = (-1 * Scratch_width - 1)
      ] )
   set Scratch (patch-set patches with [not member? self Not_Scratch])
   ask Scratch [ set pcolor grey ]        ; tags non-boundary patches
   ask turtles-on patches with [          ; clears cells from the scratch area & edges
   (member? self Scratch) and (not member? self Apops) ] [ die ]
   ifelse Seed_IFibs_Only? [              ; clears 'excess' dead cells
    ask Apops [die] ][
    let dead_pctIV14s round(.0805 * count turtles)
    ifelse count Apops = dead_pctIV14s [][
     if count Apops > dead_pctIV14s [
       ask n-of (count Apops - dead_pctIV14s ) Apops [die] ]
     if count Apops < dead_pctIV14s [
       ask n-of (dead_pctIV14s - count Apops) turtles with [
        not member? self Apops] [
        ask patch-here [Fib_apoptose] die ]]
   ]
   ]
   set Pop_t0 count turtles              ; counts remaining cells for calculations
end
```

```
;=================================================================|
;; SHORTCUTS TO SET DEFAULT VARIABLES FOR EACH FIBROBLAST STATE
to train_IFib        ; INACTIVATED FIBROBLASTS
   set color 42                  ; ~60% shaded yellow
   set size IFsize
   set Fspeed IFspeed
   set heading random 360
   set life random-normal t_life sd_life
   set fission random-normal t_div sd_div
end
to train_AFib        ; ACTIVATED FIBROBLASTS
   if Media = "FBM" [set color sky]
   if Media = "FGM" [set color turquoise]
   if Media = "CSC" [set color brown]
   set size AFsize
   set Fspeed AFspeed
   set heading random 360
   set life random-normal t_life sd_life
   set fission random-normal t_div sd_div
   set fission (fission + (t_div * (Beta_P - 1)))
end
to train_MFib        ; MYO- FIBROBLASTS
   if Media = "FBM" [set color 82.5]  ; ~50% shaded cyan
   if Media = "FGM" [set color 54]    ; ~20% shaded green
   if Media = "CSC" [set color orange]
   set size MFsize
   set Fspeed MFspeed
   set heading random 360
   set life random-normal t_life sd_life
   set fission random-normal t_div sd_div
   set fission (fission + (t_div * (Gamma_P - 1)))
end
to train_SFib        ; SENESCENT FIBROBLASTS
   if Media = "FBM" [set color 102.5]  ; ~50% shaded blue
   if Media = "FGM" [set color 72.5]   ; ~50% shaded turquoise
   if Media = "CSC" [set color red]
   set size SFsize
   set Fspeed SFspeed
   set heading random 360
   set life random-normal t_life sd_life
   set fission random-normal t_div sd_div
   set fission (fission + (t_div * (Omega_P - 1)))
end
```

```
;================================================================|
;; SHORTCUTS TO TRANSITION BETWEEN FIBROBLAST STATES

to IFib_activate       ; FIBROBLAST ACTIVATION
  set breed AFibs
  if Media = "FBM" [set color sky]
  if Media = "FGM" [set color turquoise]
  if Media = "CSC" [set color brown]
  set size AFsize
  set Fspeed AFspeed
  set fission (fission + (t_div * (Beta_P - 1)))
end

to AFib_deactivate      ; FIBROBLAST DEACTIVATION
  set breed IFibs
  set color 42                   ; ~60% shaded yellow
  set size IFsize
  set Fspeed IFspeed
  set fission (fission - (t_div * (Beta_P - 1)))
end

to AFib_transmyo        ; FIBROBLAST ACTIVATION
  set breed MFibs
  if Media = "FBM" [set color 82.5]    ; ~50% shaded cyan
  if Media = "FGM" [set color 54]      ; ~20% shaded green
  if Media = "CSC" [set color orange]
  set size MFsize
  set Fspeed MFspeed
  set fission (fission + (t_div * (Gamma_P - 1)))
end

to Fib_senesce          ; FIBROBLAST SENESCENCE
  set breed SFibs
  if Media = "FBM" [set color 102.5]     ; ~50% shaded blue
  if Media = "FGM" [set color 72.5]      ; ~50% shaded turquoise
  if Media = "CSC" [set color red]
  set size SFsize
  set Fspeed SFspeed
  set fission (fission + (t_div * (Omega_P - Beta_P)))
end
```

```
;================================================================|
;; SHORTCUT FOR STIMULATION & FIBROBLAST STATE CHANGES

to react
  ask turtles [                         ; Stimulation counter increases each step
    set stim (stim + (Zsense * m_stim))
    ]
  ask turtles [                         ; Prob of fibroblast death
    set P_die (stim / (20 * stim_max))
    if breed = IFibs [ set P_die (P_die / Alpha_D) ] ; applies IFib apoptosis resist
    if breed = AFibs [ set P_die (P_die / Beta_D)  ] ; applies AFib apoptosis resist
    if breed = MFibs [ set P_die (P_die / Gamma_D) ] ; applies MFib apoptosis resist
    if breed = SFibs [ set P_die (P_die / Omega_D) ] ; applies SFib apoptosis resist
    if random-float 1 <= P_die [
      ask patch-here [Fib_apoptose]            ; apoptotic body replaces fib
      die                               ; and fib dies/disappears
      ]]
  ask IFibs [                           ; Prob of fibroblast activation
    set P_activate (stim / (2 * stim_Ta))
    if random-float 1 <= P_activate [
      IFib_activate
      ]]
  ask AFibs [                           ; Prob of fibroblast deactivation
    set P_deactivate (((2 * stim_T-a) - stim) / (2 * (stim_T-a)))
    if random-float 1 <= P_deactivate [
      AFib_deactivate
      ]]
  ask AFibs [                           ; Prob of myofibroblast transition
    set P_transmyo ((stim - stim_Ta) / (2 * (stim_Tm - stim_Ta)))
    if random-float 1 <= P_transmyo [
      AFib_transmyo
      ]]
  ask turtles with [
    (breed = AFibs) or (breed = MFibs) ][     ; Prob of fibroblast senescence
    set P_senesce ((stim - stim_Ta) / (2 * (stim_Ts - stim_Ta)))
    if random-float 1 <= P_senesce [
      Fib_senesce
      ]]
end
```

```
;=================================================================|
;; SHORTCUT FOR PROLIFERATION COUNTER
to divide
  ask turtles [ set fission fission - 1 ]     ; division counter decreases by 1/tick
  ask turtles [
   if (fission <= 0)
   and (any? neighbors with [ ( V2_score > 0.05 )  ; rep. avg V2score @ ~100%confl.
      and (not any? other IFibs in-radius (IFsplit))
      and (not any? other AFibs in-radius (AFsplit))
      and (not any? other MFibs in-radius (MFsplit))
      and (not any? SFibs in-radius (SFsplit)) ])                [
    let parent_breed breed
    let parent_stim stim
    let parent_Zsense Zsense
    let birthplace max-one-of neighbors [ V2_score ]
    if parent_breed = IFibs [
      hatch-IFibs 1 [                 ; spawns new IFib on old IFib
        move-to birthplace              ; moves new IFib to adjacent void patch
        train_IFib                 ; applies default IFib values
        set stim parent_stim             ; stim is conserved between daughter cells
        set Zsense parent_Zsense              ]]        ; stim sensitivity is conserved
    if parent_breed = AFibs [             ; AFibs divide into AFibs
      hatch-AFibs 1 [
        move-to birthplace
        train_AFib
        set stim parent_stim
        set Zsense parent_Zsense           ]]       ; stim sensitivity is conserved
    if parent_breed = MFibs [             ; MFibs divide into MFibs
      hatch-MFibs 1 [
        move-to birthplace
        train_MFib
        set stim parent_stim
        set Zsense parent_Zsense           ]]       ; stim sensitivity is conserved
    if parent_breed = SFibs [            ; SFibs dont divide
      set stim parent_stim              ; stim remains unchanged
      set Zsense parent_Zsense         ]         ; stim sensitivity is conserved
    set fission random-normal t_div sd_div  ; resets counter of old agent
    if breed = IFibs [set fission (fission + (t_div * (Alpha_P - 1)))]
    if breed = AFibs [set fission (fission + (t_div * (Beta_P - 1)))]
    if breed = MFibs [set fission (fission + (t_div * (Gamma_P - 1)))]
    if breed = SFibs [set fission (fission + (t_div * (Omega_P - 1)))]          ]        ]
end
```

```
;================================================================|
;; SHORTCUT TO SPROUT 'APOPTOTIC BODIES' FROM DEAD FIBROBLASTS

to Fib_apoptose        ; DEAD CELLS
  sprout-Apops 1 [
    set color white
  ]
end


;================================================================|
;; SHORTCUT FOR REPLICATIVE SENESCENCE COUNTER

to age
  ask turtles [ set life life - 1 ]    ; Life counter decreases by 1 each tick.
  ask turtles with [ not member? self Apops ] [
    if life <= 0 [                  ; When life counter of living agent runs out,
      Fib_senesce                   ; fibroblast agent becomes senescent
      ]
  ]
end
```

```
;================================================================|
;; META-SHORTCUTS FOR FIB MIGRATION

to migrate                              ; Selects Migration method
  ask turtles [
    ifelse breed = SFibs [ move_rand ] [
      if Nav_Method = "Random Walk"              [ ; Completely Random Walk
        move_rand ]
      if Nav_Method = "Void Triggered Random Walk" [ ; Void-triggered Random Walk
        move_void_trig ]
      if Nav_Method = "Void Directed"            [ ; To Random Voids
        move_void_any ]
      if Nav_Method = "Void1 Score - Directed"    [ ; To Max V1-score (+sensitive)
        move_V1score ]
      if Nav_Method = "Void2 Score - Directed"    [ ; To Max V2-score (+sensitive, range)
        move_V2score ]
    ]
  ]
end


;--------------------------------------------------------------------|
;; SHORTCUT FOR FIB MOVEMENT-MODE: RANDOM WALK, ALWAYS
MOVING

to move_rand
    set heading random-float 360
    forward Fspeed
end


;--------------------------------------------------------------------|
;; SHORTCUT FOR FIB MOVEMENT-MODE: RANDOM WALK, TRIGGERED BY
VOID

to move_void_trig
    set heading random-float 360
    ifelse (any? neighbors with [(not any? other IFibs in-radius (IFmove))
      and (not any? other AFibs in-radius (AFmove))
      and (not any? other MFibs in-radius (MFmove))
      and (not any? SFibs in-radius (SFmove)) ])[
      forward Fspeed
      ]
      [ ] ; moves randomly if void space is adjacent, else doesn't move
end
```

```
;-------------------------------------------------------------------------------|
;; SHORTCUT FOR FIB MOVEMENT-MODE: DIRECTED TO RANDOM VOID,
TRIGGERED BY VOID

to move_void_any
    ifelse (any? neighbors with [(not any? other IFibs in-radius (IFmove))
      and (not any? other AFibs in-radius (AFmove))
      and (not any? other MFibs in-radius (MFmove))
      and (not any? SFibs in-radius (SFmove)) ])[
    face one-of neighbors with [(not any? other IFibs in-radius (IFmove))
      and (not any? other AFibs in-radius (AFmove))
      and (not any? other MFibs in-radius (MFmove))
      and (not any? SFibs in-radius (SFmove)) ]
    set heading heading + random-normal 0 (45 / 3)   ; biased to selected patch
    forward Fspeed
    ] [ ]   ; moves toward a void space if they are adjacent, else doesn't move
end




;-------------------------------------------------------------------------------|
;; SHORTCUT FOR FIB MOVEMENT-MODE: DIRECTED TO MAX VOID1-SCORE,
TRIGGERED BY V1SCORE

to move_V1score
    ifelse (any? neighbors with [ V1_score > 0.05 ])[
    face max-one-of neighbors [ V1_score ]
    set heading heading + random-normal 0 (45 / 3)   ; biased to selected patch
    forward Fspeed
    ] [ ]   ; moves toward a void space if they are adjacent, else doesn't move
end




;-------------------------------------------------------------------------------|
;; SHORTCUT FOR FIB MOVEMENT-MODE: DIRECTED TO MAX VOID2-SCORE,
TRIGGERED BY V2SCORE

to move_V2score
    ifelse (any? neighbors with [ V2_score > 0.05 ])[
    face max-one-of neighbors [ V2_score ]
    set heading heading + random-normal 0 (45 / 3)   ; biased to selected patch
    forward Fspeed
    ] [ ]   ; moves toward a void space if they are adjacent, else doesn't move
end
```

```
;================================================================|
;; SHORTCUT TO CALCULATE VOID SCORES

to calc_Vscores
  ;ask patches [   ; sets V0score = normalized #neighbors(n=8) devoid of cell centers
  ;  set V0_score (count neighbors with [ (not any? IFibs) and
  ;     (not any? AFibs) and (not any? MFibs) and (not any? SFibs)]) / 8
  ;  ] ; NOT SURE IF THIS METHOD WORKS OR CHANGES ANYTHING
  ask patches [   ; sets V1score = normalized #neighbors(n=8) devoid of cells
    set V1_score (count neighbors with [ (not any? IFibs in-radius IFsize) and
      (not any? AFibs in-radius AFsize) and (not any? MFibs in-radius MFsize) and
      (not any? SFibs in-radius SFsize)]) / 8
    ]
  ask patches [   ; sets V2score = mean V1score of neighborhood
    set V2_score mean [ V1_score ] of neighbors
    ]
end


;================================================================|
;; SHORTCUTS TO CALCULATE AND REPORT %HEALED AND POP.
PROPORTIONS AND PROBABILITIES

to Measure_Healed
  if Measurement = "Edge_v1" [
    set Healed ( patch-set patches with [
      member? self Scratch and ( V1_score < 0.5 ) ] )
    ]
  if Measurement = "Edge_v2" [
    set Healed ( patch-set patches with [
      member? self Scratch and ( V2_score < 0.5 ) ] )
    ]
  if Measurement = "Edge_v1+2" [
    set Healed ( patch-set patches with [
      member? self Scratch and ( V1_score < 0.5 or V2_score < 0.5 ) ] )
    ]
  set UnHealed ( patch-set patches with [
    (member? self Scratch) and (not member? self Healed)
    ] )
  set UnHealed_edge ( patch-set patches with [
    (member? self UnHealed) and (any? neighbors4 with [
      not member? self UnHealed])
    ])
```

```
if Show_Healed_Area? = true and Label_Leading_Edge? = true [
   ask Scratch [ set pcolor grey ]
   ask Healed [ set pcolor lime ]
   ask UnHealed_edge [ set pcolor 6 ] ; tinted grey
   ]
 if Show_Healed_Area? = true and Label_Leading_Edge? = false [
   ask Scratch [ set pcolor grey ]
   ask Healed [ set pcolor lime ]
   ]
 if Show_Healed_Area? = false and Label_Leading_Edge? = true [
   ask Scratch [ set pcolor grey ]
   ask UnHealed_edge [ set pcolor 6 ] ; tinted grey
   ]
end
to-report %Cover
  report 100 * ( Cell_AR / Rs_AR ) * Fibs_$
end
to-report %Healed
  ifelse Measurement = "Cell_Areas" [ report %Cover ][
    report 100 * (count patches with [member? self Healed]) / Vs_AR
  ]
end
to-report Edge_length
  report ds * (sum [
    count neighbors4 with [not member? self UnHealed]] of UnHealed_edge)
end
to-report Rel_Edge_length
  report Edge_length / Edge_length_t0
end
to-report Divs_T                          ; number of divisions - overall
  report count turtles - Pop_t0
end

to-report IFibs_T report count IFibs end          ; inactive fib pop - overall
to-report AFibs_T report count AFibs end           ; active fib pop - overall
to-report MFibs_T report count MFibs end           ; myo- fib pop - overall
to-report SFibs_T report count SFibs end          ; senescent fib pop - overall
to-report Dead_T report count Apops end          ; dead pop overall
to-report Fibs_T                          ; total fib pop - overall
  report (IFibs_T + AFibs_T + MFibs_T + SFibs_T)
end
```

```
to-report IFibs_$ report count IFibs-on Scratch end ; inactive fib pop - on scratch
to-report AFibs_$ report count AFibs-on Scratch end ; active fib pop - on scratch
to-report MFibs_$ report count MFibs-on Scratch end ; myo- fib pop - on scratch
to-report SFibs_$ report count SFibs-on Scratch end ; senescent fib pop - on scratch
to-report Dead_$ report count Apops-on Scratch end  ; dead pop - on scratch
to-report Fibs_$                          ; total fib pop - on scratch
  report (IFibs_$ + AFibs_$ + MFibs_$ + SFibs_$)
end
to-report IvTFibs_$vT    ; relative ratio of IFibs in the scratch vs overall
  let IvT_$vT 0
  ifelse (Fibs_$ = 0) or (Fibs_T = 0) or (IFibs_T = 0) [ ] [
    set IvT_$vT (IFibs_$ / Fibs_$) / (IFibs_T / Fibs_T)
  ]
  report IvT_$vT
end
to-report AvTFibs_$vT    ; relative ratio of AFibs in the scratch vs overall
  let AvT_$vT 0
  ifelse (Fibs_$ = 0) or (Fibs_T = 0) or (AFibs_T = 0) [ ] [
    set AvT_$vT (AFibs_$ / Fibs_$) / (AFibs_T / Fibs_T)
  ]
  report AvT_$vT
end
to-report MvTFibs_$vT    ; relative ratio of MFibs in the scratch vs overall
  let MvT_$vT 0
  ifelse (Fibs_$ = 0) or (Fibs_T = 0) or (MFibs_T = 0) [ ] [
    set MvT_$vT (MFibs_$ / Fibs_$) / (MFibs_T / Fibs_T)
  ]
  report MvT_$vT
end
to-report SvTFibs_$vT    ; relative ratio of SFibs in the scratch vs overall
  let SvT_$vT 0
  ifelse (Fibs_$ = 0) or (Fibs_T = 0) or (SFibs_T = 0) [ ] [
    set SvT_$vT (SFibs_$ / Fibs_$) / (SFibs_T / Fibs_T)
  ]
  report SvT_$vT
end
to-report Dead_$vT       ; relative ratio of Death in the scratch vs overall
  let DvT_$vT 0
  ifelse (Fibs_$ = 0) or (Fibs_T = 0) or (Dead_T = 0) [ ] [
  set DvT_$vT (Dead_$ / (count turtles-on Scratch)) / (Dead_T / count turtles)
  ]
  report DvT_$vT
end
```

```
to-report MeanP_activate   ; mean probability for inactive fibroblast activation
  let mean_stim 0
  ifelse any? IFibs [
    set mean_stim (Mean [stim] of turtles with [ member? self IFibs ])
    ] [
    set mean_stim (2 * stim_Ta)          ; if no IFibs, P_act = 1
    ]
  let P_act mean_stim / (2 * stim_Ta)
  if P_act < 0 [ set P_act 0 ]
  if P_act > 1 [ set P_act 1 ]
  report P_act
end
to-report MeanP_deactivate ; mean probability for activated fibroblast inactivation
  let mean_stim 0
  ifelse any? AFibs [
    set mean_stim (Mean [stim] of turtles with [ member? self AFibs ])
  ] [ ]
  let P_deact (((2 * stim_T-a) - mean_stim) / (2 * stim_T-a))
  if P_deact < 0 [ set P_deact 0 ]
  if P_deact > 1 [ set P_deact 1 ]
  report P_deact
end
to-report MeanP_transmyo    ; mean probability for senescence of active fibroblasts
  let mean_stim 0
  ifelse any? AFibs [
    set mean_stim (Mean [stim] of turtles with [ member? self AFibs ])
  ] [ ]
  let P_myo ((mean_stim - stim_Ta) / (2 * (stim_Tm - stim_Ta)))
  if P_myo < 0 [ set P_myo 0 ]
  if P_myo > 1 [ set P_myo 1 ]
  report P_myo
end
to-report MeanP_senesce    ; mean probability for senescence of active and myo-fibs
  let mean_stim 0
  ifelse (any? AFibs) or (any? MFibs) [
    set mean_stim (Mean [stim] of turtles with [(breed = AFibs) or (breed = MFibs)])
    ] [ ]
  let P_sen ((mean_stim - stim_Ta) / (2 * (stim_Ts - stim_Ta)))
  if P_sen < 0 [ set P_sen 0 ]
  if P_sen > 1 [ set P_sen 1 ]
  report P_sen
end
```

```
to-report MeanP_die        ; mean probability of fibroblast death due to stimulation
  let mean_stim (Mean [stim] of turtles with [not member? self Apops])
  report mean_stim / (2 * stim_max)
end
to-report Mean_Pact-Pdeact ; calcs mean ratio of activation / inativation rates
  let M_AvDa 1
  ifelse MeanP_deactivate = 0 [ ] [ set M_AvDa ( MeanP_activate / MeanP_deactivate ) ]
  report M_AvDa
end
to-report Mean_Pmyo-Pact   ; calcs mean ratio of myofibroblast / activation rates
  let M_MvA 1
  ifelse MeanP_activate = 0 [ ] [ set M_MvA ( MeanP_transmyo / MeanP_activate ) ]
  report M_MvA
end
to-report Mean_Psen-Pmyo   ; calcs mean ratio of senescence / myofibroblast rates
  let M_SvM 1
  ifelse MeanP_transmyo = 0 [ ][ set M_SvM ( MeanP_senesce / MeanP_transmyo ) ]
  report M_SvM
end
to-report Mean_Psen-Pdie   ; calcs mean ratio of senescence / death rates
  let M_SvD 1
  ifelse MeanP_die = 0 [ ][ set M_SvD ( MeanP_senesce / MeanP_die ) ]
  report M_SvD
end
to-report Mean_Pdie-Pmyo   ; calcs mean ratio of death / myofibroblast rates
  let M_MvD 1
  ifelse MeanP_transmyo = 0 [ ][ set M_MvD ( MeanP_die / MeanP_transmyo ) ]
  report M_MvD
end
to-report Mean_Pact-Pdie   ; calcs mean ratio of activation / death rates
  let M_AvD 1
  ifelse MeanP_die = 0 [ ][ set M_AvD ( MeanP_activate / MeanP_die ) ]
  report M_AvD
end
```

```
; Calculates Mean Void2 Scores by Patch Region's |x-coord|
to-report V2mean_0-8
  report mean [V2_score] of patches with [ (pxcor >= -8) and (pxcor <= 8) ]
end
to-report V2mean_9-16
report mean [V2_score] of patches with [
  ((pxcor >= -16) and (pxcor <= -9))
  or ((pxcor >= 9) and (pxcor <= 16))
  ]
end
to-report V2mean_17-24
report mean [V2_score] of patches with [
  ((pxcor >= -24) and (pxcor <= -17))
  or ((pxcor >= 17) and (pxcor <= 24))
  ]
end
to-report V2mean_25-33
report mean [V2_score] of patches with [
  ((pxcor >= -33) and (pxcor <= -25))
  or ((pxcor >= 25) and (pxcor <= 33))
  ]
end
to-report V2mean_34-42
report mean [V2_score] of patches with [
  ((pxcor >= -42) and (pxcor <= -34))
  or ((pxcor >= 34) and (pxcor <= 42))
  ]
end
to-report V2mean_43-50
report mean [V2_score] of patches with [
  ((pxcor >= -50) and (pxcor <= -43))
  or ((pxcor >= 43) and (pxcor <= 50))
  ]
end
```

```
;=====================================================================|
;; SHORTCUT FOR CODE USED TO SETUP IN VITRO %HEALED RANGES FOR
MODEL COMPARISONS
to plot_IV_%Healed
let x-vals (list 0 4 8 12 16 20 24)                ; Scratch Assay timepoints
let y-means (list 0.00 0.00 0.00 0.00 0.00 0.00 0.00)
let y-sds (list 0.00 0.00 0.00 0.00 0.00 0.00 0.00)
if Experiment_Type = "Scratch Healing" [
  if Cell_Line = "NHLF" [
    if Media = "FGM" [
    set y-means (list 0.00 17.40 45.29 56.79 63.88 76.65 86.64)
    set y-sds (list 0.00 5.20 3.37 7.02 6.48 10.23 5.93)
    ]
    if Media = "FBM" [
    set y-means (list 0.00 9.58 23.01 34.88 45.46 56.34 64.16)
    set y-sds (list 0.00 3.48 6.84 7.99 6.41 10.46 10.62)
    ]
    if Media = "CSC" [
    set y-means (list 0.00 6.00 14.28 23.49 34.93 45.38 52.17)
    set y-sds (list 0.00 0.86 9.32 9.70 10.59 9.96 10.16)
    ]
  ]
    if Cell_Line = "DHLF" [
    if Media = "FGM" [
    ]
    if Media = "FBM" [
    set y-means (list 0.00 12.01 19.96 21.13 24.51 28.26 39.30)
    set y-sds (list 0.00 8.96 14.90 10.68 15.94 18.87 20.47)
    ]
    if Media = "CSC" [
    set y-means (list 0.00 5.30 15.52 13.53 15.56 21.16 28.83)
    set y-sds (list 0.00 3.75 10.97 8.40 5.42 7.22 12.23)
    ]
  ]
  let index 0
  while [ index < length x-vals ] [
    plotxy (item index x-vals) ((item index y-means) + (2 * (item index y-sds)))
    plotxy (item index x-vals) ((item index y-means) - (2 * (item index y-sds)))
    set index (index + 1)
  ]
]
end
```

```
;==================================================================|
;; SHORTCUT FOR CODE USED TO SETUP IN VITRO MTT RANGES FOR MODEL
COMPARISONS
to plot_IV_MTT
let x-vals (list 0 2 12 24)                    ; MTT/CCK8 timepoints
let y-means (list 0.00 0.00 0.00 0.00 0.00 )
let y-sds (list 0.00 0.00 0.00 0.00 0.00 )
if Cell_Line = "NHLF" [
  if Media = "FGM" [
    set y-means map [( (? + 1) * Pop_t0 )] (list 1.000  1.182  0.944  1.095)
    set y-sds map [( ? * Pop_t0 )] (list 0.181  0.107  0.057  0.080)
    ]
  if Media = "FBM" [
    set y-means map [( (? + 1) * Pop_t0 )] (list 1.000  1.119  0.977  0.968)
    set y-sds map [( ? * Pop_t0 )] (list 0.181  0.132  0.127  0.120)
    ]
  if Media = "CSC" [
    set y-means map [( (? + 1) * Pop_t0 )] (list 1.000  1.047  1.018  0.765)
    set y-sds map [( ? * Pop_t0 )] (list 0.181  0.137  0.098  0.125)
    ]
  ]
let index 0
while [ index < length x-vals ] [
  plotxy (item index x-vals) ((item index y-means) + (2 * (item index y-sds)) - Pop_t0)
  plotxy (item index x-vals) ((item index y-means) - (2 * (item index y-sds)) - Pop_t0)
  set index (index + 1)
  ]
end
```

```
;===================================================================|
;; SHORTCUT FOR CODE USED TO SETUP IN VITRO Totlnorm RANGES FOR
MODEL COMPARISONS
to plot_IV_Totlnorm
let x-vals (list 0.00 0.00 0.00)
let y-means (list 0.00 0.00 0.00 )
let y-sds (list 0.00 0.00 0.00 )
if Experiment_Type = "Culture Cond." [
  set x-vals (list 0 8)                ; Staining timepoints (pre-scratch)
  if Cell_Line = "NHLF" [
  if Media = "FGM" [
    set y-means map [( (? + 1) * Pop_t0 )] (list 1.000  1.313)
    set y-sds map [( ? * Pop_t0 )] (list 0.278  0.316)
    ]
  ]
]
if Experiment_Type = "Scratch Healing" [
  set x-vals (list 0 12 24)              ; Staining timepoints (post-scratch)
  if Cell_Line = "NHLF" [
  if Media = "FGM" [
    set y-means map [( (? + 1) * Pop_t0 )] (list 1.000  1.163  1.534)
    set y-sds map [( ? * Pop_t0 )] (list 0.487  0.376  0.335)
    ]
  if Media = "FBM" [
    set y-means map [( (? + 1) * Pop_t0 )] (list 1.000  1.043  1.130)
    set y-sds map [( ? * Pop_t0 )] (list 0.487  0.497  0.524)
    ]
  if Media = "CSC" [
    set y-means map [( (? + 1) * Pop_t0 )] (list 1.000  0.948  1.114)
    set y-sds map [( ? * Pop_t0 )] (list 0.487  0.300  0.273)
    ]
  ]
  ]
let index 0
while [ index < length x-vals ] [
  plotxy (item index x-vals) ((item index y-means) + (2 * (item index y-sds)) - Pop_t0)
  plotxy (item index x-vals) ((item index y-means) - (2 * (item index y-sds)) - Pop_t0)
  set index (index + 1)
  ]
end
```

```
;==============================================================|
;; SHORTCUT FOR CODE USED TO SETUP IN VITRO Totl RANGES FOR MODEL
COMPARISONS
to plot_IV_Totl
let x-vals (list 0.00 0.00 0.00)
let y-means (list 0.00 0.00 0.00 )
let y-sds (list 0.00 0.00 0.00 )
if Experiment_Type = "Culture Cond." [
  set x-vals (list 0 8)               ; Staining timepoints (pre-scratch)
  if Cell_Line = "NHLF" [
  if Media = "FGM" [
   set y-means (list 409.4  537.8)
   set y-sds (list 113.9  129.4)
   ]
  ]
]
if Experiment_Type = "Scratch Healing" [
  set x-vals (list 0 12 24)             ; Staining timepoints (post-scratch)
  if Cell_Line = "NHLF" [
  if Media = "FGM" [
   set y-means (list 415.9  483.8  638.0)
   set y-sds  (list 202.7  156.2  139.3)
   ]
  if Media = "FBM" [
   set y-means (list 415.9  433.9  470.2)
   set y-sds  (list 202.7  206.7  217.8)
   ]
  if Media = "CSC" [
   set y-means (list 415.9  394.4  463.3)
   set y-sds  (list 202.7  124.6  113.7)
   ]
  ]
  ]
let index 0
while [ index < length x-vals ] [
    plotxy (item index x-vals) ((item index y-means) + (2 * (item index y-sds)))
    plotxy (item index x-vals) ((item index y-means) - (2 * (item index y-sds)))
    set index (index + 1)
  ]
end
```

```
;=================================================================|
;; SHORTCUT FOR CODE USED TO SETUP IN VITRO % Dead RANGES FOR
MODEL COMPARISONS
to plot_IV_dead
let x-vals (list 0.00 0.00 0.00)
let y-means (list 0.00 0.00 0.00 )
let y-sds (list 0.00 0.00 0.00 )
if Experiment_Type = "Culture Cond." [
  set x-vals (list 0 8)              ; Staining timepoints (pre-scratch)
  if Cell_Line = "NHLF" [
  if Media = "FGM" [
   set y-means (list 1.48  3.04)
   set y-sds  (list 0.56  0.54)
   ]
 ]
]
if Experiment_Type = "Scratch Healing" [
  set x-vals (list 0 12 24)              ; Staining timepoints (post-scratch)
  if Cell_Line = "NHLF" [
  if Media = "FGM" [
   set y-means (list 8.05  2.72  1.63)
   set y-sds  (list 1.85  0.50  0.63)
   ]
  if Media = "FBM" [
   set y-means (list 8.05  4.04  1.82)
   set y-sds  (list 1.85  0.57  0.21)
   ]
  if Media = "CSC" [
   set y-means (list 8.05  3.69  2.11)
   set y-sds  (list 1.85  1.99  0.71)
   ]
 ]
 ]
let index 0
while [ index < length x-vals ] [
    plotxy (item index x-vals) ((item index y-means) + (2 * (item index y-sds)))
    plotxy (item index x-vals) ((item index y-means) - (2 * (item index y-sds)))
    set index (index + 1)
 ]
end
```

```
;===================================================================|
;; SHORTCUT FOR CODE USED TO SETUP IN VITRO % SA-B-Gal RANGES FOR
MODEL COMPARISONS
to plot_IV_bgal
let x-vals (list 0.00 0.00)
let y-means (list 0.00 0.00)
let y-sds (list 0.00 0.00)
if Experiment_Type = "Culture Cond." [
  set x-vals (list 0 8)              ; Staining timepoints (pre-scratch)
  if Cell_Line = "NHLF" [
  if Media = "FGM" [
    set y-means (list 11.91  17.42)
    set y-sds  (list 3.37  1.55)
    ]
  ]
]
if Experiment_Type = "Scratch Healing" [
  set x-vals (list 0 12 24)              ; Staining timepoints (post-scratch)
  if Cell_Line = "NHLF" [
  if Media = "FGM" [
    set y-means (list 16.72  48.29  20.43)
    set y-sds  (list 5.51  7.72  1.72)
    ]
  if Media = "FBM" [
    set y-means (list 16.72  31.71  13.64)
    set y-sds  (list 5.51  2.22  3.17)
    ]
  if Media = "CSC" [
    set y-means (list 16.72  23.12  21.65)
    set y-sds  (list 5.51  11.84  2.51)
    ]
  ]
  ]
let index 0
while [ index < length x-vals ] [
    plotxy (item index x-vals) ((item index y-means) + (2 * (item index y-sds)))
    plotxy (item index x-vals) ((item index y-means) - (2 * (item index y-sds)))
    set index (index + 1)
  ]
end
```

```
;================================================================|
;; SHORTCUT FOR CODE USED TO SETUP IN VITRO % aSMA RANGES FOR
MODEL COMPARISONS
to plot_IV_asma
let x-vals (list 0.00 0.00)
let y-means (list 0.00 0.00)
let y-sds (list 0.00 0.00)
if Experiment_Type = "Culture Cond." [
  set x-vals (list 0 8)              ; Staining timepoints (pre-scratch)
  if Cell_Line = "NHLF" [
  if Media = "FGM" [
    set y-means (list 4.35  13.49)
    set y-sds  (list 1.45  0.39)
    ]
  ]
]
if Experiment_Type = "Scratch Healing" [
  set x-vals (list 0 12 24)              ; Staining timepoints (post-scratch)
  if Cell_Line = "NHLF" [
  if Media = "FGM" [
    set y-means (list 20.97  27.83  23.21)
    set y-sds  (list 3.40  3.74  4.20)
    ]
  if Media = "FBM" [
    set y-means (list 20.97  17.38  10.90)
    set y-sds  (list 3.40  0.37  1.38)
    ]
  if Media = "CSC" [
    set y-means (list 20.97  58.91  14.48)
    set y-sds  (list 3.40  22.87  4.41)
    ]
  ]
  ]
let index 0
while [ index < length x-vals ] [
    plotxy (item index x-vals) ((item index y-means) + (2 * (item index y-sds)))
    plotxy (item index x-vals) ((item index y-means) - (2 * (item index y-sds)))
    set index (index + 1)
  ]
end
```

```
;================================================================|
;; SHORTCUT TO MAKE & EXPORT A MOVIE OF THE VIEW OR INTERFACE
to make_movie
  movie-cancel                          ; cancels movie if still filming
  setup
  let movie_name "Model_0.3.7_"
  if movie_type = "World View" [        ; films movie of world view
    set movie_name (word movie_name "View_" Cell_Line"_" Media"_" Movie_Title
".mov")
    movie-start movie_name
    movie-set-frame-rate (1 / dt)       ; sets the frame rate 1 tick/sec
    movie-grab-view                     ; shows the initial state
    repeat (1 + (t_end / dt)) [
      go
      movie-grab-view                   ; shows state with each step
      ]
    ]
  if movie_type = "Interface" [         ; films movie of model interface
    set movie_name (word movie_name "UI_" Cell_Line"_" Media"_" Movie_Title ".mov")
    movie-start movie_name
    movie-set-frame-rate (1 / dt)
    movie-grab-interface
    repeat (1 + (t_end / dt)) [
      go
      movie-grab-interface
      ]
    ]
  print (word movie_name " has completed at "
    date-and-time " with " t_end " hours simulated over " movie-status)   ; prints movie
info upon completion
  repeat 3 [beep wait 1]               ; emits 3 beeps spaced 1s apart
  movie-close
end
```

# **APPENDIX B**

| Variable | Value | Unit | Description |
|---|---|---|---|
| tick | 1 | hour | Model counter |
| world-height | 101 | patches | Model world height |
| Iheight | 1677 | μm | *In vitro* image height* |
| dt | 1/3 | tick/step | Time resolution (= 20min/step) |
| ds | 16.6040 | um/patch | Spatial resolution |
| Rs_AR | 1296089.39 | $\mu m^2$ | *In vitro* scratch area* |
| N_diam | 30.0 | μm | NHLF diameter mean [61] |
| Time_seed-scratch | 6 | hours | Seed-Scratch time interval* |
| Pop_Ss | 1172 | agents | Seeded population* |
| MPop_S | 0.0435 | ratio | Seeded *MFibs** |
| SPop_S | 0.1191 | ratio | Seeded *SFibs** |
| DPop_S | 0.0148 | ratio | Seeded *DFibs** |
| IPop_S | 0 | ratio | Seeded *IFibs* [49] |
| APop_S | remaining | ratio | Seeded *AFibs* [49]* |
| Alpha_Z | 0.75 | ratio | *IFib* size coefficient |
| Alpha_M | 0 | ratio | *IFib* speed coefficient |
| Alpha_P | 1 | ratio | *IFib* division period coefficient |
| Alpha_D | 1 | ratio | *IFib* death resistance coefficient |
| Beta_Z | 1 | ratio (ref.) | *AFib* size coefficient |
| Beta_M | 1 | ratio (ref.) | *AFib* speed coefficient |
| Beta_P | 1 | ratio (ref.) | *AFib* division period coefficient |
| Beta_D | 1 | ratio (ref.) | *AFib* death resistance coefficient |
| Gamma_Z | 1.4 | ratio | *MFib* size coefficient [61] |
| Gamma_M | 0.625 | ratio | *MFib* speed coefficient [61] |
| Gamma_P | 1.4 | ratio | *MFib* division period coefficient [61] |
| Gamma_D | 1.4 | ratio | *MFib* death resistance coefficient |
| Omega_Z | 2 | ratio | *SFib* size coefficient [40] |
| Omega_M | 0.75 | ratio | *SFib* speed coefficient [124] |
| Omega_P | 1000 | ratio | *SFib* division period coefficient [40] |
| Omega_D | 1000 | ratio | *SFib* death resistance coefficient [40] |

Model constants controlling temporal-spatial resolution and initial conditions for scratch closure simulations. * indicates values determined from *in vitro* experiments with NHLF.

| Parameter | Value | Unit | Description |
|---|---|---|---|
| Migrate_rate | $ | µm/hour | *AFib* migration rate |
| Prolife_rate | $ | hour/split | *AFib* proliferation rate |
| T_myo | $ | stim | Myofibroblast stimulation threshold |
| T_sen | $ | stim | Senescence stimulation threshold |
| Stim_rate | $ | stim/hour | Environmental stimuli magnitude |
| Stim_sense | $ | ratio | Stimuli sensitivity distribution |

Model parameters controlling agent characteristics and responses to stimulation during scratch closure simulations. $ indicates parameters calibrated to *in vitro* experiments.

| UI Setting | Value | Description |
|---|---|---|
| Cell_Line | NHLF | Counter-plot NHLF in vitro data ranges |
| | DHLF | Counter-plot DHLF in vitro data ranges |
| Media | FGM | Green-gradient agents |
| | FBM | Blue-gradient agents |
| | CSC | Red-gradient agents |
| Experiment_Type | Culture Cond. | No voided region; no gradients. |
| | Scratch Healing | Whole region seeded with N agents; central region denuded of ~N/2 agents at time T to instigate invasive behaviors |
| | Barrier Removal | Central region is filled with ~N/2 agents; allowed to invade at time T |
| Seed_Density | In Vitro | Seed same number of agents as in vitro |
| | Max Confluency | Seed max number of agents sans overlap |
| Seed_IFibs_Only? | On/Off | Toggles "all inactive" or "*in vitro* ratios" |
| Precondition? | On/Off | Toggles precondition interval |
| Show_Healed_Area? | On/Off | Toggles green-labeled *Healed* region |
| Label_Leading_Edge? | On/Off | Toggles grey-labeled *Unhealed Edge* |

User interface settings that control the model display and additional functionalities.

# **APPENDIX C**

| Group | Parameter Modulation | | Total Population | | %Dead | |
|---|---|---|---|---|---|---|
| | | | **12 HR** | **24 HR** | **12 HR** | **24 HR** |
| **NHLF FGM** | M | + | -5.9 | -4.3 | 3.4 | 2.3 |
| | | - | -10.9 | -10.0 | 4.9 | 4.6 |
| | P | + | -6.3 | -5.8 | 5.4 | 7.0 |
| | | - | -7.2 | -5.4 | 3.9 | 3.0 |
| | $L_M$ | + | -10.5 | -9.1 | 2.4 | 1.8 |
| | | - | -6.7 | -6.1 | 4.3 | 3.7 |
| | $L_S$ | + | -7.4 | -5.2 | 2.3 | -0.2 |
| | | - | -10.5 | -10.0 | 3.1 | 3.2 |
| | $A_M$ | + | -9.5 | -8.7 | 3.1 | 3.8 |
| | | - | -4.2 | -2.5 | 2.5 | 2.6 |
| | $A_S$ | + | -12.5 | -11.1 | 1.8 | 0.4 |
| | | - | -4.8 | -3.9 | 2.9 | 3.9 |
| **NHLF FBM** | M | + | -1.5 | -4.0 | 0.2 | 1.6 |
| | | - | 1.2 | -2.7 | 1.9 | 5.5 |
| | P | + | -2.2 | -4.7 | 1.8 | 3.0 |
| | | - | -2.1 | -5.0 | -0.4 | 2.5 |
| | $L_M$ | + | -5.4 | -7.6 | 1.4 | 3.7 |
| | | - | -1.4 | -5.0 | 1.2 | 4.7 |
| | $L_S$ | + | -1.0 | -3.3 | 0.9 | 3.4 |
| | | - | -4.3 | -7.8 | 0.4 | 3.5 |
| | $A_M$ | + | -4.0 | -7.6 | 2.0 | 5.4 |
| | | - | -1.4 | -3.4 | 0.8 | 2.0 |
| | $A_S$ | + | 0.9 | -1.5 | 3.0 | 5.5 |
| | | - | -2.9 | -5.4 | 1.1 | 3.6 |

(Table continued on next page)

| Group | Parameter Modulation | | Total Population | | %Dead | |
|---|---|---|---|---|---|---|
| | | | 12 HR | 24 HR | 12 HR | 24 HR |
| NHLF | M | + | -3.9 | -3.1 | 1.2 | 2.1 |
| CSM | | - | 0.8 | 0.4 | 2.4 | 2.5 |
| | P | + | -3.8 | -4.1 | 1.7 | 3.0 |
| | | - | -4.4 | -3.8 | 0.3 | -1.2 |
| | $L_M$ | + | -1.5 | -1.5 | 1.2 | 0.4 |
| | | - | -0.6 | -0.8 | 0.0 | 2.4 |
| | $L_S$ | + | -0.6 | 0.3 | 1.8 | 3.1 |
| | | - | -0.9 | -1.6 | 2.1 | 3.1 |
| | $A_M$ | + | -5.3 | -5.2 | 1.8 | 0.6 |
| | | - | -5.1 | -4.9 | 1.3 | 1.4 |
| | $A_S$ | + | 1.2 | 0.8 | 1.8 | 5.8 |
| | | - | -4.0 | -4.6 | 0.7 | 3.1 |
| DHLF | M | + | -1.7 | -2.0 | -0.6 | 0.8 |
| | | - | 0.5 | 0.7 | 2.0 | 3.8 |
| | P | + | -5.6 | -5.9 | 1.3 | 3.3 |
| | | - | 0.2 | 0.4 | -0.5 | -1.3 |
| | $L_M$ | + | -4.7 | -5.0 | 0.9 | 3.2 |
| | | - | -4.6 | -5.1 | 0.7 | 2.2 |
| | $L_S$ | + | 4.7 | 5.1 | -0.6 | 0.3 |
| | | - | -1.3 | -1.7 | -0.9 | 0.7 |
| | $A_M$ | + | -1.1 | -1.3 | 2.3 | 6.4 |
| | | - | -6.1 | -5.1 | 0.6 | 0.2 |
| | $A_S$ | + | 0.1 | 0.2 | -0.8 | 0.1 |
| | | - | 0.8 | 0.8 | 1.2 | 1.6 |

Heat-map of each calibrated parameter-set's sensitivity to parameter changes; expressed as the percentage difference from the calibrated parameter-set's mean output when each parameter is independently modulated by $\pm$ 10%. Model outputs are shown for the total population and percentage of dead cells after 12 or 24 hours. Parameter-set mean outputs were calculated from 10 simulations with the same conditions. A blue-red gradient was applied across all outputs and parameter modulations within each group.

# **<u>VITA</u>**

I, James Alexander Ratti, am a U.S. citizen native to Virginia Beach, Virginia; born December 08, 1990. I earned a Bachelor of Science in Biomedical Engineering with a Concentration in Biomechanics and Biomaterials, along with a Minor in Applied Mathematics from Virginia Commonwealth University in May 2013. I have submitted abstracts and poster presentations of this work, or iterations, to annual conferences for BMES (2015), VAS (May 2016) and BAMM (May 2016); along with oral presentations to annual conferences for SIAM-SEAS (March 2018) and BAMM (May 2018).

While working on this project, I began working with Sosipatros Boikos, MD and Steven Grossman, MD, PhD to investigate cancer resistance to hypoxia and cytotoxins within sarcomas in search of novel treatment strategies. I've also begun working as a communications liaison for the Pityriasis Rubra Pilaris Alliance non-profit patient advocacy organization to raise awareness and funds for research into treatments for this disease. It is my sincere hope that people with these and other rare conditions will one day have the efficacious treatments they desperately need.